Deutsches Zentrum
für Luft- und Raumfahrt e.V.
in der Helmholtz-Gemeinschaft

EnMAP Ground Segment

Mission Quarterly Report #14

01.10.2025 to 31.12.2025

Public

Doc. ID	EN-GS-RPT-1114
Issue	1.0
Date	23.03.2026

Configuration Controlled: Yes

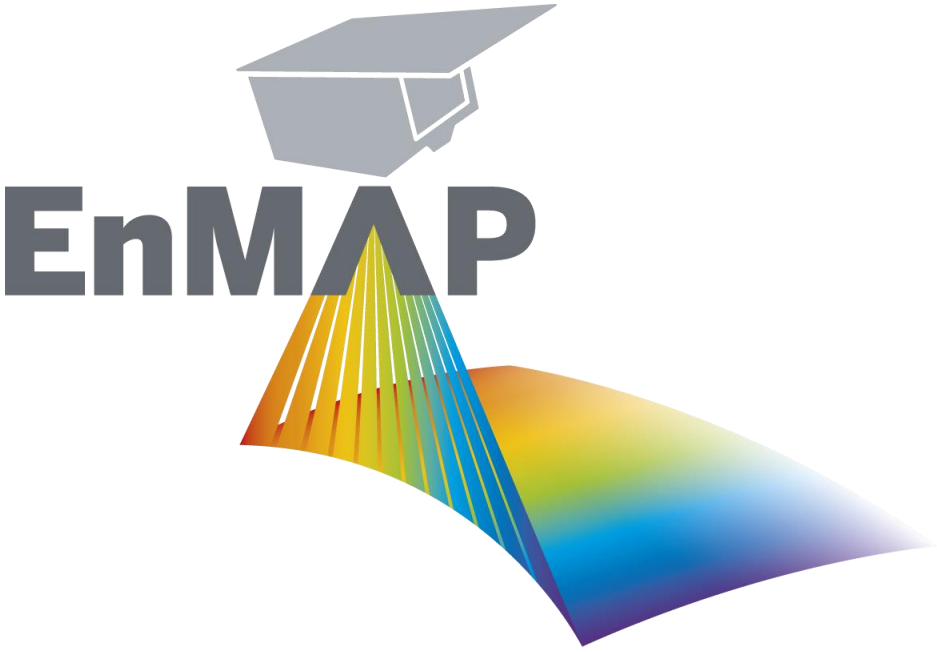

German Remote Sensing Data Center (DFD)
Remote Sensing Technology Institute (IMF)
German Space Operations Center (GSOC)
Helmholtz Centre for Geosciences (GFZ)
German Space Agency at DLR

TABLE OF SIGNATURES

Prepared	Emiliano Carmona Flores Digitally signed by Emiliano Carmona Flores DN: C=DE, CN=Emiliano Carmona Flores, O=Deutsches Zentrum fuer Luft- und Raumfahrt e. V. (DLR), ST=Nordrhein-Westfalen, E=emiliano.carmona@dlr.de, postalCode=51147, street=Linder Höhe Reason: I am the author of this document Location: Date: 2026.03.30 14:00:57+02'00' Foxit PDF Reader Version: 2025.3.0	Date
	Emiliano Carmona, (DLR MF-ASP, EnMAP OMM)	
	Sabine Chabrillat Digital unterschrieben von Sabine Chabrillat Datum: 2026.03.30 23:13:33 +02'00'	Date
	Sabine Chabrillat, (GFZ, EnMAP SciLead)	
Reviewed	i.A. D. Schulze Digital signiert von Daniel Schulze Datum: 2026.03.31 09:10:47+02'00'	Date
	Daniel Schulze, (DLR RB-MIB, dep. EnMAP OMM)	
	Sabine Engelbrecht Digital signiert von Sabine Engelbrecht DN: C=DE, CN=Sabine Engelbrecht, O=Deutsches Zentrum fuer Luft- und Raumfahrt e. V. (DLR), ST=Nordrhein-Westfalen, E=sabine.engelbrecht@dlr.de, postalCode=51147, street=Linder Höhe Grund: Ich habe dieses Dokument geprüft Ort: DLR Oberpfaffenhofen Datum: 2026.03.31 09:26:10+02'00' Foxit PDF Editor Version: 14.0.2	Date
	Sabine Engelbrecht, (DLR DFD-INF, EOC PAD)	
	Robert Größel Digital signiert von Robert Größel DN: C=DE, CN=Robert Größel, O=Deutsches Zentrum fuer Luft- und Raumfahrt e. V. (DLR), ST=Nordrhein-Westfalen, E=robert.groessel@dlr.de, postalCode=51147, street=Linder Höhe Grund: Ich bin der Verfasser dieses Dokuments Ort: Datum: 2026.03.31 08:57:24+02'00' Foxit PDF Reader Version: 2025.3.0	Date
	Robert Größel, (DLR RB-CTA, GSOC PAD)	
	Karl Segl Digitally signed by Karl Segl Date: 2026.03.31 08:05:37 +02'00'	Date
	Karl Segl, (GFZ, dep. EnMAP SciLead)	
Approved & Released	i.A. Laura La Porta 2026.03.31 15:50:05+02'00' 14.0.2	Date
	Laura La Porta, (DLR AR-AO, EnMAP MM)	

DISTRIBUTION LIST

The document is publicly available via www.enmap.org.

CHANGE RECORD

Version	Date	Chapter	Comment
1.0	23.03.2026	All	First issue of Mission Quarterly Report #14 corresponding to 01.10.2025 to 31.12.2025.

Custodian of this document is Carmona, Emiliano.

CONTENTS

LIST OF FIGURES

LIST OF TABLES

1 Introduction

1.1 Purpose

This mission quarterly report (MQR) states information on the EnMAP mission status with regard to the registered user community, announcements-of-opportunities and observations as well as the status of the user interfaces, satellite (platform and payload), ground stations (S-band and X-band), processor (Archive, Level 1B, Level 1C, Level 2A (land and water)), calibration (spectral, radiometric, geometric), data quality control and validation of EnMAP.

Please visit www.enmap.org for further information on EnMAP.

1.2 Scope

This 14th Mission Quarterly Report (MQR) applies to the operations of EnMAP in the reporting period of Routine Phase (RP) from **01.10.2025 to 31.12.2025 (Q4 2025)**.

2 References

Reference Identifier	Document Identifier and Title
[1]	L. Guanter et al. (2015) The EnMAP Spaceborne Imaging Spectroscopy Mission for Earth Observation. Remote Sensing, Issue 7, pp. 8830-8857.
[2]	EN-GS-UM-6020 Portals User Manual, Version 1.4
[3]	EN-PCV-ICD-2009-2 Product Specification, Version 1.9
[4]	EN-PCV-TN-4006 Level 1B ATBD, Version 1.10
[5]	EN-PCV-TN-5006 Level 1C ATBD, Version 1.7
[6]	EN-PCV-TN-6007 Level 2A (land) ATBD, Version 2.4
[7]	EN-PCV-TN-6008 Level 2A (water) ATBD, Version 3.1
[8]	Chabrillat, S. et al. (2022) EnMAP Science Plan. EnMAP Technical Report, DOI: 10.48440/enmap.2022.001
[9]	Storch, T.; Honold, H.-P.; Chabrillat, et al. The EnMAP imaging spectroscopy mission towards operations. Remote Sens. Environ. 2023, 294, 113632. DOI: 10.1016/j.rse.2023.113632

Table 2-1 References

3 Terms, Definitions and Abbreviations

Terms, definitions and abbreviations for EnMAP are collected in a database which is publicly accessible via Internet on www.enmap.org.

An Earth observation of swath length *n* × 30 km (and swath width 30 km) is separated into *n* tiles of size 30 km × 30 km.

4 Mission

4.1 Mission Objectives

The primary goal of EnMAP (Environmental Mapping and Analysis Program) is to measure, derive and analyze quantitative diagnostic parameters describing key processes on the Earth's surface [1].

During the mission operations, with the successful launch on 1st of April 2022 and an expected operational mission lifetime of at least 5 years, EnMAP will provide valuable information for various application fields comprising soil and geology, agriculture, forestry, urban areas, aquatic systems, ecosystem transitions.

4.2 Mission Description

The major elements of the EnMAP mission are the EnMAP Space Segment, built by OHB System AG and owned by the German Space Agency at DLR, the EnMAP Ground Segment built and operated by DLR institutes DFD, MF, RB, and the EnMAP User and Science Segment represented by GFZ. The project management of the EnMAP mission is responsibility of the German Space Agency at DLR.

The EnMAP Space Segment is composed of

- the platform providing power and thermal stability, orbit and attitude control, memory, S-band uplink/downlink for TM/TC data transmission/reception, X-band downlink for payload data transmission, and

- the payload realized as a pushbroom imaging dual-spectrometer covering the wavelength range between 420 nm and 2450 nm with a nominal spectral resolution ≤ 10 nm and allows in combination with a high radiometric resolution and stability to measure subtle reflectance changes.

The EnMAP satellite is operated on a sun-synchronous repeat orbit to observe any location on the globe with comparable illumination conditions. This allows a maximum reflected solar input radiance at the sensor with an acceptable risk for cloud coverage.

The EnMAP Ground Segment is the interface between Space Segment and User and Science Segment. It comprises functionalities to

- perform planning of imaging, communication and orbit maneuver operations, provision of orbit and attitude data, command and control of the satellite, ground station networks (in particular: Weilheim, Germany, for S-band and Neustrelitz, Germany, for X-Band), receive satellite data, perform long-term archiving and delivery of products, and

- perform processing chain (for systematic and radiometric correction, orthorectification, atmospheric compensation), instrument calibration operations, and the data quality control of the products.

The EnMAP mission interfaces to the international science and user community through the EnMAP Portal www.enmap.org with official information related to EnMAP by DLR and GFZ-Potsdam (as the document in hand) and links for ordering observations and products.

The EnMAP Science Segment is represented by the EnMAP Science Advisory Group chaired by the mission principal investigator at the GFZ-Potsdam. The Science Segment addresses aspects such as

- supporting and performing validation activities to improve sensor performance and product quality

- developing scientific and application research to fully exploit the scientific potential of EnMAP [8] including provision of software tools for EnMAP data processing and analyses (EnMAP-Box) and provision of teaching and education materials (HYPERedu)

- Organizing workshops, summer schools and in general information, training and networking activities for the user community

The EnMAP User Segment is the community of German and international users ordering acquisitions and accessing products of EnMAP.

4.3 Mission Status Summary

The mission successfully finished the commissioning phase (CP) on 01.11.2022 [9] and entered its routine phase (RP) on 02.11.2022. In the reporting period, from 01.10.2025 to 31.12.2025, there have been no major issues affecting the instrument or the satellite, only some minor issues have caused the loss of a small fraction of observation time. The Ground Segment services have been operating normally.

During the period 01.10.2025 to 31.12.2025 (92 days in total), only two issues resulted in several hours of no acquisitions. The two issues were caused by HSI SAFE_ERRORs (18.11.2025 and 15.12.2025), that resulted in no observations during 22 hours and 26 hours. In all cases the data quality is analyzed after resuming operations and no effect was found on the newly acquired data. During normal operations, the mission is regularly surpassing the initially planned maximum acquisition capacity of 5000 km / day.

In this period, 1754 Earth observations of 30 km swath width and up to 990 km swath length were successfully performed which resulted in 19123 archived Earth observation tiles of 30 km × 30 km and 22 calibration acquisitions. In addition, 20586 products were delivered from catalog orders. In total, 21526 Earth observations were performed until 31.12.2025 by the EnMAP team and the 4862 registered users with at least one active user role. This results in 193749 archived Earth observation images (233882 products including the different versions of the re-processed products) and 363235 Earth products delivered from observations requests (200587) and catalogue orders (162648) since the start of the mission. More details are presented in sections 5 and 6.

The mission acquisition process has been updated to improve cloud forecast handling during planning. The forecast request window to obtain cloudiness predictions from the German Meteorological Service (DWD) has been reduced to ensure EnMAP acquisitions are planned with the most up-to-date information. Additionally, acquisitions with negative forecasts (predicted cloudiness exceeding the threshold specified in the request) are now excluded from planning, whereas previously they could still be considered and scheduled if no better alternative was available. As a result, the total number of acquisitions will likely decrease in future quarters, but the quality of acquired data should improve significantly thanks to a reduced cloud presence in the EnMAP products. This update was activated on November 21.

No major limitations are applicable at 31.12.2025. For minor limitations affecting data processing, check section 7.4. Other effects observed in the data by our Quality Control team are reported in section 7.6 where they are investigated in more detail.

Activities within the EnMAP Mission and in particular the Ground Segment are periodically reported in conferences and workshops. More details are available in Section 9.

The following changes were implemented in the reporting period:

- Since 21 November 2025, the logic of the cloud forecast for preparation of the mission timeline has been updated. Cloud estimates are updated on a time window closer to the acquisition date and observation requests with a negative forecast are rejected (see above).
- New version of the processing software (**V01.05.05**).
- Reprocessing of L0 products to L2A ARD products with processor version **V01.05.02** in progress. During this re-processing, L1B and L1C ARD products for the complete EnMAP archive will also be generated and made available along 2026.

The list of changes introduced in this and previous processor updates is available at:

https://www.enmap.org/data/doc/EnMAP_processor_changelog.pdf

Since August 2024, EnMAP L2A ARD products have been available for download through the EOC Geoservice (https://geoservice.dlr.de/) and the EO-Lab platform (https://eo-lab.org/). These possibilities allow the direct download of EnMAP L2A products generated by the EnMAP Ground Segment with a standard set of parameters. Since these L2A products are already processed, users can directly download these products without waiting times, allowing a fast way to get large amounts of EnMAP products from the mission archive. Notice that both EOC Geoservice and EO-Lab are not part of the standard services offered by the EnMAP mission but are accessible with the GS/IPS EnMAP account. More information on the number of products downloaded through Geoservice can be found in section 6.2.1.

The following changes are expected to be performed in the next quarters:

- New processor version (**V01.05.06**). For more details on this new version see section 7.4.
- Implementation of stricter policy concerning use of private emails for registration as an EnMAP user
- Implementation of updated FGM flightlines and switch to normal mode (form winter mode)
- Implementation of new linearity calibration (and updated calibration) to improve the VNIR-SWIR matching between spectrometers, specially at low radiances.

5 Users and Announcements-of-Opportunities

5.1 Users

	Country/Continent (No of Countries) *(of reporting period)*	Reporting Period 01.10.2025 to 31.12.2025		Country/Continent (No of Countries) *(since beginning of routine phase)*	Since beginning of routine phase until 31.12.2025 (end of reporting period)
Total European Users	Europe *(24)*	122		Europe *(33)*	1999
European Countries	• Germany	34		• Germany	731
	• France	17		• France	194
	• Greece	7		• Italy	183
	• Hungary	6		• Spain	126
	• Czechia	5		• United Kingdom	123
	• Switzerland	5		• Netherlands	95
	• United Kingdom	5		• Poland	85
	• Austria	4		• Finland	47
	• Italy	4		• Greece	44
	• Netherlands	4		• Belgium	39
	• Spain	4		• Switzerland	39
	• Belgium	3		• Austria	34
	• Finland	3		• Czechia	33
	• Lithuania	3		• Sweden	32
	• Poland	3		• Hungary	30
	• Ukraine	3		• Norway	29
	• Others *(8)*	12		• Others *(17)*	135
Non European	North America *(5)*	46		North America *(11)*	597
	South America *(6)*	22		South America *(11)*	285
	Asia *(23)*	185		Asia *(37)*	1557
	Africa *(14)*	25		Africa *(32)*	232
	Oceania *(2)*	25		Oceania *(3)*	192
	Total *(74)*	**425**		**Total *(127)***	**4862**

Table 5-1 Number of registered users per continent with **at least one active user role** (number of user countries during reporting period)

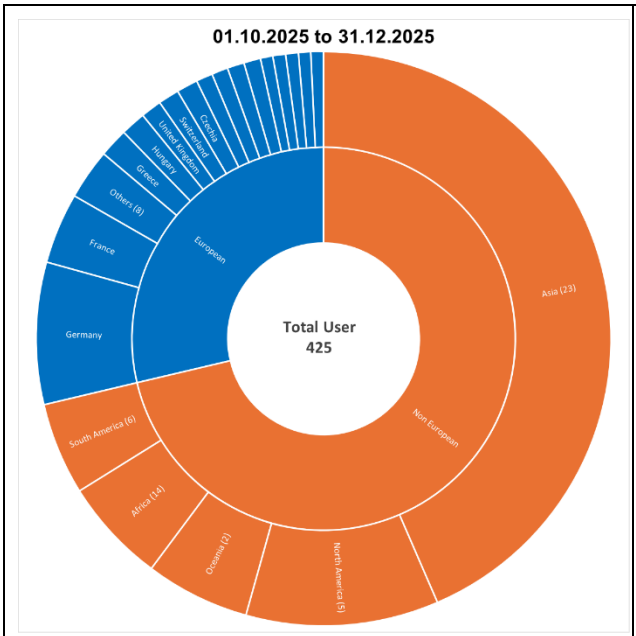

Reporting Period 01.10.2025 to 31.12.2025 with a total of 425 Users of 74 different countries.

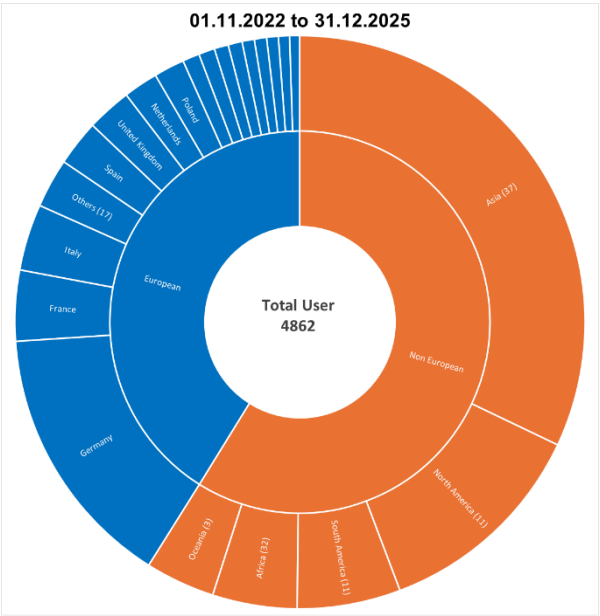

Since beginning of operational phase until 31.12.2025 (end of reporting period) with total of 4862 Users of 127 different countries.

Figure 5-1 Number of registered users (with at least one active user role) per country

User per Category		New within reporting period 01.10.2025 to 31.12.2025	Since beginning of routine phase start until 31.12.2025 (end of reporting period)
Registered users	Total*	573	7122
	with active role assignment**	425	4862
Cat-1 Science	Total	398	4779
	AO Process 00001**	398	3913
	AO Process 00002**	0	641
	AO Process 00003**	0	225
Cat-2 Commercial	Total	12	54
Cat-1 Distributor***	Total	308	3638

Table 5-2 Number of registered users and number of released user roles per category (Cat-1 Science, Cat-2 Commercial and Cat-1 Distributor)

* Registered users inhibited user accounts excluded

**Registered users with at least one active user role

***Catalogue User, ordering EnMAP data from archive

Notice that registered users belong to different categories, therefore the sum of Cat-1 Science and Cat-1 Distributors or other categories does not correspond to the total registered users.

5.2 Announcements-of-Opportunities

Announcement -of-Opportunity	New within reporting period 01.10.2025 to 31.12.2025		Since beginning of routine Phase until 31.12.2025 (end of reporting period)	
	Proposals	Total tiles granted	Proposals	Total tiles granted
A00001	67	4088	916	41324
A00002	0	0	126	10395
A00003	0	0	4	127
Total	67	4088	1046	51846

Table 5-3 Number of released science proposals per Announcement-of-Opportunity (AOs#) and total number of granted tiles per AO#.

Icon	Topic	New within reporting period 01.10.2025 to 31.12.2025		Since beginning of routine Phase until 31.12.2025 (end of reporting period)	
		Proposal	Total tiles granted	Proposal	Total tiles granted
	ATMOSPHERE	4	279	57	3568
	CAL/VAL	2	345	41	5675
	GEO/SOIL	24	713	346	10569
	HAZARD/RISK	2	370	25	1092
	METHODS	3	156	24	968
	SNOW/ICE	1	42	25	1589
	URBAN	2	98	17	691
	VEGETATION	22	1779	392	22370
	WATER	7	306	119	5324
	Total	**67**	**4088**	**1046**	**51846**

Table 5-4 Number of accepted science proposals and total number of granted tiles per topic

6 Archived and Delivered Observations

The following table shows the number of archived Earth Observation and Calibration products and their sizes within the specified time frames.

Acquisition Type	Archived	Reporting Period 01.10.2025 to 31.12.2025		Since beginning of Commissioning Phase until 31.12.2025 (end of reporting period)	
		Number Tiles / Observations	Size (in GB)	Number Tiles / Observations	Size (in GB)
Earth Observation (EO)	Total	19123 / 1754	9318.023	233882 / 21526	113963.21
	Average / Day	207.86 / 19.07	101.28	170.59 / 15.70	83.12
Calibration (CAL)	Total	22	91.87	488	2037.75
	Average / Day	0.24	1.00	0.36	1.49

Table 6-1 Number and size of archived and not archived products (more than one version of the same image can be archived)

The following table shows the number of delivered products and their sizes within the specified time frames. Product deliveries result either directly from acquisition orders (“Acquisition”) or catalog orders (“Archive”).

Acquisition Type	Order Type		Reporting Period 01.10.2025 to 31.12.2025		Since beginning of Commissioning Phase until 31.12.2025 (end of reporting period)	
			Number Tiles / Observations	Size (in GB)	Number Tiles / Observations	Size (in GB)
Earth Observation (EO)	Acquisition	Total	20236 / 1766	9136.77	200587 / 18488	88987.40
		Average / Day	219.96 / 19.2	99.31	146.31 / 13.4916	64.91
	Catalogue	Total	20586	7327.37	162648	60557.01
		Average / Day	223.76	79.65	118.63	44.17
Calibration (CAL)	Acquisition	Total	22	90.2	319	1352.14
		Average / Day	0.4	0.98	0.23014	0.99
	Catalogue	Total	0	0.0	77	394.94
		Average / Day	0.0	0.0	0.06	0.29

Table 6-2 Number and size of delivered products

6.1 Archived Acquisitions

The following figures show the heatmaps for the whole world and for Europe within the specified time frames. The heatmaps represent the frequencies of products at a geographic location, where the number of products increases from blue over red to yellow.

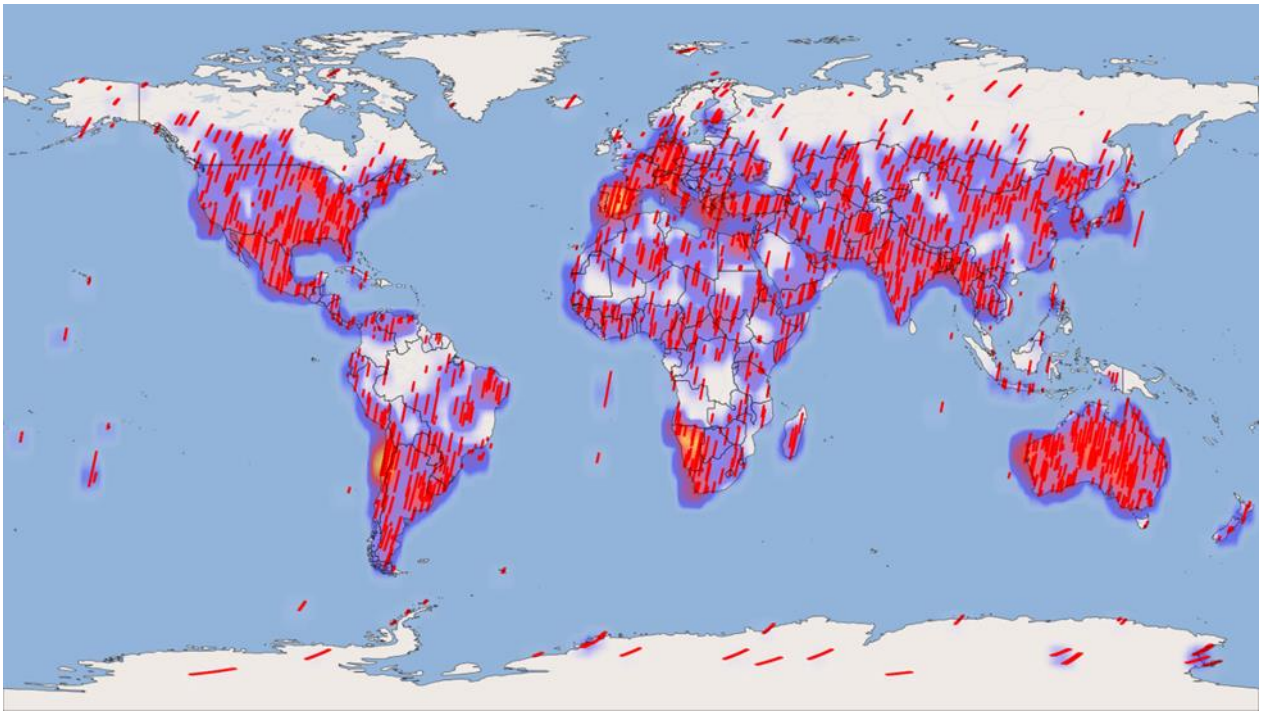

reporting period 01.10.2025 to 31.12.2025

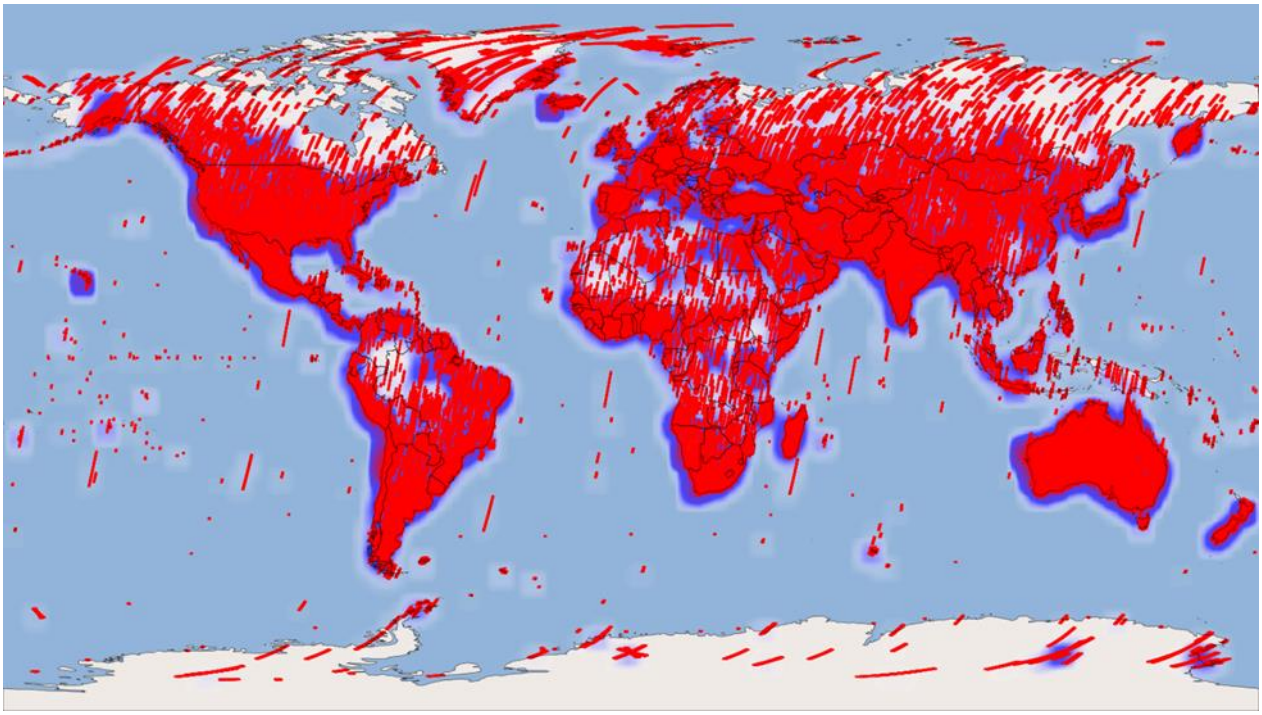

reporting period 2022-04-01 to 31.12.2025 includes commissioning phase acquisitions and different versions of the same tiles)

Figure 6-1 Geographic location of all Earth observation tiles archived, World

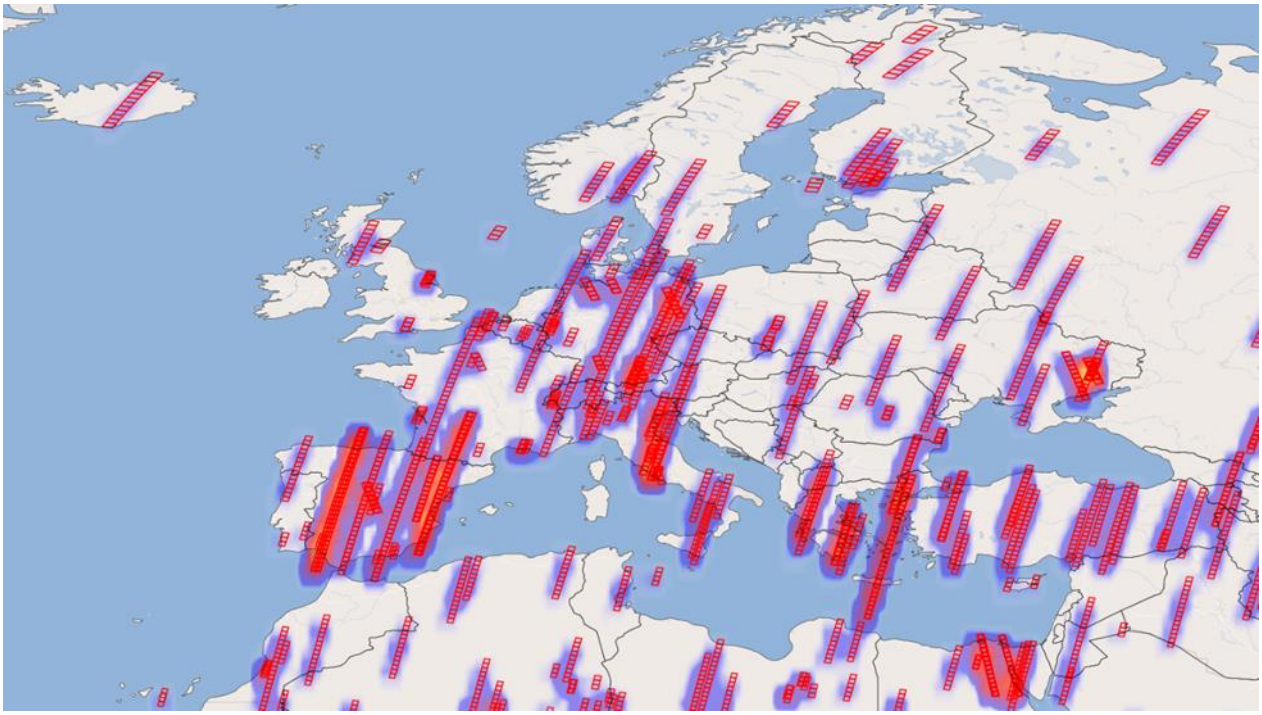

reporting period 01.10.2025 to 31.12.2025 Europe

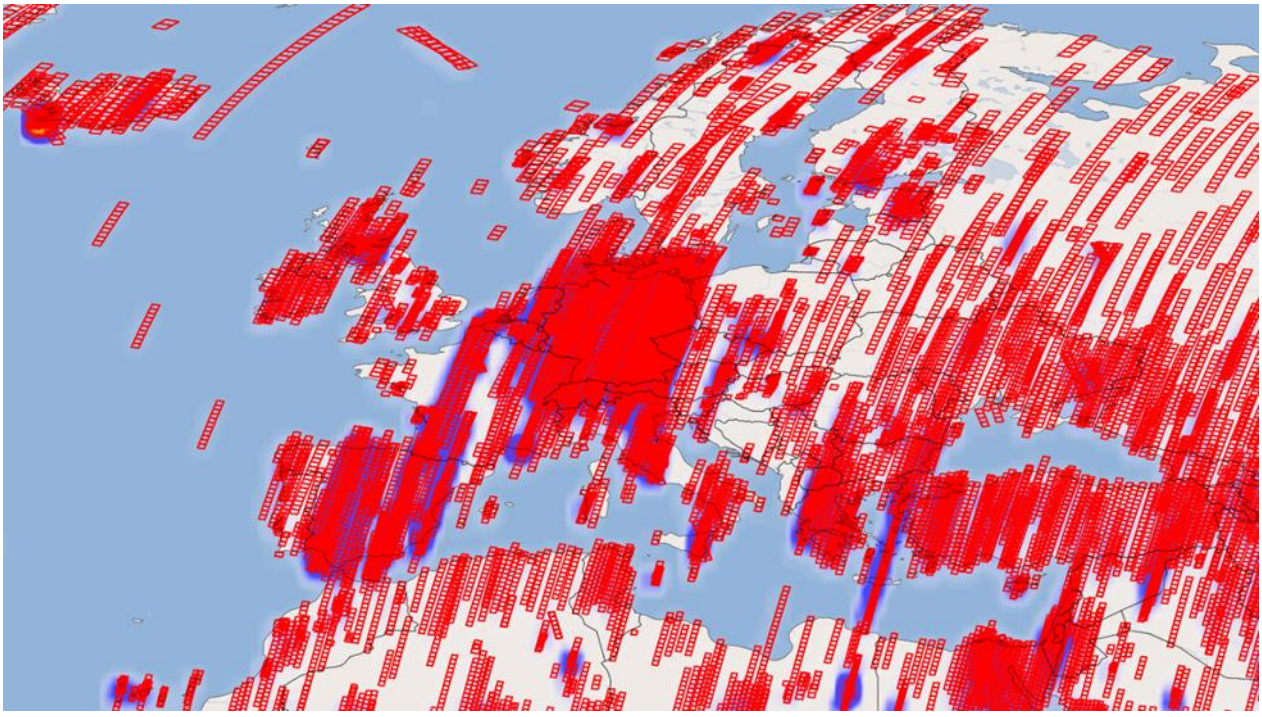

reporting period 2022-04-01 to 31.12.2025 Europe (includes commissioning phase acquisitions)

Figure 6-2 Geographic location of all Earth observation tiles archived, Europe

The following figures show the distribution of cloud coverage for the archived products.

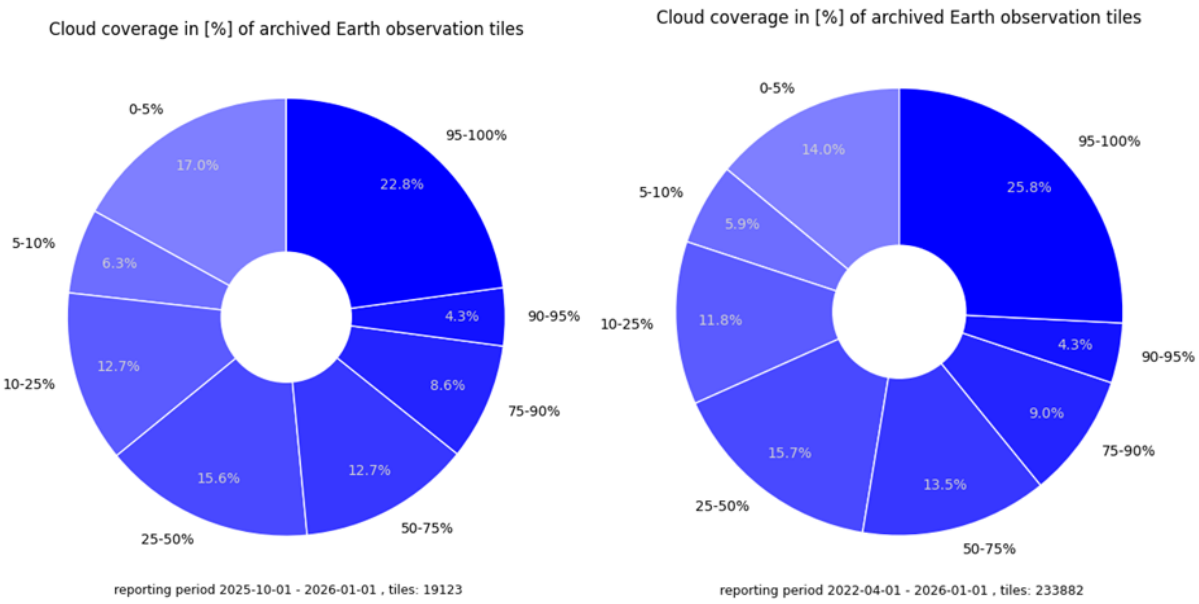

Figure 6-3 Cloud coverage in [%] of archived Earth observation tiles

The following figures show the distribution of observation angles for the archived products.

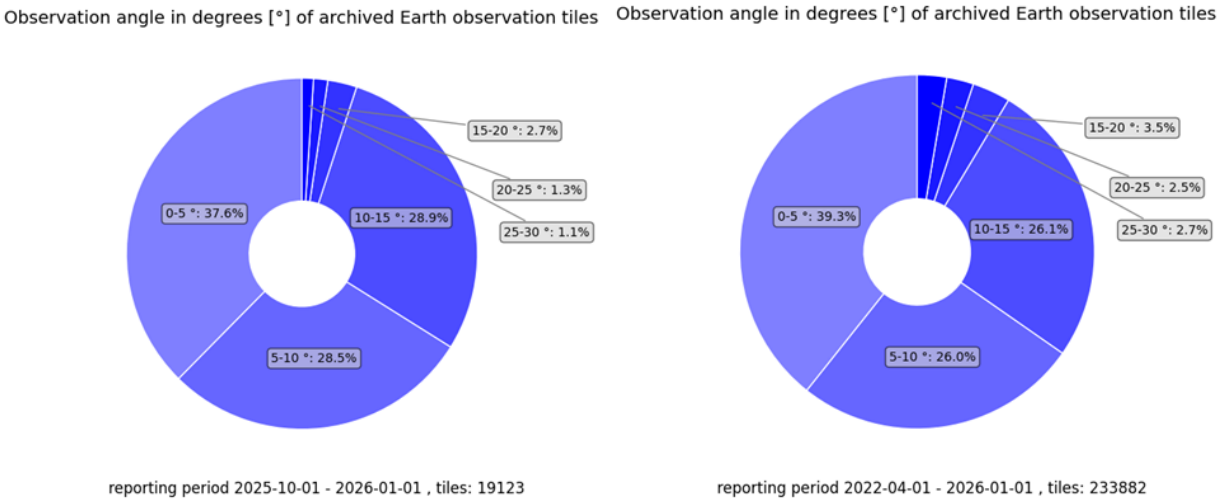

Figure 6-4 Observation angle of archived Earth observation tiles

6.2 Delivered Observations

The following figures show the distribution of processing level of the delivered products from acquisition orders.

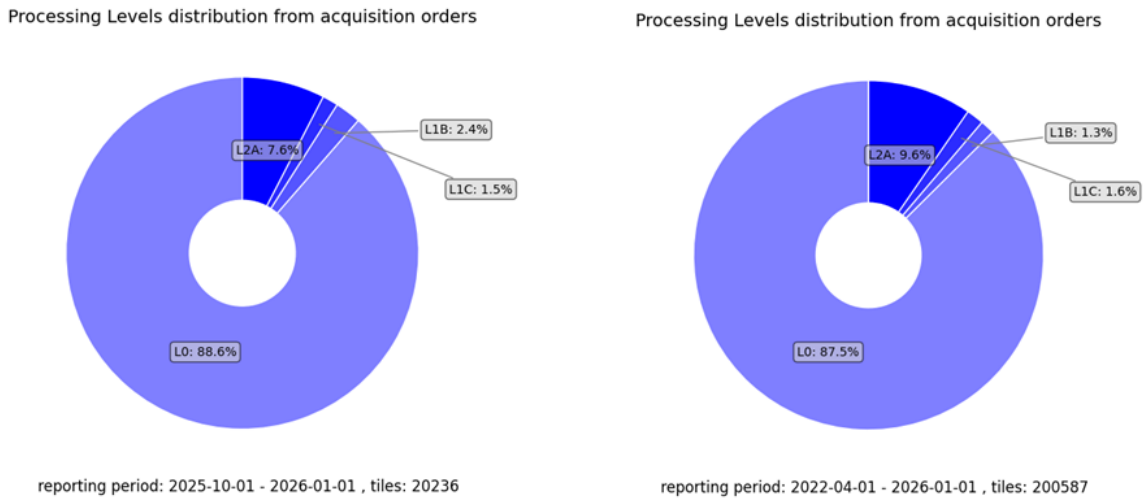

Figure 6-5 Levels of delivered Earth observation tiles from acquisition orders

The following figures show the distribution of processing level and correction type (for L2A) of the delivered products from catalog orders.

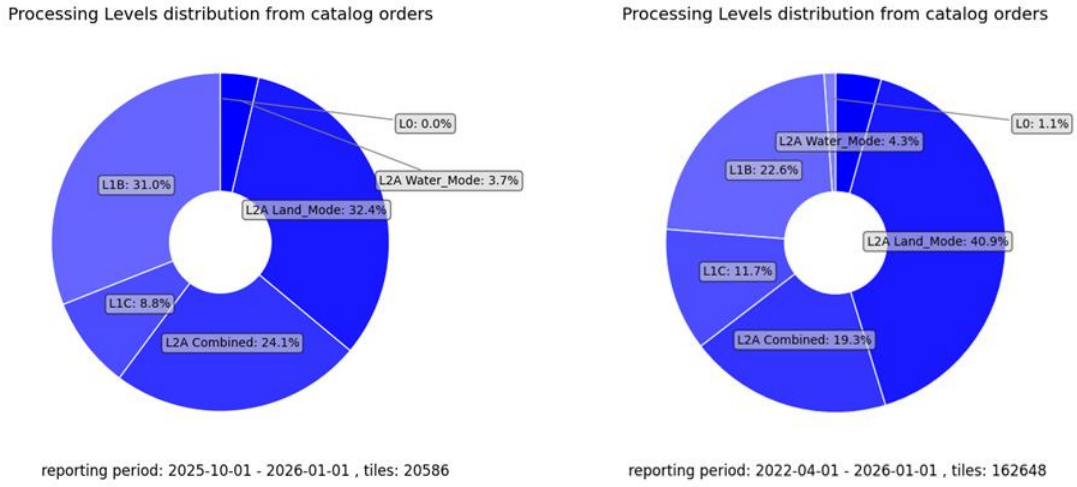

Figure 6-6 Levels of delivered Earth observation tiles from catalog orders

6.2.1 Delivered L2A products from the Download service (EOC Geoservice)

The Ground Segment also produces products already processed with standard parameters. CEOS certified L2A ARD products are available for direct download using the EOC Geoservice and the EOLab platforms. Since July 2025, the IPP account credentials also grant access to the EOC Geoservice to download EnMAP products.

EnMAP's Ground Segment processes all recorded data to L2A ARD format, saving computational and processing time. The default processing parameters of the L2A ARD are the following:

Product_Format = **GeoTIFF+Metadata**
Map Projection = **UTM_Zone_of_Scene_Center**
Image Resampling = **Bilinear_Interpolation**
Correction Type = **Land_Mode**
Cirrus Haze Removal = **No**
Band Interpolation = **No**
Terrain Correction = **Automatic**
Season = **Automatic**
Ozone column = **Automatic**

Table 6-3 Processing parameters used for the L2A ARD products in Geoservice / EOLab

In addition, take into account that:

- the versions of the L2A ARD products may differ depending on their generation time. The processor changelog (https://www.enmap.org/data/doc/EnMAP_processor_changelog.pdf) provides an overview of the software changes. During re-processing of the L2A ARD products, new versions of the products will replace older versions of the products. Currently a re-processing is in progress that shall bring all L2A products to at least version **V01.05.02**.

- No L2A-water products are available as L2A ARD products in Geoservice. For the moment water processing is only available using the on-demand processing options in EOWeb.

- The L2A ARD archive is now complete. All EnMAP products available in the Mission archive are also available as L2A ARD products at Geoservice / EOLab.

The total number of downloads* using the EOC Geoservice is **2370099** for this reporting period (01.10.2025 to 31.12.2025). Number of monthly downloads for this quarter are given in Table 6-4 and the graph with their evolution since the start of the service is shown in Figure 6-7.

Product	Month	# Downloads
ENMAP-L2A	2025-10	478872
ENMAP-L2A	2025-11	912512
ENMAP-L2A	2025-12	978715
Total in period		2370099

Table 6-4 Absolut amount of downloads in Geoservice.

*Downloads count the download of a file from the EOC Geoservice. A EnMAP L2A product consists of 13 different files

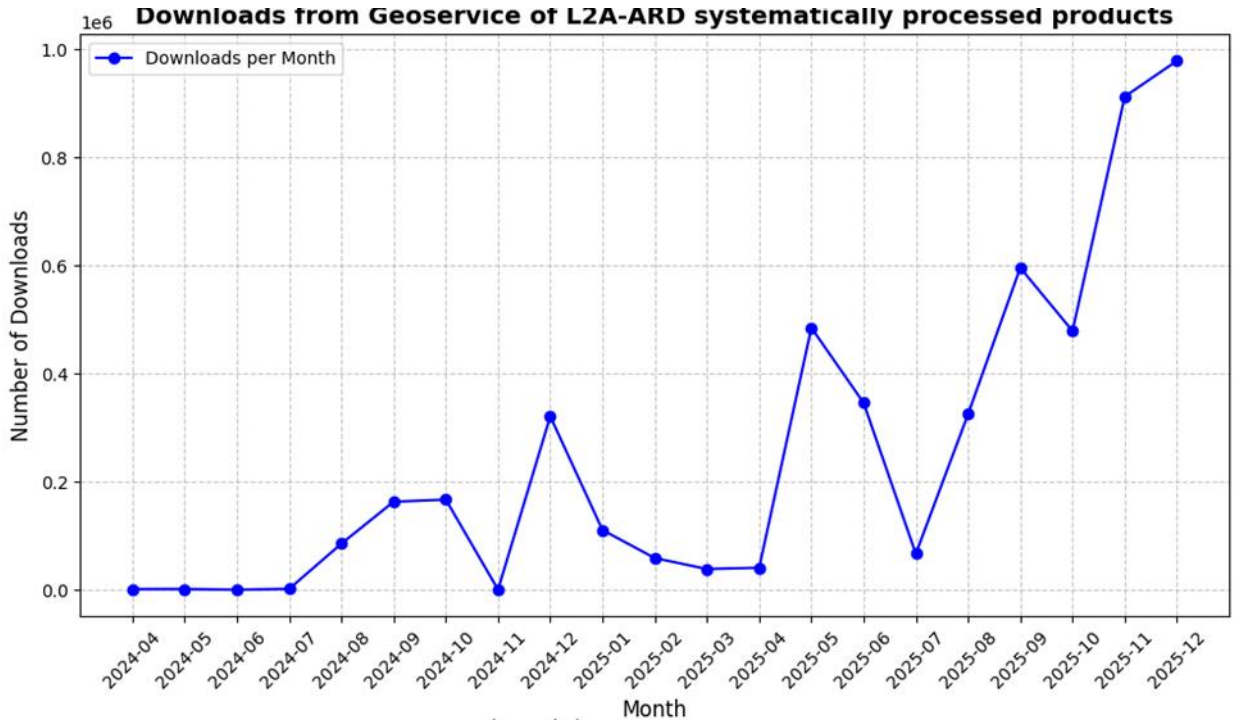

Figure 6-7 Downloads in Geoservice per month

7 Detailed Status

7.1 Satellite

During the reporting period the mission has experienced 2 HSI SAFE_ERROR events that have resulted in the loss of observation time. The events took place on 18.11.2025 and on 15.12.2025 but only resulted in some hours of outage since the operations could be resumed next day. No DSHA Safety Mode event took place during the reporting period. As reported in all the previous events of these types, no consequences on the image or data quality are observed as a result of these events. For more details on data quality see sections 7.6 and 8.

The sporadic cancellation of acquisitions when the satellite is coming from the eclipse phase (known as “3-minute events”), has been observed during the reporting period, as it was expected given the seasonal variability of this phenomenon. It is expected that these events will disappear towards the end of Q1 2026.

More details about different satellite aspects are reported in the following subsections.

7.1.1 Orbit

The reference orbit is a Sun-synchronous polar orbit with a mean local time of descending node of 11:00 hrs and a repeat cycle of 398 revolutions in 27 days at an altitude of 643 km.

The satellite orbit is controlled with respect to an Earth-fixed reference track over the entire orbit, analogous to a rim, with a control box of +/- 6 km in radial direction and +/- 22 km in normal direction.

During Q4 2025, a total of 1696 ACS Precise Modes were executed onBoard, compared to 1824 during the previous quarter. Due to the implementation of Back-to-Back Image Acquisitions, the number of ACS Precise Modes does not represent the number of performed activities. By executing two or three Images as one sequence, the total number of ACS Precise Modes decreases whereas the number of Image Acquisitions remains stable or increases. Over the whole mission, a total of 23054 ACS Precise Modes have been successfully executed.

During Q4 2025, two in-plane and two out-of-plane maneuvers were executed. No collision avoidance maneuvers were required. The resulting performance error off all maneuvers was estimated by FDS to range between +0.43% and +1.5%. No actuations of the Ball Latch Valve or other OCS configuration changes were performed during Q4 2025**.**

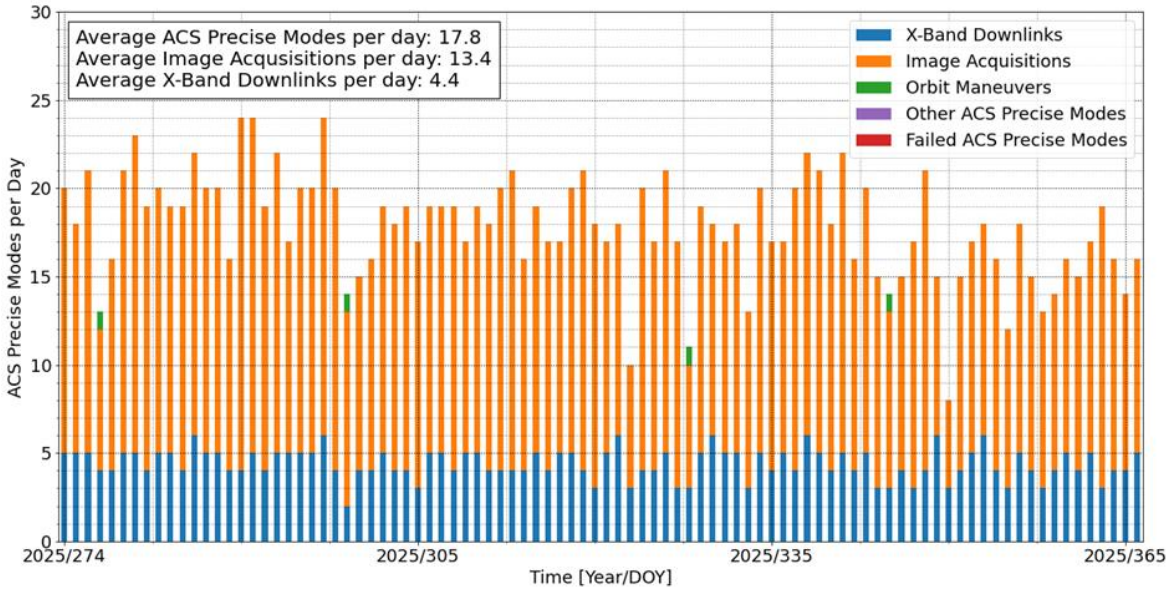

Figure 7-1 Number of ACS Precise Modes per day during Q4 2025

7.1.2 Life Limited Items

The life cycle of the life limited items is evaluated depending on their use. The life-limited items include the following optical and mechanical components:

Life-Limited Item	01.10.2025 to 31.12.2025	until 31.12.2025	Estimated minimum total lifetime / health of the system
Fuel(*)	+0.5 kg	9.3 kg	17.1 years
Battery and Solar Cells(**)	nominal	nominal	Nominal
Shutter Usage	+2.02%	25.11%	15.0 years (@ daily use)
FAD movements	+2.00%	32%	15.1 years (@ bimonthly use)
Diffuser exposure time based on sole measurement time(***)	+3.33%	53.33%	8.4 years (@ bimonthly use to reach 100% originally planned used)
Diffuser exposure time based on real cyclogram duration(***)	+4.00%	63.96%	6.8 years (@ bimonthly use to reach 100% originally planned used)
On-Board Calibration Equipment Usage	On-board calibration equipment:		
- OBCA SPC lamp 1	+1.20%	18.07%	19.4 years (@ biweekly use)
- OBCA RAD lamp 1/LED 1	+1.83%	37.05%	13.0 years (@ biweekly use)
- FPA LEDs 1	+0.56%	8.43%	44.5 years (@ monthly use)

Table 7-1 Status of life-limited items

(*) During periods with higher temperature and pressure fluctuations due to e.g., an Instrument shutdown and startup, the calculation of the propellant mass via the Pressure-Volume-Temperature method contains a relatively large margin of errors.

(**) The Power Subsystem is working nominally and as expected. Voltage stays above any critical level.

(***) A 100% Sun diffuser exposure time corresponds to a total planned exposure of 2 hours after 5 years when performing monthly Solar calibrations. The contribution of the diffuser to the total radiometric uncertainty after reaching the reference 100% value is estimated to be **0.6%** according to the instrument manufacturer. This value is significantly below the 5% total radiometric uncertainty requirement, which indicates that the diffuser will not be a relevant contributor to the total radiometric uncertainty of the instrument even if the diffuser were to be used significantly above the originally allocated 2 hours of exposure time (reference 100% value). Nevertheless, the use of the diffuser is continuously monitored and accounted for in the Life-Limited Item list and thanks to the instrument stability the Sun calibration frequency is adjusted to reduce the number of necessary Solar calibrations.

The consumed resources (except fuel) are calculated based on the processed L0 product metadata, i.e. only successfully processed calibrations can be considered.

7.1.3 Redundancies

To date, the SWIR wavelength range is covered by SWIR-A (SWIR-B can be activated using a one-time switch mechanism).

All satellite subsystems are using nominal configurations.

7.2 Ground Stations

7.2.1 S-Band

S-Band Ground Stations	01.10.2025 to 31.12.2025		
	Total Passes	Non-Routine Passes (e.g. Anomaly Handling/SW Updates)	Failed Passes
All stations (Weilheim-Germany, Neustrelitz-Germany, Inuvik-Canada, O'Higgins-Antarctica, Svalbard-Norway)	558 (171 WHM, 234 NSG, 153 INU)	0	4

Table 7-2 S-Band Ground Station Passes

7.2.2 X-Band

X-Band Ground Stations	01.10.2025 to 31.12.2025	
	Executed Passes	Successful Passes
All stations (Neustrelitz-Germany, Inuvik-Canada)	404 (286 NZ, 118 INU)	404 (286 NZ, 118 INU)

Table 7-3 X-Band Ground Station Passes

Inuvik (Canada) station was integrated in Q4 2023 into the regular operations of the EnMAP Ground Segment for X-Band and S-Band downlinks. After integration, more data and more flexibility in S-band and X-band data reception is achieved, especially concerning image acquisitions over Europe.

7.3 User Interfaces

Further improvements to the user interfaces are continuously on-going and will be reported in this section.

During the reporting period the Ground Segment of EnMAP continues to update the information on future high priority observations of the EnMAP mission (*Foreground Mission*). The tool displaying this information is available at the EnMAP web site (under https://www.enmap.org/data_tools/foreground_mission/).

With this tool the users can get informed weeks in advance about future priority observations with EnMAP. Initially, a set of long flight-lines (990km) over Germany and other European countries have been identified together with the user community and will be regularly scheduled. Since July 2024, the Foreground mission has expanded to include additional European regions. The foreground mission continued in Q4 2025 to focus on Europe. It entered the so-called *winter mode* since November 2025, when it shifts to southern Europe and the southern hemisphere during winter time. At the end of Q1 2026 and with the return to the normal mode, an update of the foreground mission flightlines for 2026 will be introduced.

7.4 Processors

Reference [3] provides the product specification and [4], [5], [6], [7] the algorithm theoretical basis for Level 1B, Level 1C and Level 2A (land / water).

In the reporting period (01.10.2025 to 31.12.2025) there has been one update in the EnMAP processing chain. A new version of the EnMAP processing software, **V01.05.05**, was available to the users since **05.11.2025**.

The following changes are part of the **V01.05.05** release:

- L2A atmospheric correction over water update (water quality rating and height dependency)
- L2A improvements in regions around cirrus (fix for aura effects)
- Fixed WV, VIS and SZA criterion for overall atmospheric quality

- Fixed adjacency correction around saturated pixels in L2A products
- Treat visibility of neighboring tiles consistently in WV regions in L2A products
- Adapted path radiance rescaling, including an adjacency correction, in L2A products

The changelog document was updated during Q4 2025 to include the list of changes. The document contains the history of EnMAP processor updates and shows the updates performed in the processing software. The document can be downloaded from the EnMAP website:

https://www.enmap.org/data/doc/EnMAP_processor_changelog.pdf

The following changes are expected to be performed in the future quarters:

- New processor version **V01.05.06** (available to users at the time of writing this report):
  - Fixed creation of black L2A products under certain (rare) conditions
  - Switched the entries for scene azimuth and zenith angles for the lower corners in the metadata files for Lx products (they are now all in clock-wise order)
- Update of the linearity calibration to improve the matching between VNIR and SWIR spectrometers, specially at low radiance level.

7.5 Calibrations

Table 7-4 summarizes the radiometric calibration observations acquired in this quarter and which will be described in the rest of this section. The calibration acquisitions were generally acquired according to the routine operations plan.

Category	01.10.2025 to 31.12.2025	
	Number of Archived Observations	Size (in GB)
Total	22	91.5
Deep Space	4	5.2
Rel. Radiometric	7	27.3
Abs. Radiometric	2	2.6
Linearity	3	51
Spectral Calibration	6	5.4

Table 7-4 Number and size of archived radiometric and spectral calibration observations

The continuous degradation of the VNIR sensor was monitored and quantified. The rate of degradation is constantly decreasing as illustrated in Figure 7-2 and by the end of March 2023 it has reached the point where it is practically negligible and has been kept that way during the reporting period. It shall be noted, though, that this average trend is different at different parts of the detector as illustrated for individual pixels in Figure 7-3. The effect on the radiometric calibration coefficients of a few selected bands is shown in Figure 7-4.

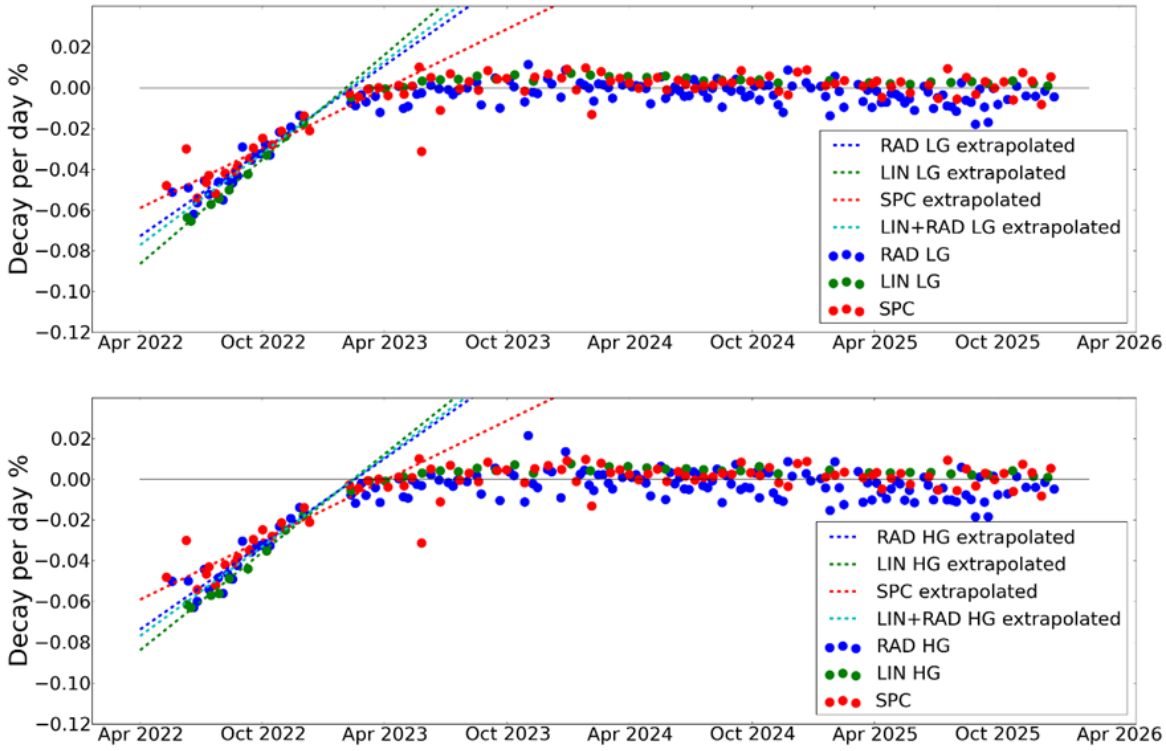

Figure 7-2 Decay per day from Lamp (RAD), Linearity (LIN) and Spectral (SPC) measurements for low gain (top) and high gain (bottom)

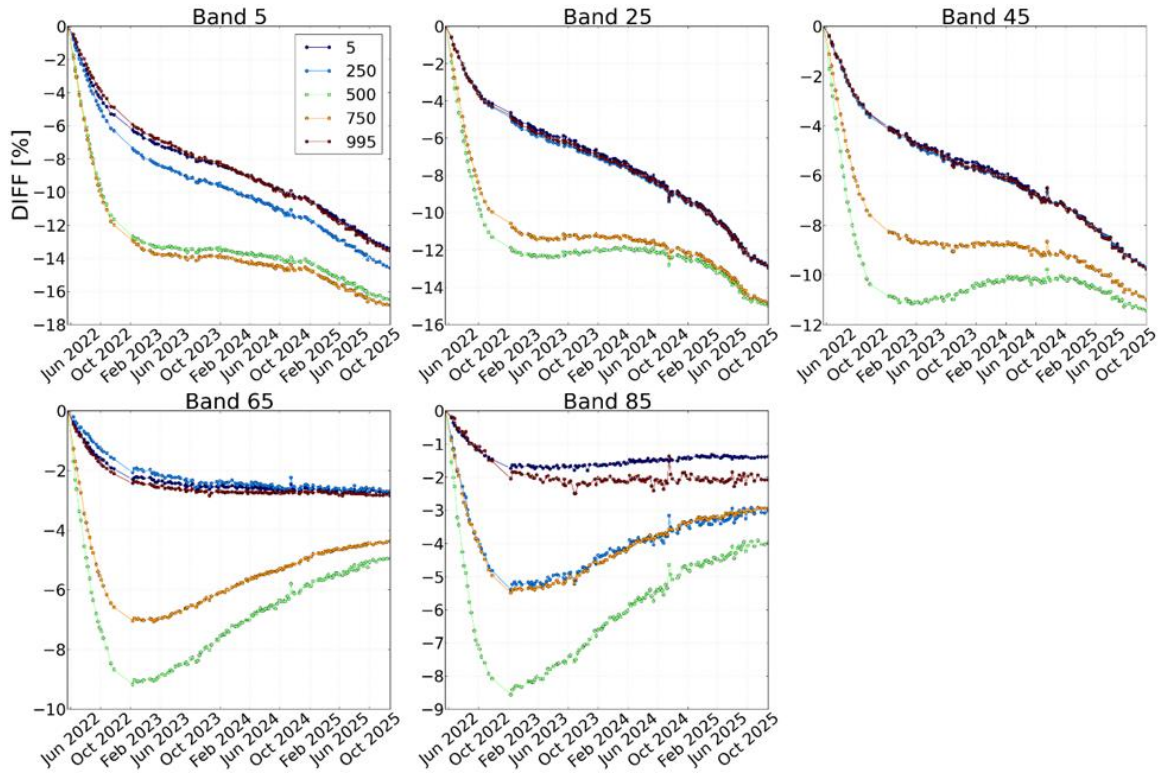

Figure 7-3 Change in percentage for individual pixels based on OBCA-Lamp measurements given for 5 bands and 5 cross track elements (coloured lines).

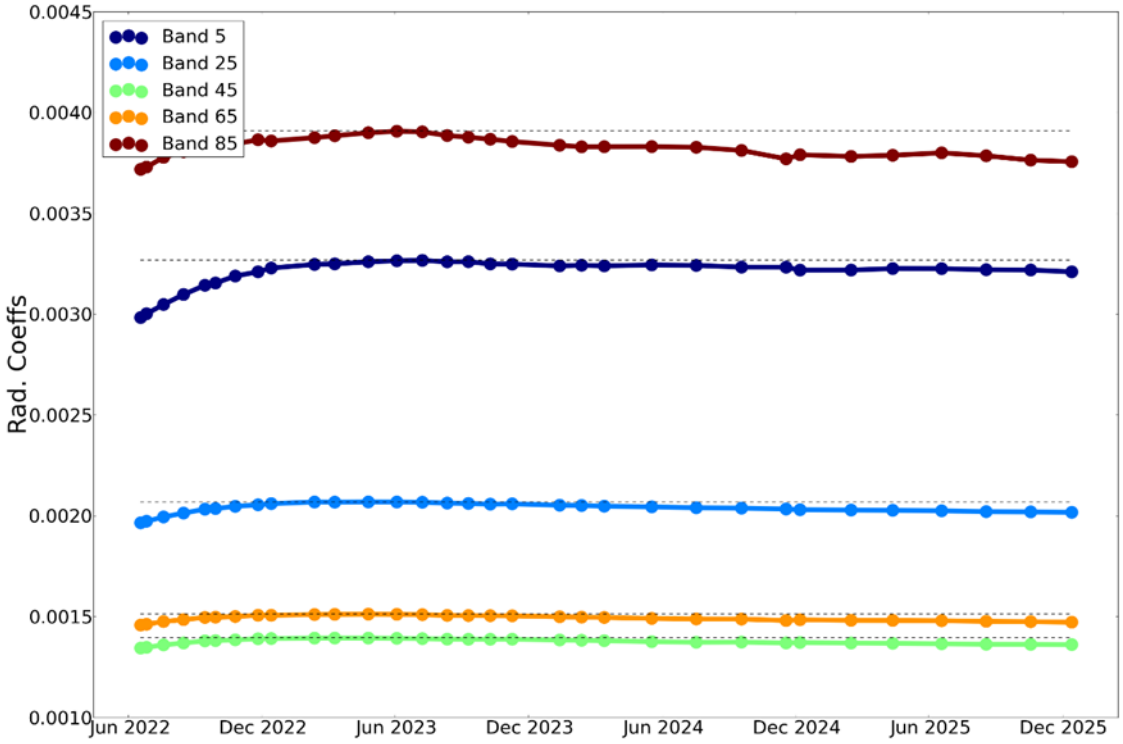

Figure 7-4 Average percentage change in the VNIR radiometric coefficients for five selected bands since launch

7.5.1 Dead Pixels

The following table shows the number and percentage of dead pixels. Figure 7-5 and Figure 7-6 show the position of the dead pixels in the focal plane of VNIR and SWIR sensors respectively. There have been no updates since 31.08.2022.

Defect Pixels	01.10.2025 to 31.12.2025	
	Number of Pixels	Percent
Total	1921	0.8
VNIR	137	0.2
SWIR	1784	1.2

Table 7-5 Number and percent of dead pixels

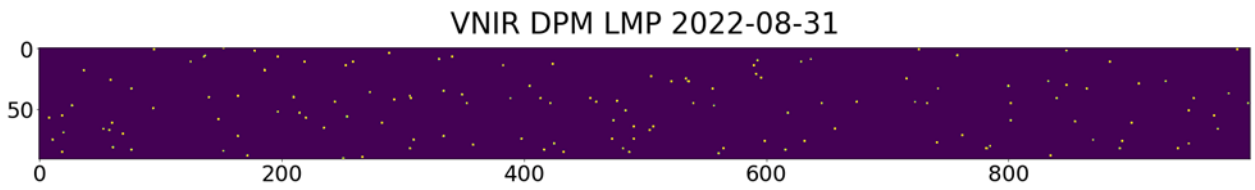

Figure 7-5 VNIR Dead Pixel Mask

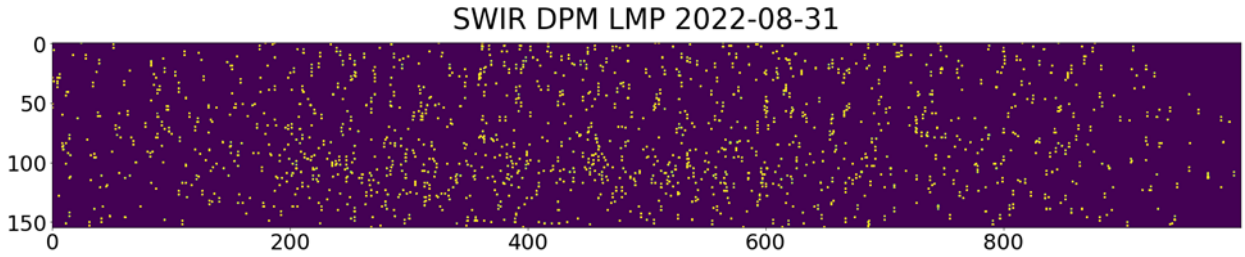

Figure 7-6 SWIR Dead Pixel Mask

There are no clusters of more than three spectrally or spatially adjacent dead pixels.

7.5.2 Spectral Calibration

Remark: In the following figures, OBCA is abbreviation for On-Board Calibration Assembly for spectral and radiometric calibrations.

Category	01.10.2025 to 31.12.2025	
	Number of Archived Observations	Size (in GB)
Total	6	5.4
Spectral Calibration	6	5.4

Table 7-6 Number and size of archived spectral calibration observations

The spectral properties – in particular center wavelength (CW) (see Figure 7-7 and Figure 7-8) and full width at half maximum (FWHM) (see Figure 7-10) for each band (spectral coordinate) and pixel (spatial coordinate) – have been characterized, considering all bands and pixels provided in Level 1B, Level 1C and Level 2A products.

The major conclusions of the monitoring of the spectral performance are summarized as follows:

- During the reporting period, 7 spectral calibration measurements were made which took place on: 10.10.2025, 24.10.2025, 07.11.2025, 21.11.2025, 05.12.2025 and 19.12.2025.
- The VNIR spectral range in this reporting period was found to be 418.4 – 993.3 nm over 91 bands (Figure 7-7). The average spectral sampling distance was 6.4 nm with a total range of 4.7 – 8.2 nm. This meets the requirement for overall wavelength coverage [HSI-POSS-0210], average spectral sampling distance [HSI-POSS-0310] and spectral sampling distance range [HSI-POSS-0320].
- The SWIR spectral range in this reporting period was found to be 902.2 – 2445.5 nm over 155 bands (Figure 7-7). The average spectral sampling distance was 10.0 nm with a total range of 7.5 – 12.0 nm. This meets the requirement for overall wavelength coverage [HSI-POSS-0210], average spectral sampling distance [HSI-POSS-0310] and spectral sampling distance range [HSI-POSS-0320].
- The spectral calibration measurements from this quarter show good temporal stability – measurements showed an absolute <0.15 nm change from the VNIR sensor and <0.35 nm change in SWIR (Figure 7-8) with respect to current spectral calibration table. All changes were below 0.5 nm between measurements for VNIR and below 0.5 nm SWIR. Long-term VNIR and SWIR spectral shifts are reported in Figure 7-9. This meets the requirement for consecutive spectral stability [HSI-POSS-0510] and overall spectral stability [HSI-POSS-0520].
- FWHM for VNIR and SWIR (Figure 7-10) are shown below but are not recalculated inflight.
- A VNIR degradation pattern is not clearly visible between consecutive spectral reference measurements acquired in this period, but there are positive and negative changes across the detector and on average the signal appears to have increased by 0.07% across all pixels from 26.09.2025 to 19.12.2025. A comparable change was reported in the previous quarter (0.05%). Although now very small, the monitoring of this behavior will continue in the next reporting period.

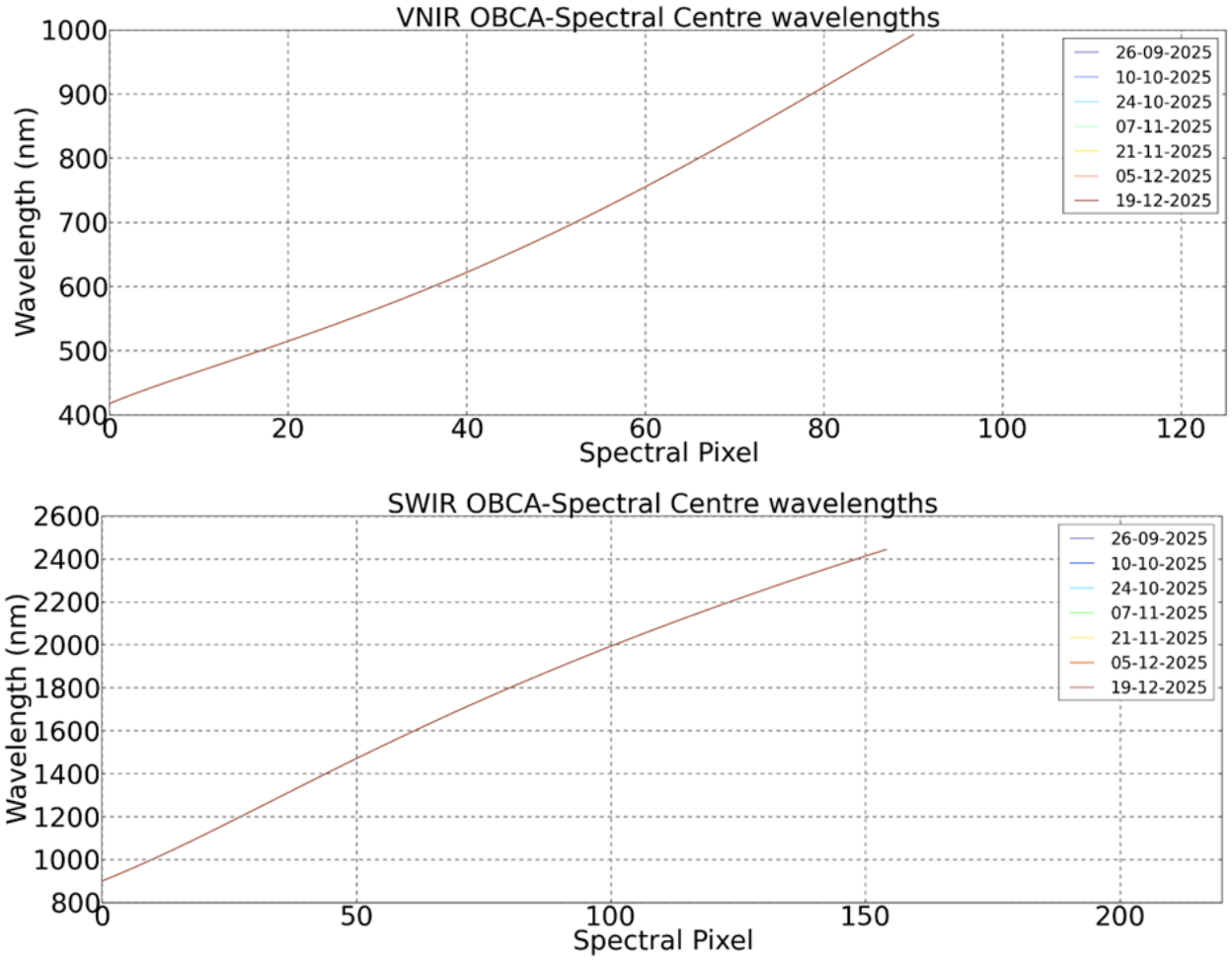

Figure 7-7 VNIR (top) and SWIR (bottom) center wavelength in nm

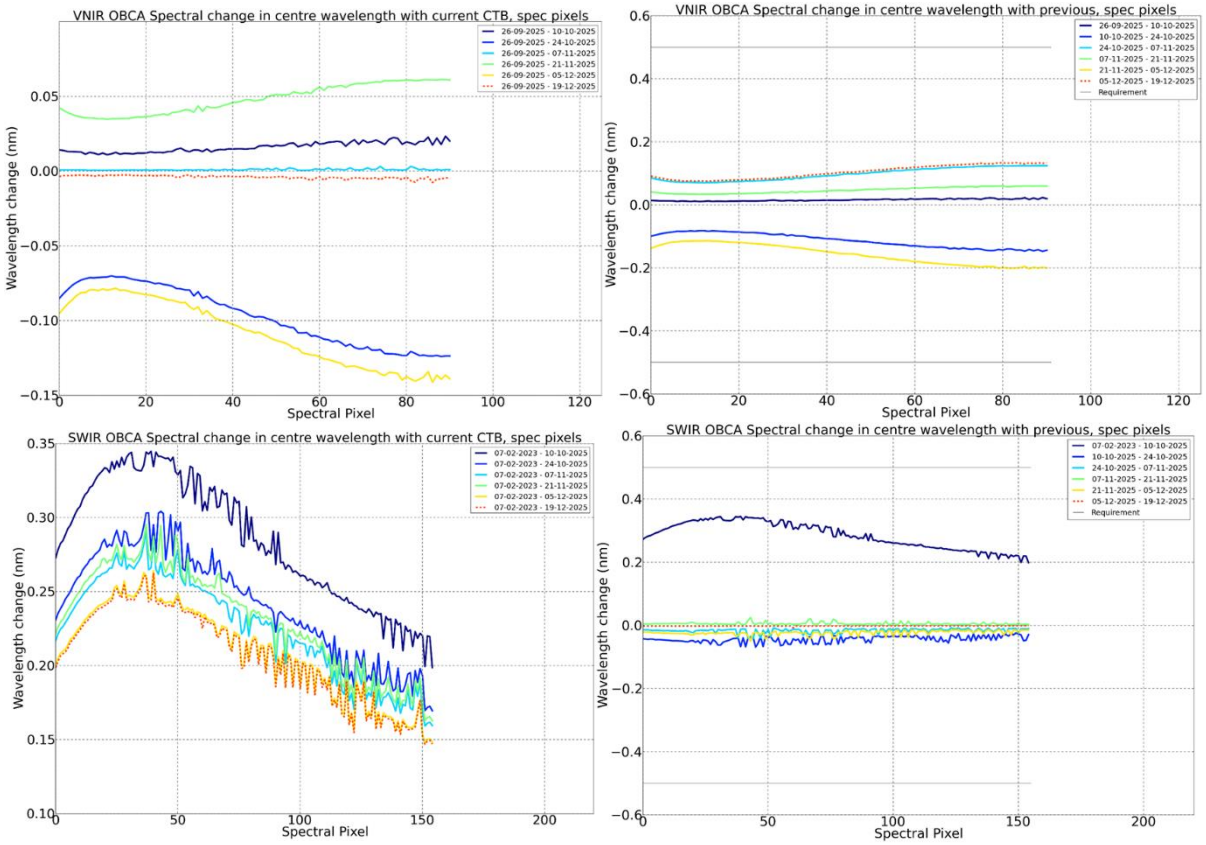

Figure 7-8 Change in center wavelength per spectral pixel for VNIR (top) and SWIR (bottom). Left panels show the changes with respect to current spectral calibration table in use and right panels with respect to the previous measurements.

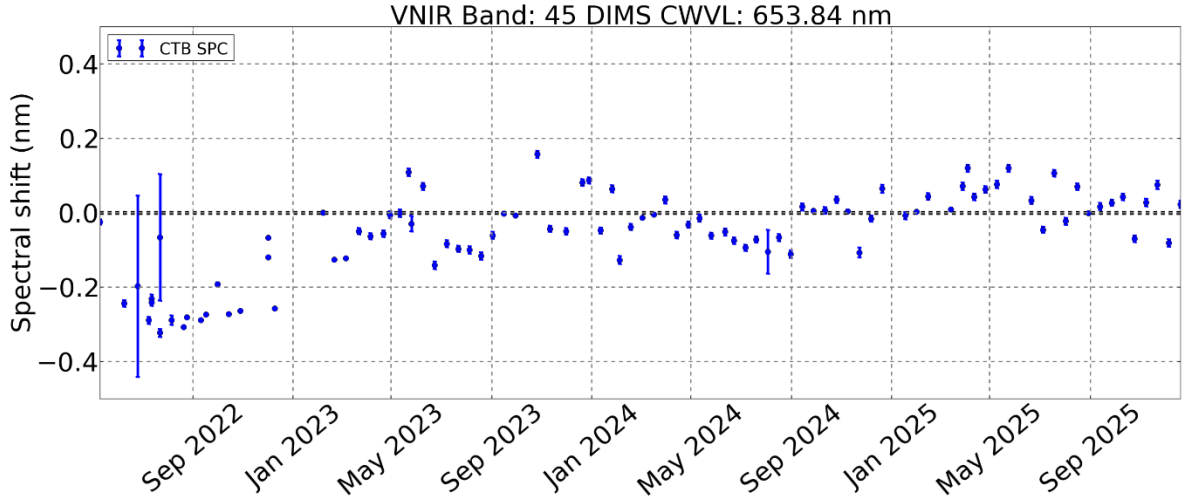

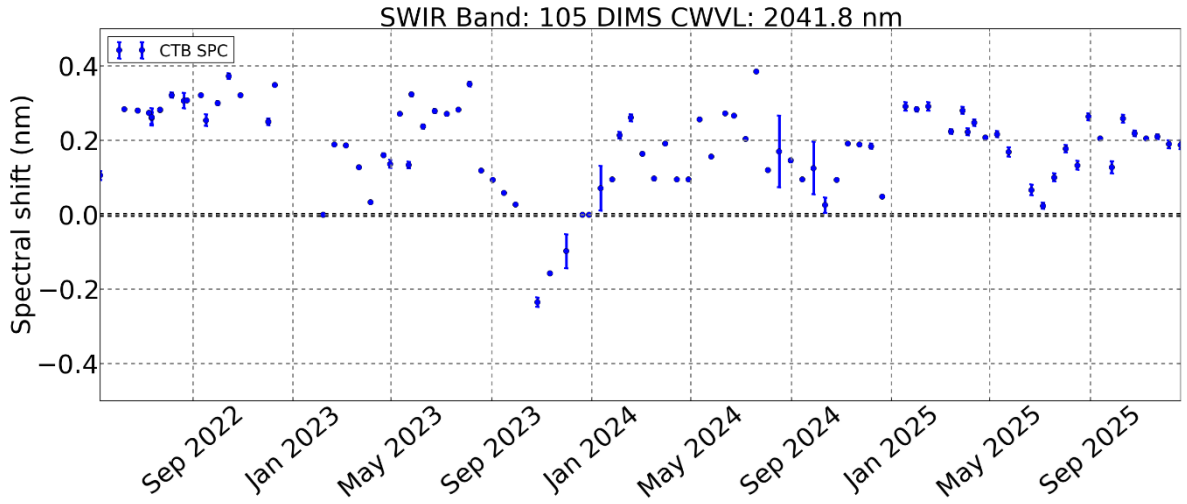

Figure 7-9 Long-term VNIR (top) and SWIR (bottom) spectral shifts since the beginning of the mission for VNIR band 45 at 654 nm and SWIR band 105 at 2042 nm.

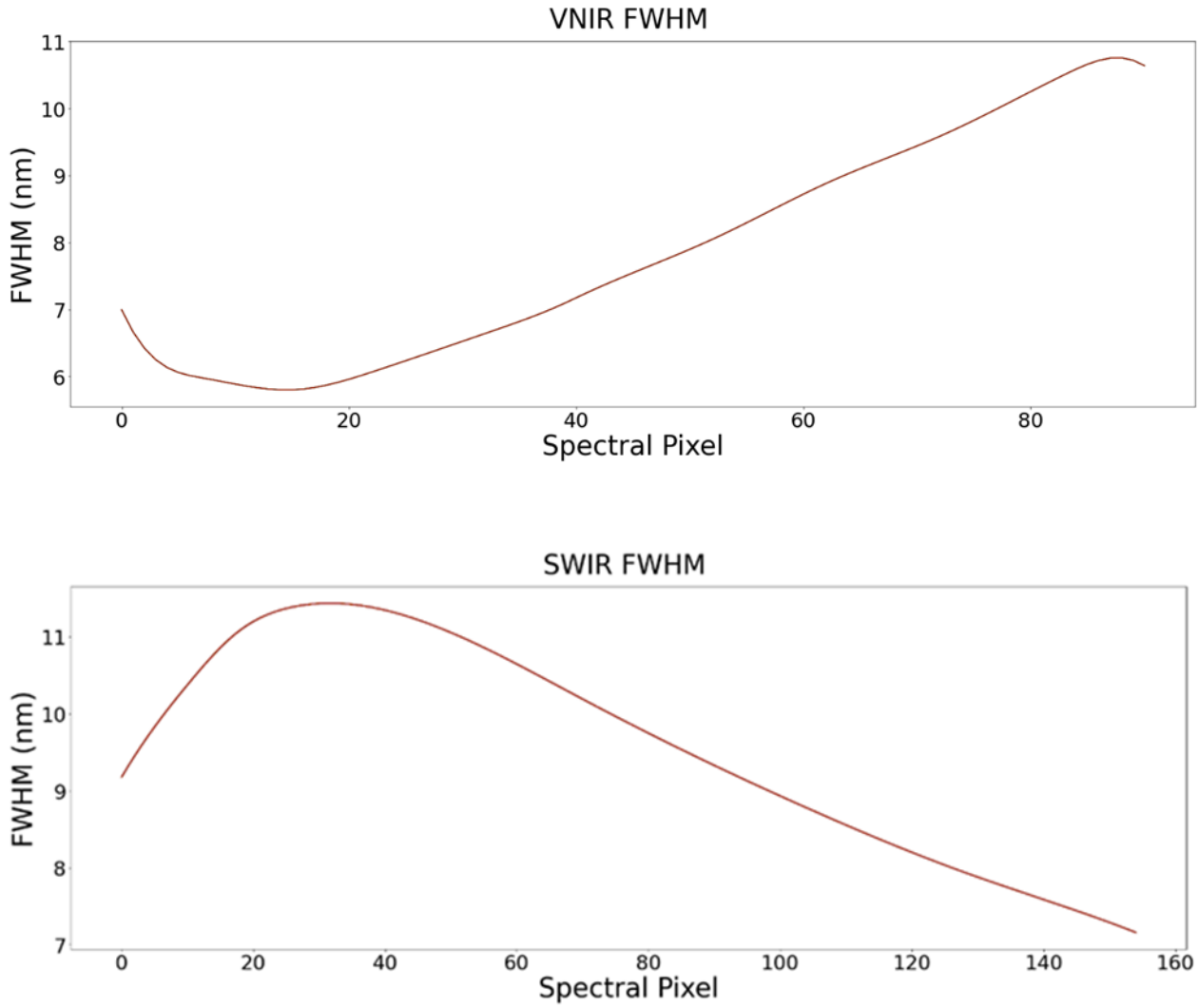

Figure 7-10 VNIR (top) and SWIR (bottom) FWHM in nm

CW and FWHM are available in the spectral calibration tables (see Table 7-7) and System Response Functions (SRF) per band are modelled by a Gaussian shape using those parameters.

Spectral calibration updates

No new calibration products were generated and delivered during the reporting period.

Product	Type	Date of Generation	Date of Validity Start	Date of Validity End	Delivered to
none					

Table 7-7 Generated spectral calibration tables

7.5.3 Radiometric Calibration

Category	01.10.2025 to 31.12.2025	
	Number of Archived Observations	Size (in GB)
Total	16	86.1
Deep Space	4	5.2
Rel. Radiometric	7	27.3
Abs. Radiometric	2	2.6
Linearity	3	51

Table 7-8 Number and size of archived radiometric calibration observations

The radiometric properties – characterized in particular by the calibration coefficient for each band (spectral coordinate) and pixel (spatial coordinate) and radiance – during this reporting period are investigated, considering all bands and pixels and radiances provided in Level 1B, Level 1C and Level 2A products.

Radiometric calibration coefficients (see Figure 7-11, Figure 7-12 and Table 7-10) and VNIR RNU (response non-uniformity, see Figure 7-14) were affected by the degradation of the VNIR sensor during commissioning but have stabilized from Q1 2023. In-flight, the gain matching coefficients (see Figure 7-13), the SWIR calibration coefficients, and the SWIR RNU (response non-uniformity, see Figure 7-14) have been stable.

During the reporting period, two Absolute Radiometric Calibration measurement were obtained. They took place on: 18.10.2025 and 13.12.2025.

Albeit now relatively small in magnitude, changes in the VNIR sensor have led to the creation of new calibration and reference tables for the new absolute radiometric measurement.

Although the VNIR degradation has almost stopped, the overall effects are visible in the reference measurements of the sun. However geometric conditions (sun-earth distance, pointing angle) also play a role in the absolute magnitude so the degradation cannot be quantified with these reference measurements.

The major conclusions of the monitoring of the absolute performance are summarized as follows:

- Changes in the VNIR sensor have affected the absolute Radiometric calibration coefficients: the increasing signal in the VNIR sensor, although not homogeneous, has resulted in decreasing radiometric coefficients. In this reporting period, the calibration coefficients decreased by about -0.24% to offset the increase in absolute (Figure 7-11 and Figure 7-12). Regarding RNU, the degradation features are still visible in the focal plane (Figure 7-14). Lastly, the Gain Matching correction has been relatively stable during this reporting period (Figure 7-13).

- The SWIR sensor has shown good stability during this reporting period, with no significant changes in the gain matching, RNU or radiometric calibration coefficients (Figure 7-11 and Figure 7-12).

- Regarding the total change in calibration corrections as a result of the VNIR degradation, almost all pixels experienced a change of less than 2.5% between consecutive measurements as set in

requirement [HSI-POSR-0410]. The only pixels which exceeded this value were already marked as dead during inflight assessment. No SWIR pixels experienced a change of more than 2.5% between consecutive absolute calibration measurements.

- New VNIR and SWIR calibration and reference tables were created for the absolute radiometric measurements from 18.10.2025 and 13.12.2025, mainly due to the changes in the VNIR sensor. The VNIR radiometric calibration coefficients have decreased in this reporting period to offset the increasing VNIR signal. The changes are small, and within requirements, so the dynamic coefficients are not calculated and calibration coefficients are taken directly from the most recent calibration table as envisioned at the beginning of the mission.

- Since April 2024, Absolute Radiometric Calibration measurements are planned at intervals of two months, following the stable performance of both sensors, and to allow for the extension of the lifetime of the solar diffuser.

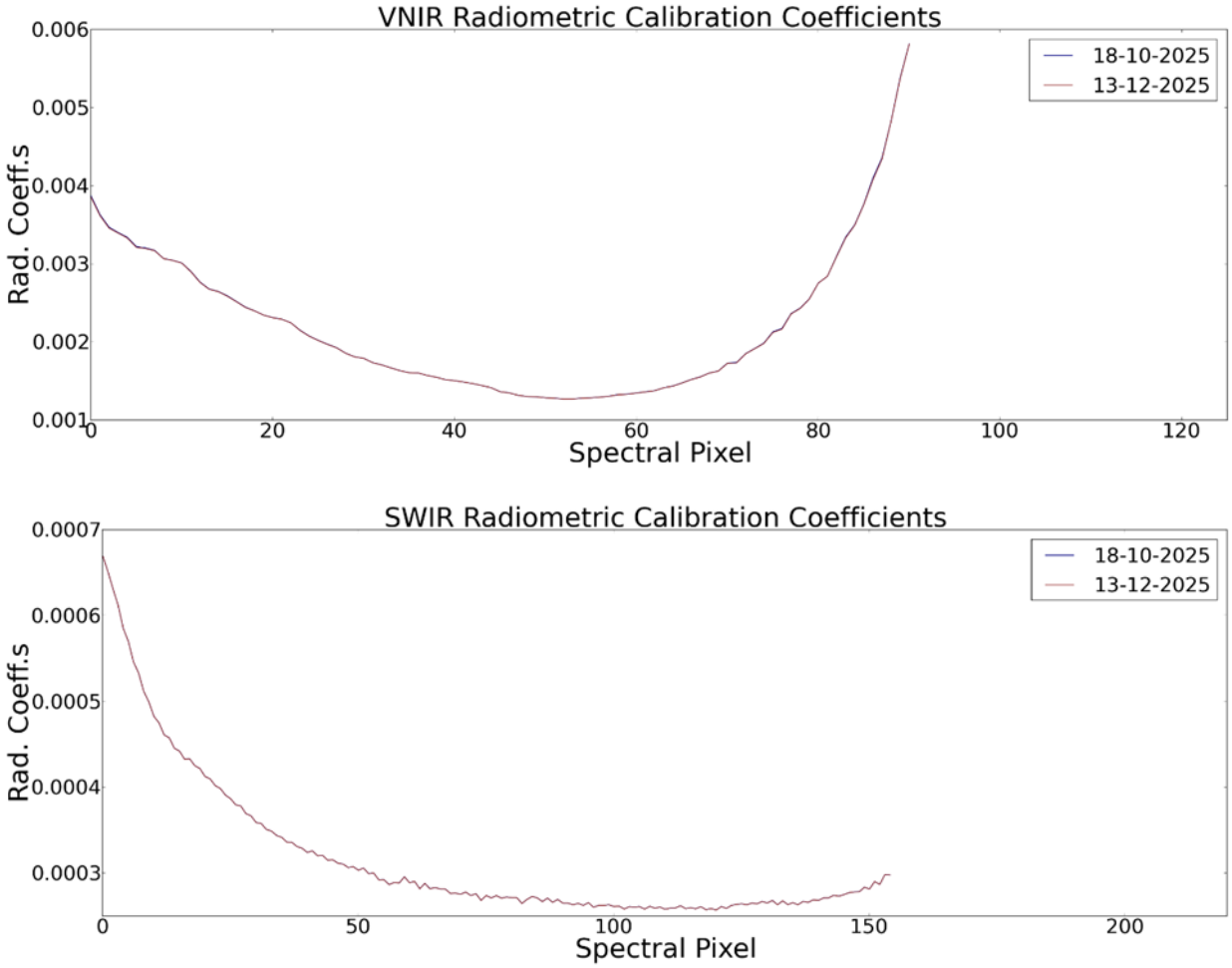

Figure 7-11 VNIR (top) and SWIR (bottom) calibration coefficient in mW/cm²/sr/µm

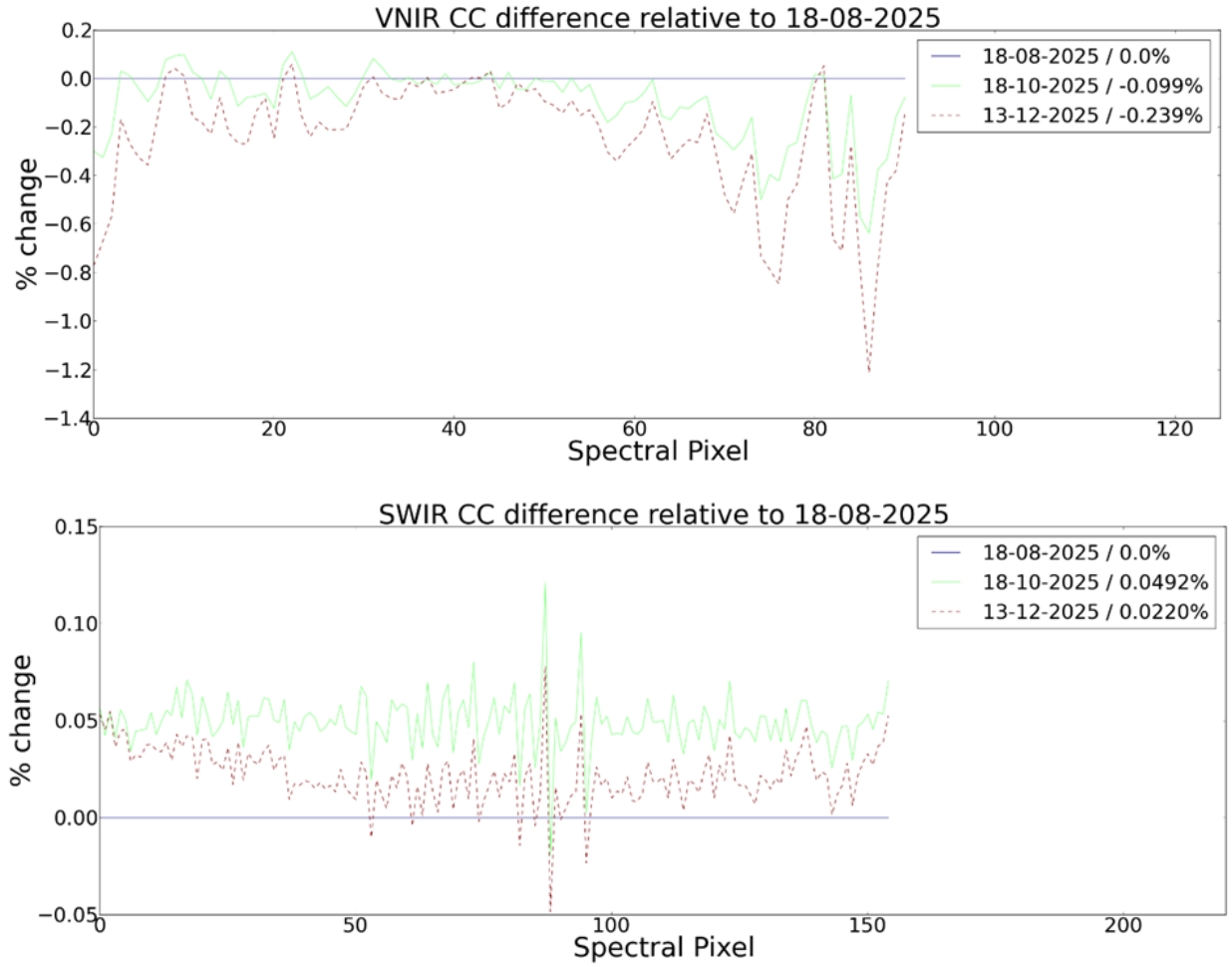

Figure 7-12 Percentage change in VNIR Calibration Coefficients (top) and SWIR Calibration Coefficients (bottom)

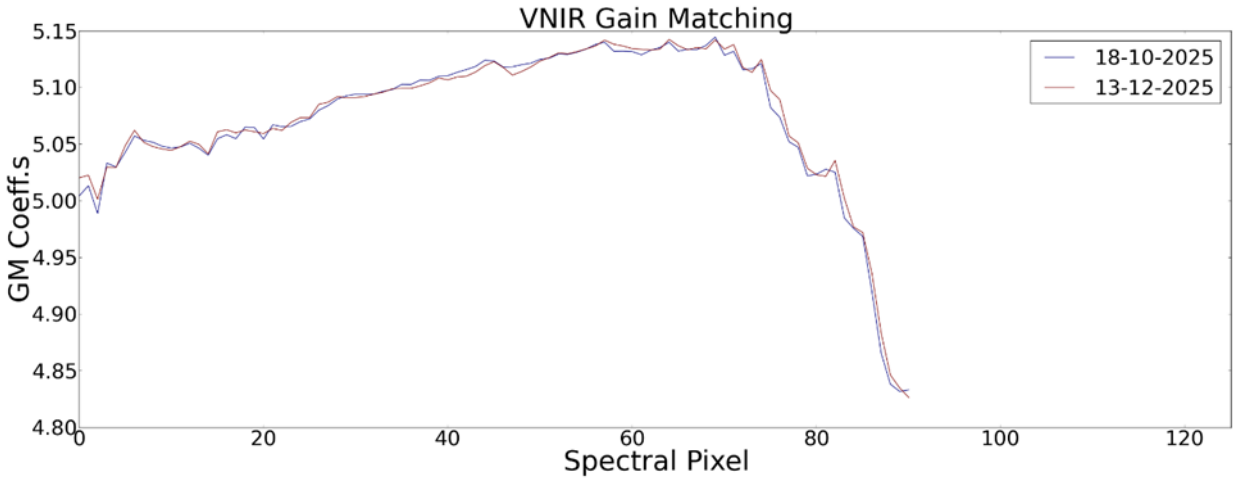

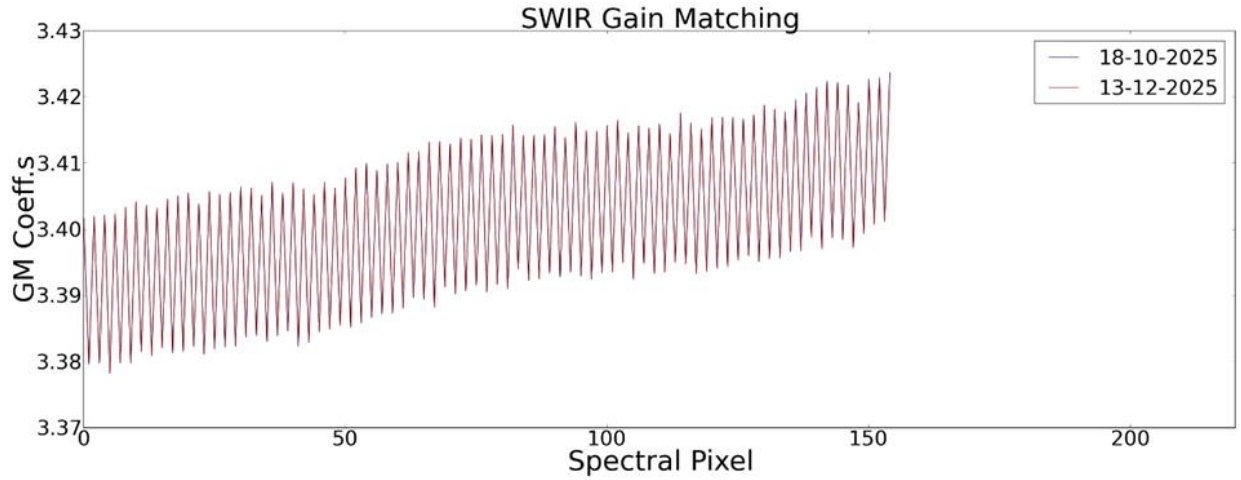

Figure 7-13 VNIR (top) and SWIR (bottom) gain matching calibration coefficients

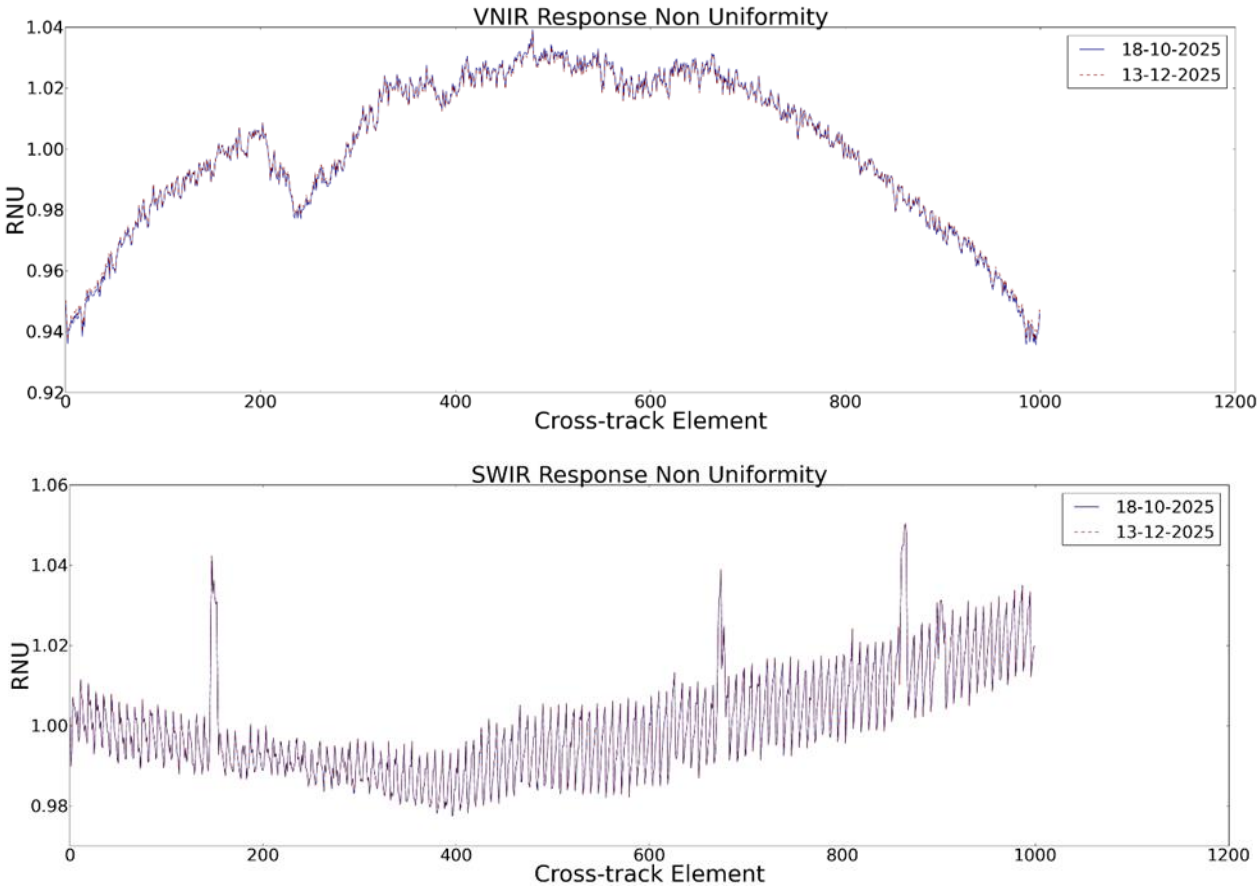

Figure 7-14 VNIR (top) and SWIR (bottom) response non-uniformity coefficients

Signal-to-Noise Ratio

The Signal-to-Noise Ratio (SNR) is derived from the Linearity reference measurements. This is not a perfect set-up for the assessment of the SNR as the linearity measurements only cover a single wavelength and light level at increasing integration times. However, it is well constrained, covering a wide range of radiances

including the levels of the reference radiance spectrum that is used to evaluate the requirements (30% reflectance, 30° sun incidence angle, 21 km visibility, target 500 m above sea level). The lamp reference measurements are not used, as the reference spectrum is not well covered at the radiances of the lamp and extrapolation would be required to test the performance at the SNR requirements. Those requirements are: SNR greater than 500 at 495 nm in VNIR for the reference spectrum value given a 10 nm pixel; and SNR greater than 150 at 2200 nm in SWIR for the reference spectrum given a 10 nm pixel.

For the VNIR sensor, SNR is computed from the linearity calibration measurement. SNR values are shown as a contour map with the reference radiance spectrum as a blue line. Contour lines with SNR values of 150 and 500 are also shown in black. The plot in low gain mode includes the mission requirement which is evaluated at 495 nm for a radiance value of 36 mW/cm^2/µm/sr and is expected to be greater than 500: the calculated value here is **599**. The radiance value used here for the evaluation is the value at 495 nm of the reference radiance spectrum after bandwidth normalization to a 10 nm pixel (see Figure 7-16).

For the SWIR sensor, SNR is also computed from the linearity calibration measurement. SNR values for the high gain mode are shown as a contour map with the reference radiance spectrum as a blue line. Contour lines with SNR values of 150 and 500 are also shown in black. The plot in high gain mode includes the mission requirement which is evaluated at 2200 nm for a radiance value of 0.5 mW/cm^2/µm/sr and is expected to be greater than 150: the calculated value here is **199**. The radiance value used here for the evaluation is the value at 2200 nm of the reference radiance spectrum after bandwidth normalization to a 10 nm pixel (see Figure 7-17).

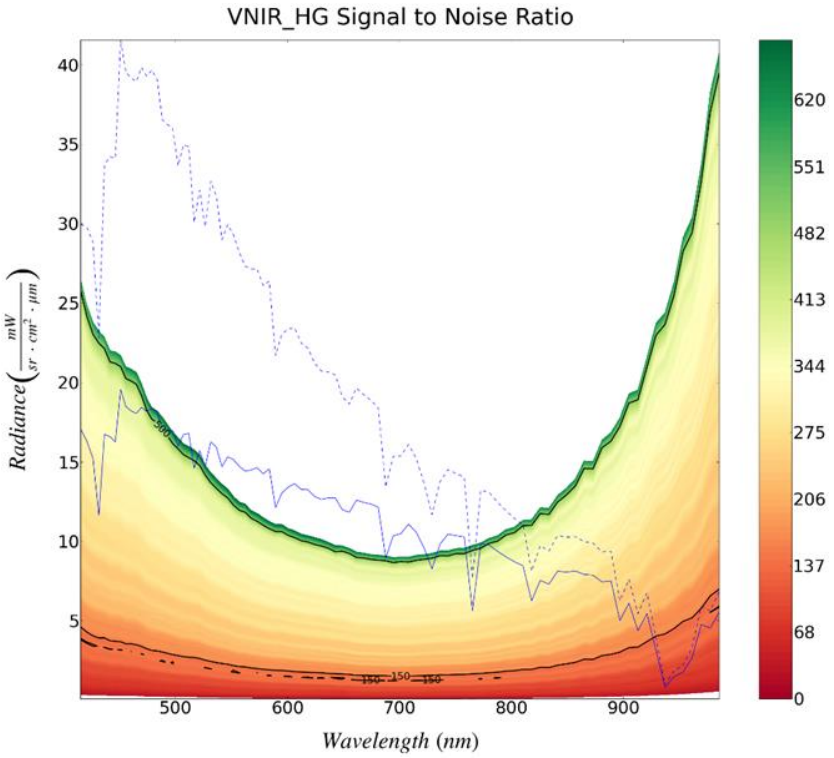

Figure 7-15 SNR contour map for VNIR high gain from the LED linearity observations observed on 15.12.2025. The reference radiance is shown with a blue line and after bandwidth normalization to a 10 nm pixel (dotted). Contour lines with SNR values of 150 and 500 are also shown in black.

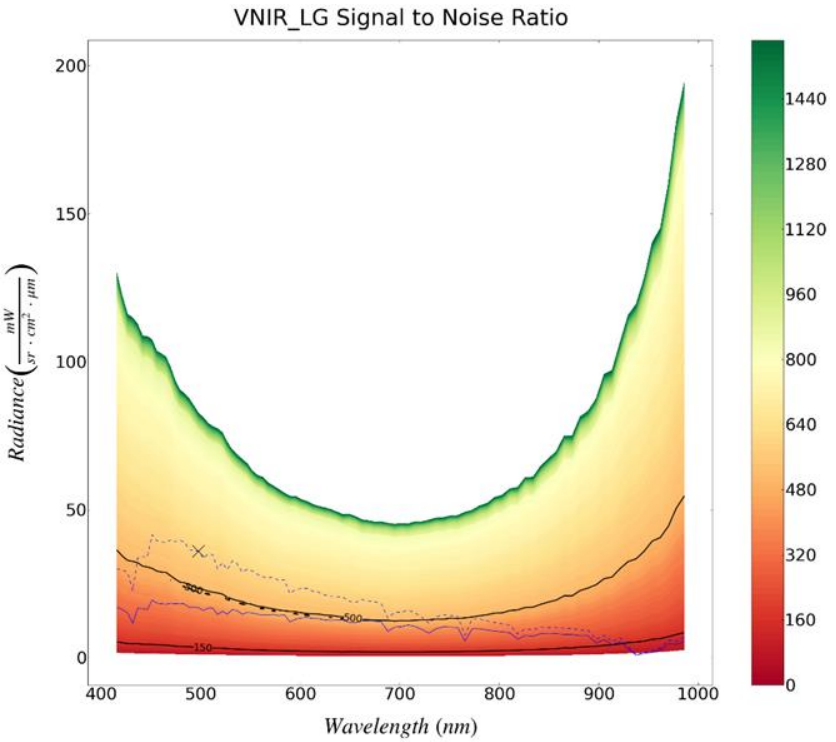

Figure 7-16 SNR contour map for VNIR low gain from the LED linearity observations observed on 15.12.2025. The reference radiance is shown with a blue line and after bandwidth normalization to a 10 nm pixel (dotted). Contour lines with SNR values of 150 and 500 are also shown in black. The mission requirement is evaluated at 495 nm for a radiance value of 36 mW/cm^2/μm/sr (marked with a black cross) and is expected to be greater than 500.

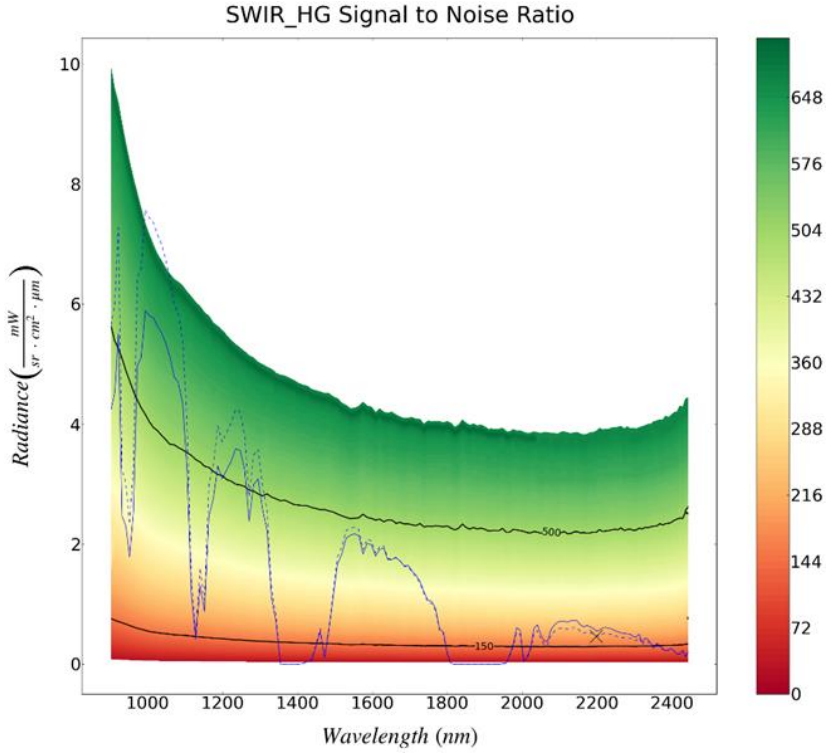

Figure 7-17 SNR contour map for SWIR high gain from the LED linearity observations observed on 15.12.2025. The reference radiance is shown with a blue line and after bandwidth normalization to a 10 nm pixel (dotted). Contour lines with SNR values of 150 and 500 are also shown in black. The mission requirement is evaluated at 2200 nm for a radiance value of 0.5 mW/cm^2/μm/sr (marked with a black cross) and is expected to be greater than 150.

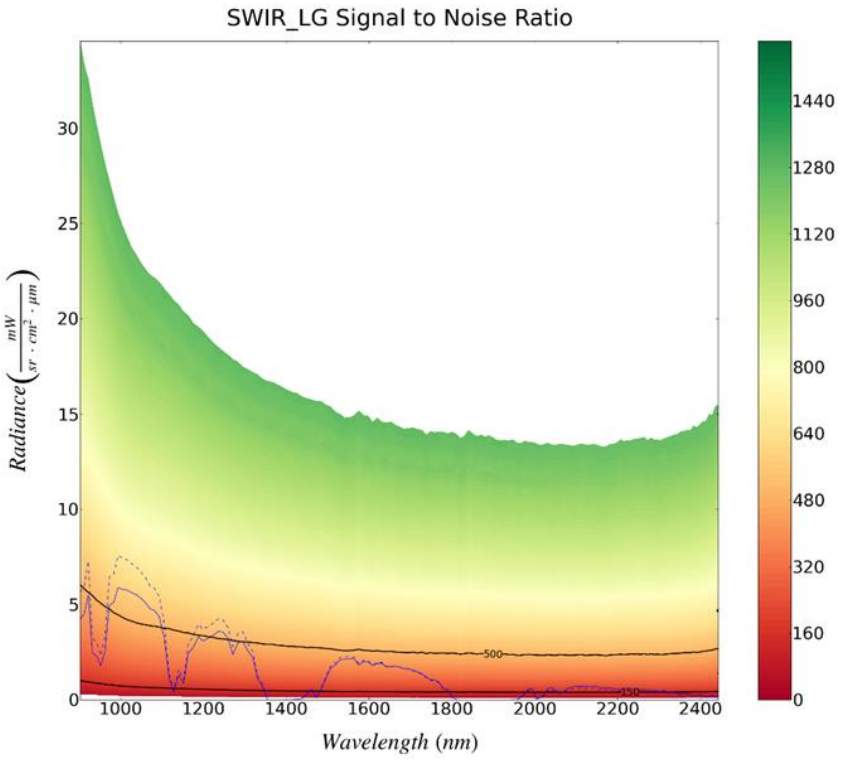

Figure 7-18 SNR contour map for SWIR low gain from the LED linearity observations observed on 15.12.2025. The reference radiance is shown with a blue line and after bandwidth normalization to a 10 nm pixel (dotted). Contour lines with SNR values of 150 and 500 are also shown in black.

The SNR values at the reference radiance spectrum are given in the table below (Table 7-9). The SNR is not determined in absorption regions and when the reference is too low or too high relative to the measured values in the linearity calibration.

Sensor	Wavelength (nm)	Reference Radiance (mW/sr/cm2/µm)	SNR Low gain	SNR High gain
VNIR	418.42	15.62	300.11	311.71
VNIR	424.04	15.32	302.34	312.96
VNIR	429.46	12.09	262.41	280.24
VNIR	434.69	15.07	305.09	310.81
VNIR	439.76	15.69	311.68	340.27
VNIR	444.7	17.29	330.36	344.03
VNIR	449.54	18.44	350.06	367.99
VNIR	454.31	18.18	351.1	367.01
VNIR	459.03	18.29	369.29	375.39
VNIR	463.73	18.2	370.45	376
VNIR	468.41	18.62	378.04	376.69
VNIR	473.08	18.2	381.19	381.03
VNIR	477.74	18.8	392.1	
VNIR	482.41	18.42	394.88	
VNIR	487.09	15.98	371.54	375.49
VNIR	491.78	16.46	381.8	396.16
VNIR	496.5	17.36	394.18	
VNIR	501.24	15.97	385.59	462.93
VNIR	506.02	17.31	415.09	
VNIR	510.83	16.57	403.96	
VNIR	515.67	15.92	394.01	
VNIR	520.55	15.48	389.82	
VNIR	525.47	15.6	397.8	
VNIR	530.42	15.98	423.99	
VNIR	535.42	15.84	434.46	
VNIR	540.46	14.72	416.65	

VNIR	545.55	15.36	444.33	
VNIR	550.69	15.03	447.76	
VNIR	555.87	15.02	459.97	
VNIR	561.11	15.03	464.28	
VNIR	566.41	14.13	452.32	
VNIR	571.76	14.36	467.47	
VNIR	577.17	14.47	465.93	
VNIR	582.64	14.61	473.4	
VNIR	588.17	13.5	466.51	
VNIR	593.77	13.32	466.89	
VNIR	599.45	13.48	465.12	
VNIR	605.19	13.77	476.18	
VNIR	611.02	13.33	466.33	
VNIR	616.92	12.67	464.28	
VNIR	622.92	13.07	469.56	
VNIR	628.99	12.85	464.04	
VNIR	635.11	12.9	475.9	
VNIR	641.3	12.76	479.64	
VNIR	647.54	12.04	459.95	
VNIR	653.84	12.4	479.75	
VNIR	660.21	12.43	487.88	
VNIR	666.64	12.48	483.69	
VNIR	673.13	12.41	484.43	
VNIR	679.69	12.21	482.8	
VNIR	686.32	10.69	445.45	
VNIR	693.02	10.52	445.63	
VNIR	699.78	10.76	453.01	
VNIR	706.62	10.96	458.9	
VNIR	713.52	10.96	458.19	
VNIR	720.5	7.95	364.47	380.41
VNIR	727.54	8.29	375.32	366.09
VNIR	734.65	10.03	414.18	
VNIR	741.83	10.13	412.13	
VNIR	749.06	10.45	426.92	
VNIR	756.35	10.32	413.37	
VNIR	763.7	3.91	227.79	276.72
VNIR	771.11	9.86	396.29	
VNIR	778.57	9.87	388.67	
VNIR	786.08	9.53	368.72	413.46
VNIR	793.64	9.01	362.44	382.92
VNIR	801.25	8.78	335.12	359.24
VNIR	808.91	8.66	328.63	343.79
VNIR	816.61	6.28	280.64	311.81
VNIR	824.36	7.09	290.7	311.13
VNIR	832.15	7.15	285.45	313.22
VNIR	839.98	8.18	303.98	328.97
VNIR	847.85	8.25	295.99	307.13
VNIR	855.76	7.74	284.91	304.5
VNIR	863.7	8.09	284.42	307.28
VNIR	871.68	7.88	266.02	296.03
VNIR	879.69	7.66	256.7	280.95
VNIR	887.73	7.41	245.22	269.92
VNIR	895.79	5.56	199.98	247.22
VNIR	903.87	6.03	203.83	244.16
VNIR	911.97	4.85	169.88	220.56
VNIR	920.08	5.54	182.5	227.18
VNIR	928.2	3.8	134.13	160.94
VNIR	936.34	0.89		69.43
VNIR	944.47	1.48		83.33
VNIR	952.61	1.65		87.64
VNIR	960.75	2.58	86.75	103.21
VNIR	968.89	4.74	128.08	133.4
VNIR	977.04	4.53	116.63	143.26
VNIR	985.19	5.41	122.23	146.24
VNIR	993.34	5.87	124.8	146.08

SWIR	901.96	6.12	506.06	
SWIR	911.57	4.75	444.86	
SWIR	921.32	5.38	484.64	
SWIR	931.2	1.91	261.14	
SWIR	941.22	1.95	274.06	
SWIR	951.36	2.03	285.93	
SWIR	961.63	2.7	349.43	
SWIR	972.02	4.85	505.12	
SWIR	982.52	5.13	535.42	
SWIR	993.14	5.87	584.46	
SWIR	1003.88	5.75	585.49	
SWIR	1014.72	5.73	591.34	
SWIR	1025.66	5.66	596.69	
SWIR	1036.7	5.51	591.32	
SWIR	1047.84	5.38	589.41	
SWIR	1059.07	5.07	576.16	
SWIR	1070.39	4.89	569.35	
SWIR	1081.78	4.67	554.24	
SWIR	1093.26	4.06	515.5	
SWIR	1104.81	3.18	450.98	
SWIR	1116.43	0.67	159.7	
SWIR	1128.11	0.35	94.64	
SWIR	1139.84	1.37	278.04	
SWIR	1151.62	0.97	217.87	
SWIR	1163.44	2.76	434.82	
SWIR	1175.3	3.18	476.81	
SWIR	1187.2	2.99	463.34	
SWIR	1199.11	2.91	457.77	
SWIR	1211.05	3.18	485.21	
SWIR	1223	3.39	507.89	
SWIR	1234.97	3.64	534.9	
SWIR	1246.95	3.54	528.44	
SWIR	1258.94	3.18	498.87	
SWIR	1270.93	2.82	470.27	
SWIR	1282.92	3.04	492.26	
SWIR	1294.91	3.02	496.3	
SWIR	1306.89	2.46	442.76	
SWIR	1318.87	1.92	383.98	
SWIR	1330.85	0.89	232	
SWIR	1342.82	0.56	167.2	
SWIR	1354.76	0.01		
SWIR	1366.69	0.01		
SWIR	1378.59	0.01		
SWIR	1390.47	0.01		
SWIR	1402.33	0.01		
SWIR	1414.17	0.01		
SWIR	1425.95	0.07		
SWIR	1437.7	0.06		
SWIR	1449.43	0.23	82.61	
SWIR	1461.1	0.38	126.87	
SWIR	1472.74	0.2	75.11	
SWIR	1484.33	0.61	187.53	
SWIR	1495.9	1.11	291.26	
SWIR	1507.41	1.68	379.6	
SWIR	1518.87	1.86	406.32	
SWIR	1530.29	2.09	437.22	
SWIR	1541.67	2.15	449.37	
SWIR	1553.02	2.17	450.17	
SWIR	1564.3	2.14	444.83	
SWIR	1575.55	1.87	404.1	
SWIR	1586.77	2	429.77	
SWIR	1597.91	1.97	423.3	
SWIR	1609.03	1.74	398.68	
SWIR	1620.08	1.92	418.7	
SWIR	1631.1	1.91	421.32	

SWIR	1642.07	1.74	399.67	
SWIR	1653	1.76	402	
SWIR	1663.87	1.73	398.54	
SWIR	1674.69	1.71	397.66	
SWIR	1685.46	1.67	393.15	
SWIR	1696.19	1.59	380.17	
SWIR	1706.88	1.49	366.94	
SWIR	1717.5	1.55	378.07	
SWIR	1728.07	1.42	355.55	
SWIR	1738.59	1.25	334.27	
SWIR	1749.08	1.21	325.02	
SWIR	1759.52	1.19	322.04	
SWIR	1769.9	0.91	270.44	
SWIR	1780.21	0.59	197.58	
SWIR	1790.5	0.44	152.9	
SWIR	1800.73	0.07		
SWIR	1810.92	0.01		
SWIR	1821.06	0		
SWIR	1831.16	0		
SWIR	1841.2	0		
SWIR	1851.19	0		
SWIR	1861.16	0		
SWIR	1871.06	0		
SWIR	1880.92	0		
SWIR	1890.73	0		
SWIR	1900.52	0		
SWIR	1910.22	0		
SWIR	1919.91	0		
SWIR	1929.55	0		
SWIR	1939.15	0		
SWIR	1948.69	0.02		
SWIR	1958.19	0.04		30.26
SWIR	1967.66	0.23		120.99
SWIR	1977.07	0.43		186.56
SWIR	1986.45	0.56		222.87
SWIR	1995.79	0.45		194.99
SWIR	2005.08	0.06		41.24
SWIR	2014.33	0.1		57.86
SWIR	2023.54	0.37		174
SWIR	2032.7	0.68		253.59
SWIR	2041.83	0.66		248.51
SWIR	2050.92	0.4		183.98
SWIR	2059.96	0.46		197.72
SWIR	2068.96	0.4		183.38
SWIR	2077.93	0.63		241.61
SWIR	2086.85	0.68		253.61
SWIR	2095.74	0.71		262.52
SWIR	2104.59	0.74		269.07
SWIR	2113.41	0.73		263.74
SWIR	2122.17	0.71		261.79
SWIR	2130.91	0.74		268.77
SWIR	2139.6	0.74		265.57
SWIR	2148.27	0.7		259.23
SWIR	2156.89	0.68		253.61
SWIR	2165.46	0.61		240.02
SWIR	2174.03	0.64		246.81
SWIR	2182.54	0.61		237.12
SWIR	2191.02	0.63		243.58
SWIR	2199.45	0.55		221.7
SWIR	2207.86	0.59		232.16
SWIR	2216.24	0.61		235.93
SWIR	2224.58	0.61		235.21
SWIR	2232.89	0.6		234.83
SWIR	2241.16	0.59		229.11
SWIR	2249.41	0.57		225

SWIR	2257.61	0.54		216.9
SWIR	2265.8	0.53		212.83
SWIR	2273.93	0.51		211.82
SWIR	2282.05	0.49		205.54
SWIR	2290.13	0.49		205.02
SWIR	2298.17	0.46		196.74
SWIR	2306.18	0.47		202.07
SWIR	2314.17	0.45		195.63
SWIR	2322.14	0.39		175.44
SWIR	2330.06	0.43		188.68
SWIR	2337.94	0.36		168.68
SWIR	2345.81	0.35		160.37
SWIR	2353.64	0.29		139.81
SWIR	2361.43	0.37		169.07
SWIR	2369.2	0.24		124.36
SWIR	2376.94	0.26		127.88
SWIR	2384.66	0.21		111.4
SWIR	2392.34	0.26		127.25
SWIR	2399.99	0.27		134.51
SWIR	2407.61	0.19		101.77
SWIR	2415.21	0.12		69.71
SWIR	2422.79	0.19		100.77
SWIR	2430.32	0.24		115.93
SWIR	2437.83	0.19		94.84
SWIR	2445.31	0.18		89.99

Table 7-9 SNR values per wavelength for VNIR and SWIR low and high gains

Radiometric calibration updates

The following calibration products were generated and delivered:

Product	Type	Date of Generation	Date of Validity Start	Date of Validity End	Delivered to
ENMAP01-CTB_RAD-20251101T000000Z_V040100_20251020T061628Z	CTB_RAD	20.10.2025	01.11.2025	19.12.2025	DIMS
ENMAP01-REF_SUN-20251101T000000Z_V040100_20251020T061628Z	REF_SUN	20.10.2025	01.11.2025	19.12.2025	DIMS
ENMAP01-CTB_RAD-20251220T000000Z_V040100_20251218T152543Z	CTB_RAD	18.12.2025	20.12.2025	-	DIMS
ENMAP01-REF_SUN-20251220T000000Z_V040100_20251218T152543Z	REF_SUN	18.12.2025	20.12.2025	-	DIMS

Table 7-10 Generated radiometric calibration tables

7.5.4 Geometric Calibration

There have been no new geometric calibration tables generated in the reporting period.

Type of Calibration Table	ID of Calibration Table	Date of Generation	Date of Validity Start	Date of Validity End
None				

Table 7-11 Generated new geometric calibration tables

The performance of the geometric calibration table is assessed in chapter 7.6.3.

7.6 Internal Quality Control

7.6.1 Archive

Within the given time period (01.10.2025 to 31.12.2025), 1754 datatakes with a total of 19123 tiles were acquired and archived (remark: additional datatakes acquired during this period but for which the archiving is pending might be missing in the statistics).

The overall quality rating statistics are listed in Table 7-12, and in relation to the Solar Zenith Angle (SZA) in Table 7-13. Also these ratings are further detailed for the VNIR and SWIR detector in Table 7-14, showing a nominal performance rating for the given quality thresholds.

In addition, the rating for the atmospheric conditions for the scenes are depicted in Table 7-15. When setting the atmospheric quality rating in relation to the illumination conditions (i.e., large SZA) during data acquisition (Table 7-16), For the reporting period, a slight increase of “low quality” scenes can be observed, but the numbers are still very small, 396 scenes (2.07%) compared to 88 scenes (0.4%) in Q3; this increase is related both to the increase in scenes with low light conditions (100% of the “low quality” scenes), and to a slight increase in the detected general radiometric artefacts.

Parameter	Value	Number of tiles	Percentage
overallQuality	Nominal	18700	97,79%
	Reduced	27	<0.14%
	Low	396	2.07%

Table 7-12 Overall quality rating statistics

Parameter	Sub-Parameter	Number of tiles	Percentage
overallQuality = Low		396	
	Thereof with SZA > 70°	396	100%

Table 7-13 Overall quality rating in relation to Sun Zenith Angle (SZA)

Parameter	Sub-Parameter	Number of tiles	Percentage
overallQuality = Reduced		27	
	Thereof with qualityVNIR nominal	16	59.26%
	Thereof with qualitySWIR nominal	11	40.74%
overallQuality = Low		396	
	Thereof with qualityVNIR nominal or reduced	7	1.77%
	Thereof with qualitySWIR nominal or reduced	319	80.56%

Table 7-14 Reduced and low quality rating statistics

Parameter	Value	Number of tiles
QualityAtmosphere	Nominal	6953
	Reduced	2892
	Low	9278

Table 7-15 QualityAtmosphere rating statistics

Parameter	Sub-Parameter	Number of tiles	Percentage
overallAtmosphere = Reduced		2892	
	Thereof with SZA > 65°	75	2.59%
	Thereof with SZA > 70°	30	1.04%
	Thereof with SZA > 80°	3	0.10%
overallAtmosphere = Low		9278	
	Thereof with SZA > 65°	2454	26.45%
	Thereof with SZA > 70°	1360	14.66%
	Thereof with SZA > 80°	514	5.54%

Table 7-16 QualityAtmosphere rating in realtion to Sun Zenith Angle (SZA)

Parameter	Sub-Parameter	Number of tiles	Percentage
overallAtmosphere = Low		9278	
	Thereof with Cloud Cover > 66%	4603	49.61%
	Thereof with DDV warnings	7084	76.35%

Table 7-17 QualityAtmosphere rating in relation to Cloud Cover and DDV availability

Remark about definition of EnMAP low quality collection

The quality rating of EnMAP products is based on image parameters, such as illumination conditions (i.e., sun elevation angle) and image defects, and on possible anomalies in the image data or instrument telemetry. These parameters are retrieved during the pre-processing and are added to the metadata and quality layers for every archived L0 product. In EOWEB GeoPortal two collections of EnMAP L0 products are available: “EnMAP-HSI (L0)” and “EnMAP-HSI (L0), Low Quality”. An L0 product is assigned to the low-quality collection if the corresponding metadata item qualityFlags.overallQuality is equal to 2 (low quality). This happens for products with a significant number of striping, saturation, artefact or dead pixels, when the screening of data and instrument indicates non-nominal behavior or, in the majority of cases, when the sun elevation angle is less than or equal to 0 (e.g., night scenes). A detailed definition of qualityFlags. overallQuality is given in Sec. 4.4.9 in the L1B ATBD (EN-PCV-TN-4006).

7.6.2 Level 1B

7.6.2.1 Radiometric Performance

Defective / de-calibrated detector elements

Using the Detector Map components, an offline check of possibly defective or de-calibrated detector elements is conducted. In particular, a detector element is identified as “possibly defective” if it is suspicious in at least 75% of the useful tiles. Note that this analysis is based on L1B_RAD data, so no dead / defective pixel interpolation was carried out. Within the given reporting period, the following indications for defective pixels are found for the VNIR and the SWIR camera:

VNIR (total of 16021 tiles, with 15891 suitable for analysis):

Newly found suspicious pixels in green, previously detected in **black**, no longer present ones in ~~red~~.

Band	Cross-track element
~~77~~	~~600~~
85	14
89	395

Note that the band index starts at 1.

SWIR (total of 16021 tiles, with 15782 suitable for analysis):

Newly found suspicious pixels in green, previously detected in **black**, no longer present ones in ~~red~~.

NOTE: due to the change in SWIR band configuration within the period Q3 2023, the band index from band 45 till 75 did change by +1 (with bands 45, 74 & 75 newly added) w.r.t. the reports before Q3 2023.

Band	Cross-track element	Band	Cross-track element	Band	Cross-track element
1	817	33	560	85	525
2	235, 286, 593, 673	38	241, 919	89	285
3	381	48	511	91	973
4	362, 363, 418	50	311, 344, 395	92	677, 973
5	687	53	97, 98	96	341, 819

7	472, 910	54	941	101	318
8	801	56	221, 965	106	107
9	124	58	632, 667, 922	107	265, 764
11	715	59	89, 90	108	886
14	29, 684	61	312	111	315
16	535	63	123	118	837
29	855, 928	66	93		
30	360, 855	69	864		
31	360	72	801, 845		
		75	737		

Dead detector elements

Within the given reporting period, the statistics for dead pixels are provided in Table 7-18 and Table 7-19. When comparing these numbers to the estimates in Ch. 7.5.1, one must bear in mind that the latter is based on the full detector readout configuration, while the numbers provided in the following are related to the standard readout configuration as provided in the user product. Because of the smaller readout area, these following dead pixel numbers are lower in comparison.

Parameter	Value (number of pix)	Number of tiles	Percentage
DeadPixelsVNIR	137	19123	100%

Table 7-18 Dead pixel statistics, VNIR

Parameter	Value (number of pix)	Number of tiles	Percentage
DeadPixelsSWIR	1509	19123	100%

Table 7-19 Dead pixel statistics, SWIR

Saturation and radiance levels

Within the given reporting period, no indications for increased saturation defects are found for the VNIR and the SWIR camera (see Table 7-20 and Table 7-21).

Parameter	Value (per mille of scene)	Number of tiles	Percentage of tiles
SaturationCrosstalkVNIR	0	17963	93.93%
	> 0 per mille	1160	6.07%
	> 10 per mille	258	1.35%

Table 7-20 Saturation statistics, VNIR

Parameter	Value (per mille of scene)	Number of tiles	Percentage of tiles
SaturationCrosstalkSWIR	0	18034	94.31%
	> 0 per mille	1089	5.69%
	> 10 per mille	87	0.45%

Table 7-21 Saturation statistics, SWIR

Other radiometric artifacts

Within the given reporting period, the striping performance is similar to the one encountered during the Commissioning Phase. Within PCV, different de-striping approaches were tested, and the selected one by M. Brell (GFZ) is implemented in processor version V01.02.00 (07.03.2023).

Apart from this, no indications for an increase in general radiometric artifacts are found for the VNIR and the SWIR camera (see following tables).

Parameter	Value (number of pix)	Number of tiles	Percentage
generalArtifactsVNIR	0	0	0%
	> 0	19123	100%
	> 10	1216	6,36%
	> 100	436	2,28%
	> 1000	0	0%

Table 7-22 Artifacts statistics (without striping), VNIR

Parameter	Value (number of pix)	Number of tiles	Percentage
generalArtifactsSWIR	0	0	0%
	> 0	19123	100%
	> 10	19123	100%
	> 25	1005	5.26%
	> 100	464	2.43%
	> 1000	0	0%

Table 7-23 Artifact statistics (without striping), SWIR

7.6.2.2 Spectral Performance

For the analysis of the spectral stability, the Detector Maps of all Earth datatakes acquired in the reporting period were used. Note that no smile correction was applied, so the analysis shows only on the instrument characteristics. At the wavelengths of stable atmospheric features (760 nm Oxygen absorption and CO2 absorption at ~2050 nm), simulations of spectral shifts were carried out by resampling the absorption in the interval of +/- 3.0 nm with steps of 0.05 nm. Then the signal of the Detector Maps and the simulated shifted

absorptions were normalized, and a least-square fit was used where the sensed absorption matches the simulations. Also an additional polynomial fitting was applied, as especially the CO2 absorption band region has low signal an is thus significantly influenced by noise.

For the VNIR, when aggregating the shifts (Figure 7-19) the mean derivation is almost constant in across-track direction and -as before- around 0.5 nm towards shorter wavelengths, underpinning the consistency with the in-orbit spectral calibration and especially regarding the shape of the spectral smile. Note that of course these results are consistent within the limitations of this vicarious approach. Additionally, the variability of the vicariously estimated spectral calibration can be expressed as the standard deviation at 1 sigma is below 0.4 nm, which includes the spectral stability of EnMAP and as well the variations of the used Earth datatakes and the limitations of the method.

In summary, for the VNIR the estimated differences to the CTB_SPC consistent with the results of previous reporting periods, confirming the validity of the spectral calibration and the spectral stability of the instrument taking into accounts the limitations of the vicarious approach.

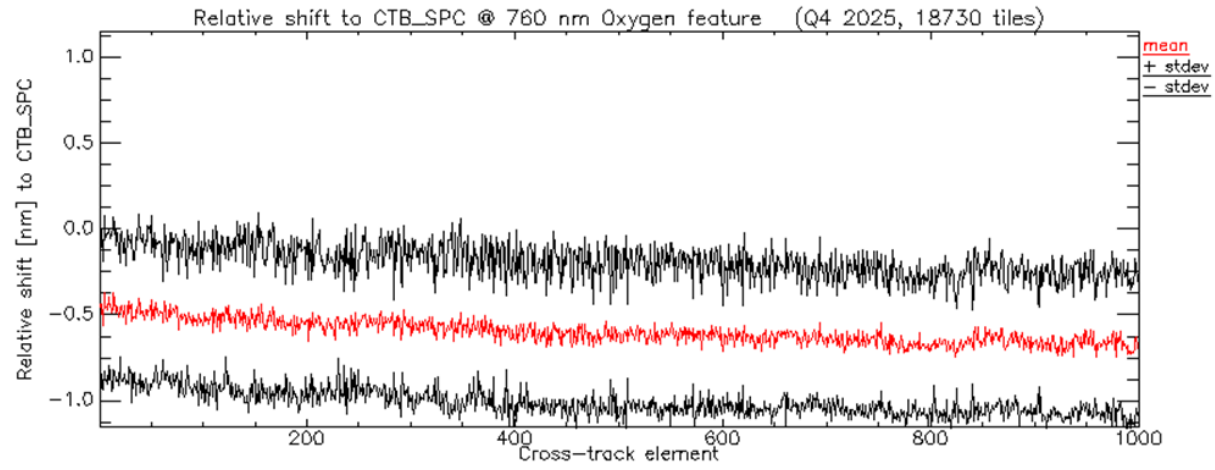

Figure 7-19 VNIR estimated spectral shift at 760 nm w.r.t the valid spectral calibration table (CTB_SPC), and relative spectral stability expressed at 1 sigma (Q4 2025, 15920 tiles)

For this analysis, the reference is thus not the nominal center wavelengths (i.e., a single number per band), but the CW per cross-track pixel, thus explicitly including the spectral smile (see Figure 7-20).

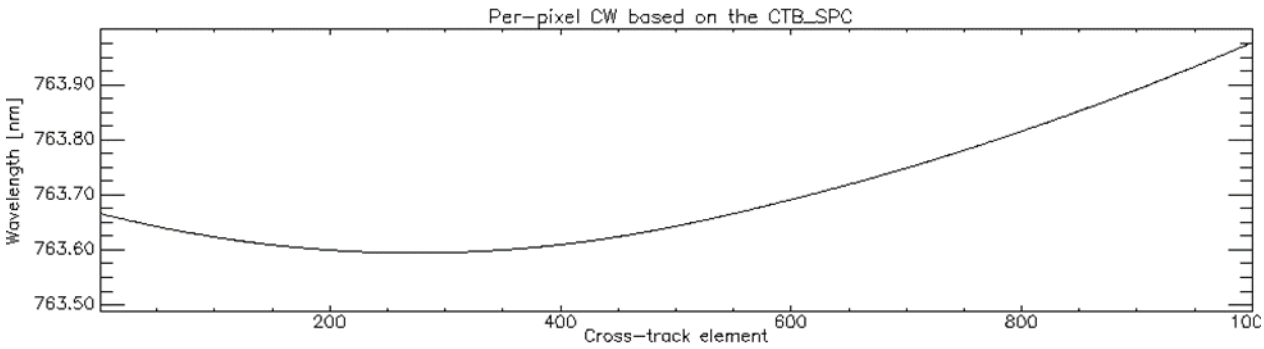

Figure 7-20 Center wavelengths per cross-track pixel based on the spectral calibration table (VNIR band 62) in the calibration table (CTB_SPC).

For the SWIR having less pronounced atmospheric absorption features, more influence of the background and a much lower signal level, the fitting also results in more clutter, as shown in Figure 7-21.

In order to demonstrate that the mean derivation to the CTB_SPC is within the spread of the data, the mean and standard deviation are calculated using the relative values, as shown in Figure 7-21. For Q4 2025, a small shift of ~0.45 nm towards longer wavelengths is visible when comparing to CTB_SPC (Figure 7-22) ,

and having a standard deviation of ~0.6 nm. This shift is equal for all cross-track elements, so the shape of the spectral smile did not change and is well represented in the CTB_SPC. When comparing this small spectral shift to the results in the past quarter, the tendency towards longer wavelengths by ~0.4 nm was also present, but then with a larger magnitude and within a larger clutter in the fitted data. In addition, the spread around the estimated mean with a standard deviation of ~0.6 nm (1 sigma) indicates no significant change of the good overall stability of the instrument.

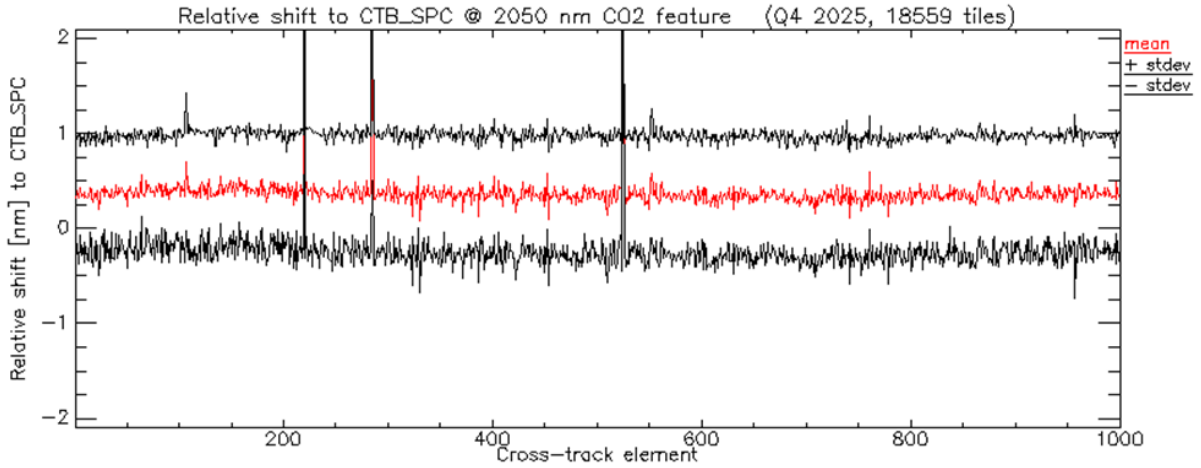

Figure 7-21 SWIR estimated spectral shift at 2050 nm w.r.t the valid spectral calibration table (CTB_SPC, shown below), and relative spectral stability expressed at 1 sigma (Q4 2025, 17894 tiles)

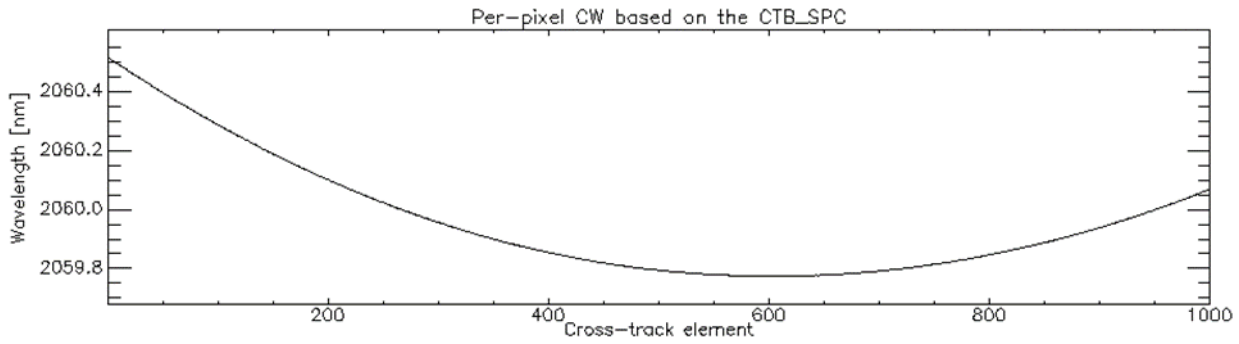

Figure 7-22 Center wavelengths per cross-track pixel based on the spectral calibration table (SWIR band 86).

7.6.3 Level 1C

This report covers the timeframe from 01.10.2025 to 31.12.2025. No geometric calibration was performed during this period.

In the timeframe of this report, 1754 datatakes have been acquired. In 1317 of those datatakes (~75 %), enough ground control points (GCP) and independent check points (ICP) were found to perform a geometric accuracy assessment. The datatakes without enough GCPs were not assessed quantitatively, but a random subset of them was inspected visually. The vast majority of those datatakes was either almost fully covered with clouds or showing only water, desert or rain forest. The behavior is thus as expected.

The assessment of the RMSE values in the metadata is shown below in Figure 7-23.

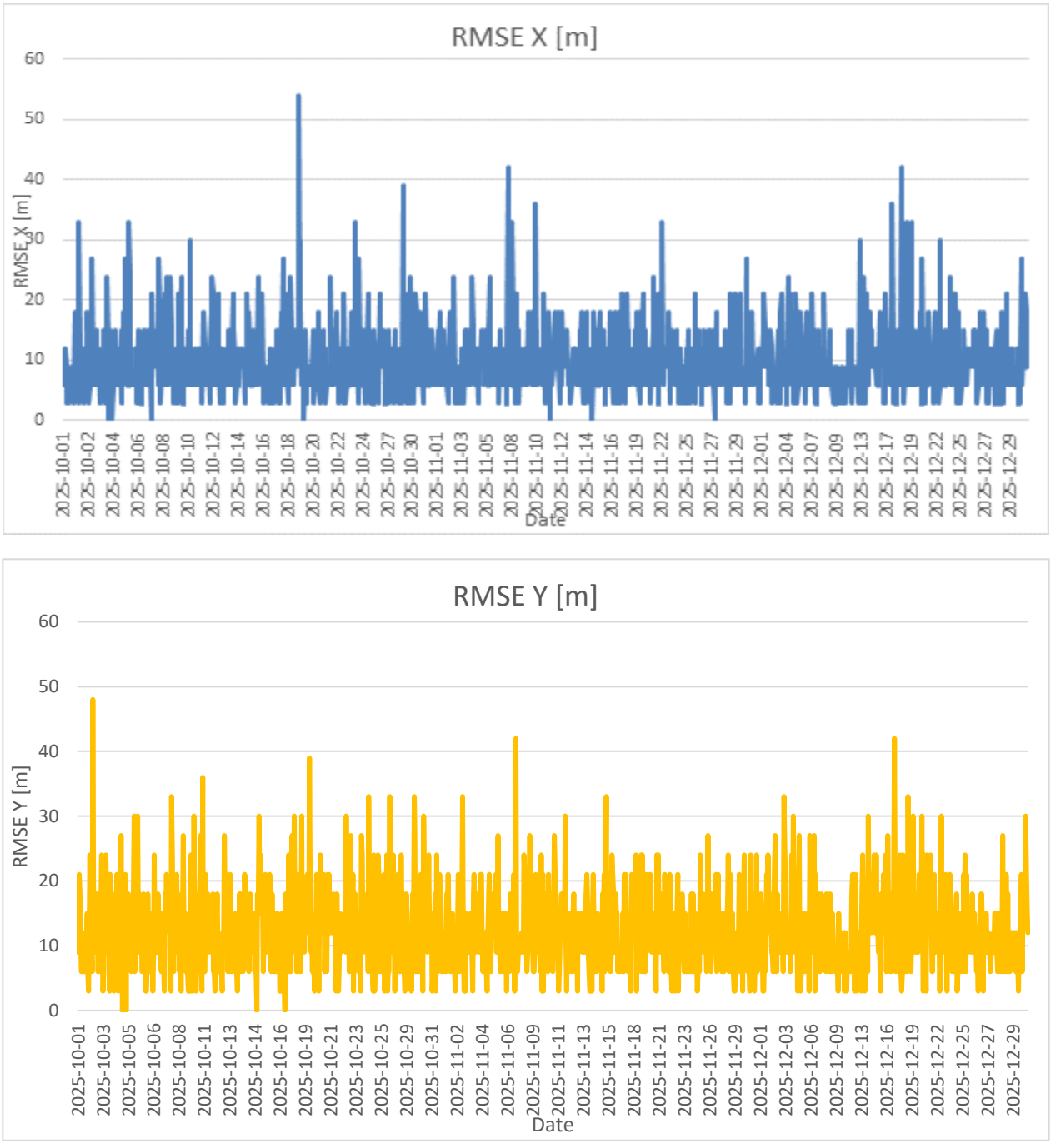

Figure 7-23 Assessment of RMSE X values (top) and RMSE Y values (bottom), calculated based on found ICPs, for all datatakes where ICP could be found

In x-direction, 13 datatakes (~1.0%) had an RMSE value above 30 m (1 GSD), whereas in y-direction, 30 datatakes (~1.0%) are above this threshold. For most of those datatakes, only very few GCP and ICP could be found during processing, making the results less reliable. The mean values are 10.08 m in x-direction and 12.41 m in y direction. This shows a very high geolocation accuracy for the datatakes where matching was possible. The requirement GRD-PCV-0155 (1 GSD) is thus fulfilled.

The average boresight angles, which can be interpreted as the correction and thus the error of the scene if no GCPs could have been found, correspond to approximately -20 m in x direction with a standard deviation of approximately 25 m and -31 m in y direction with a standard deviation of approximately 20 m on ground. It is reasonable to assume that the scenes where no GCPs could be found are in the same accuracy range

and thus well within the requirement of 100 m (GRD-PCV-0150). Note that the x and y direction mentioned in this report are not in the image coordinate system but in UTM, as the evaluation is done on L1C products.

7.6.3.1 Geometric accuracy

EnMAP L1C products are matched against a reference image (Sentinel-2 data, if not stated otherwise) by using image matching techniques to assess the geometric accuracy. At the obtained checkpoints (CP), statistics are calculated to provide mean and RMSE values (Figure 7-24) for each scene. Note that the obtained accuracy in the analysis is always w.r.t. the reference image. This report covers EnMAP data from 01.10.2025 to 31.12.2025. A random sample of 565 L1C tiles was selected based on visual inspection of the catalogue quicklooks (e.g. to avoid cloudy images).

The requirement GRD-PCV-0155 shall be fulfilled:

The geolocation accuracy at nadir look direction of level 1C and 2A products shall be better than 1 GSD (1 sigma) in each direction with respect to reference images provided that reference images are available and sufficient similarity.

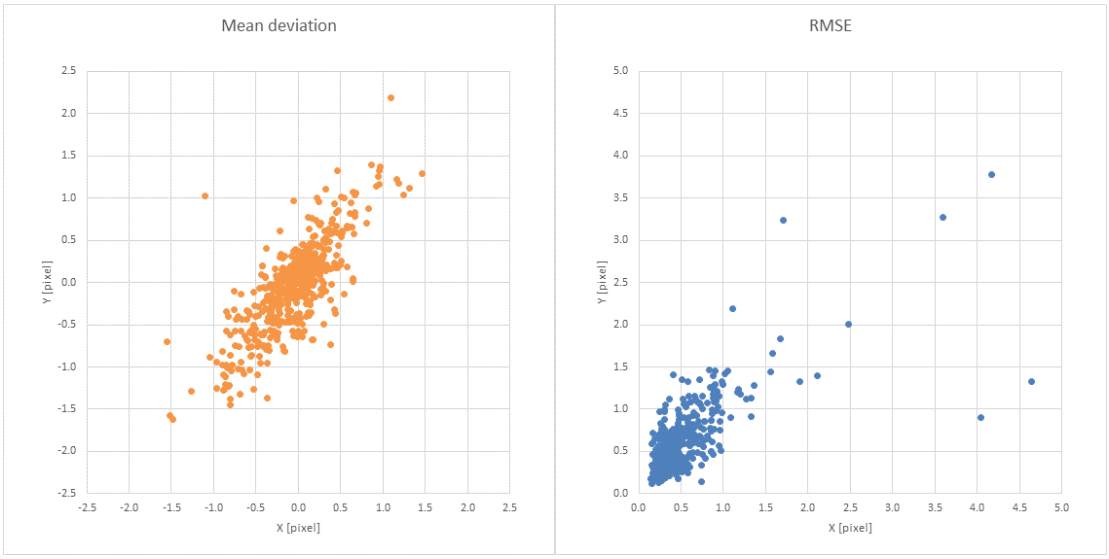

Figure 7-24 Mean deviation of EnMAP L1C products in pixel (left). RMSE value for EnMAP L1C products in pixel (right)

Note, that during processing the boresight angles and the geometric accuracy related quality flags are calculated on datatake level while in the figures and tables above, the accuracy is assessed per tile. The mean values over all 565 L1C tiles are -0.05 and -0.02 pixel in mean deviation with a standard deviation of 0.43 and 0.51 pixel while the mean RMSE values are 0.49 and 0.58 pixel, all in x and y direction respectively. The data show that for the vast majority of scenes the accuracy wrt. reference image is better than one pixel and thus the requirements are fulfilled. Compared to the last geometric QC report, the values are very stable (see Figure 7-26).

7.6.3.2 Co-registration accuracy

In this section, the co-registration accuracy is checked against the Space Segment requirement SRDS-PIM-0050 (EN-KT-RFW-003 is also to be considered here):

*The HS-Imager shall be designed such, that the geometric co-registration is ≤ 20 % of the nominal Ground Sampling Distance (0.2 * GSD linear displacement in both directions).*

For the assessment of co-registration accuracy, the SWIR data of EnMAP L1C products are matched against the corresponding VNIR data and the mean deviation values shown in this section (Figure 7-25).

This report covers EnMAP data from 01.10.2025 to 31.12.2025. A random sample of 568 L1C tiles was selected based on visual inspection of the catalogue quicklooks (e.g. to avoid cloudy images).

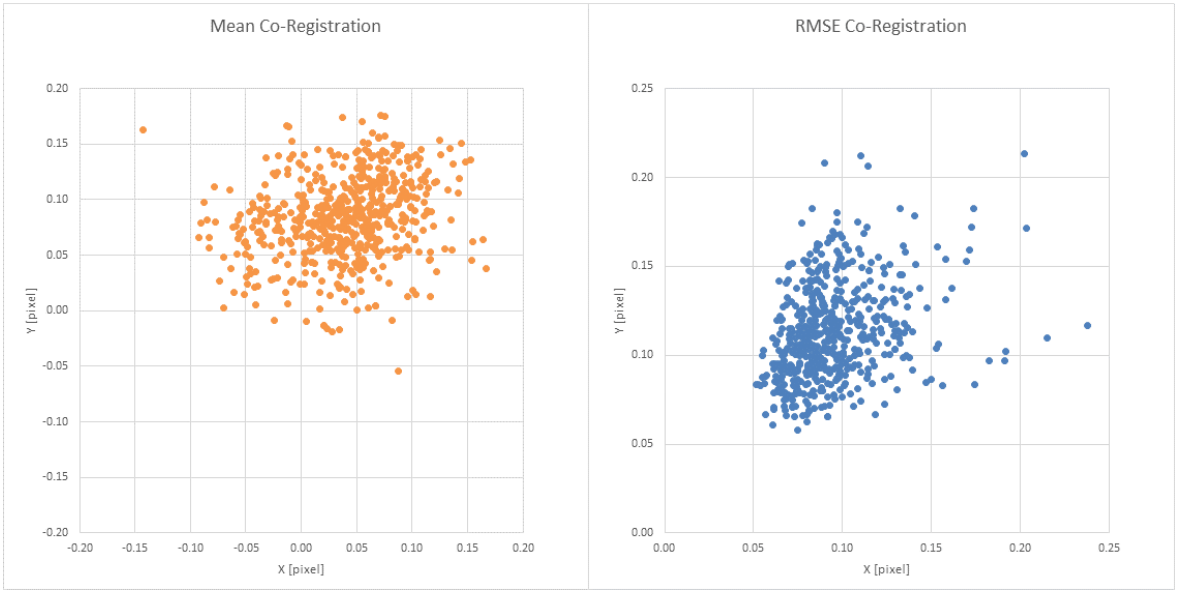

Figure 7-25 Mean deviation in pixel between VNIR and SWIR data of EnMAP L1C products (left). RMSE in pixel between VNIR and SWIR data of EnMAP L1C Products (right)

The data show, that the mean co-registration is well within the requirement. Note that the theoretical accuracy of the used matching algorithm is 0.1 pixel, and as can be seen in the RMSE values, still some mismatches were not removed by the blunder detection techniques that were applied. The mean deviation over all analyzed tiles are 0.04 pixel in x-direction with a standard deviation of 0.05 pixel and 0.08 pixel in y direction with a standard deviation of 0.04 pixel. Compared to the results in the previous geometric QC report, the values are very stable as can be seen in Figure 7-26.

7.6.3.3 **Development of geometric performance**

Since the launch of EnMAP on April 1st 2022, the geometric performance has been improved significantly. This was achieved by different geometric calibrations and processor updates. Table 7-24 shows the measures performed, their date and their effect.

Date	Measure	Effect
01.08.2022	Fix of attitude processing	Improvement of absolute geolocation (w/o matching)
20.09.2022	Boresight Calibration	Improvement of absolute geolocation (w/o matching)
03.11.2022	1st Geometric Calibration	Improvement of absolute geolocation (w/o matching) Improvement of VNIR/SWIR co-registration (~0.8 pix -> ~0.4 pix)
11.02.2023	2nd Geometric Calibration	Improvement of VNIR/SWIR co-registration (~0.4 pix -> ~0.15 pix)
29.03.2023	Processor update (v01.02.00)	Improvement of VNIR/SWIR co-registration (~0.15 pix -> ~0.06 pix)
05.05.2023	Processor update (v01.03.01)	Improvement of geolocation accuracy

Table 7-24 Improvement of geometric performance

Figure 7-26 shows the development of the co-registration accuracy, measured as described in previous section. Again, after a significant improvement since commissioning phase, over the last report periods the accuracy has been very stable.

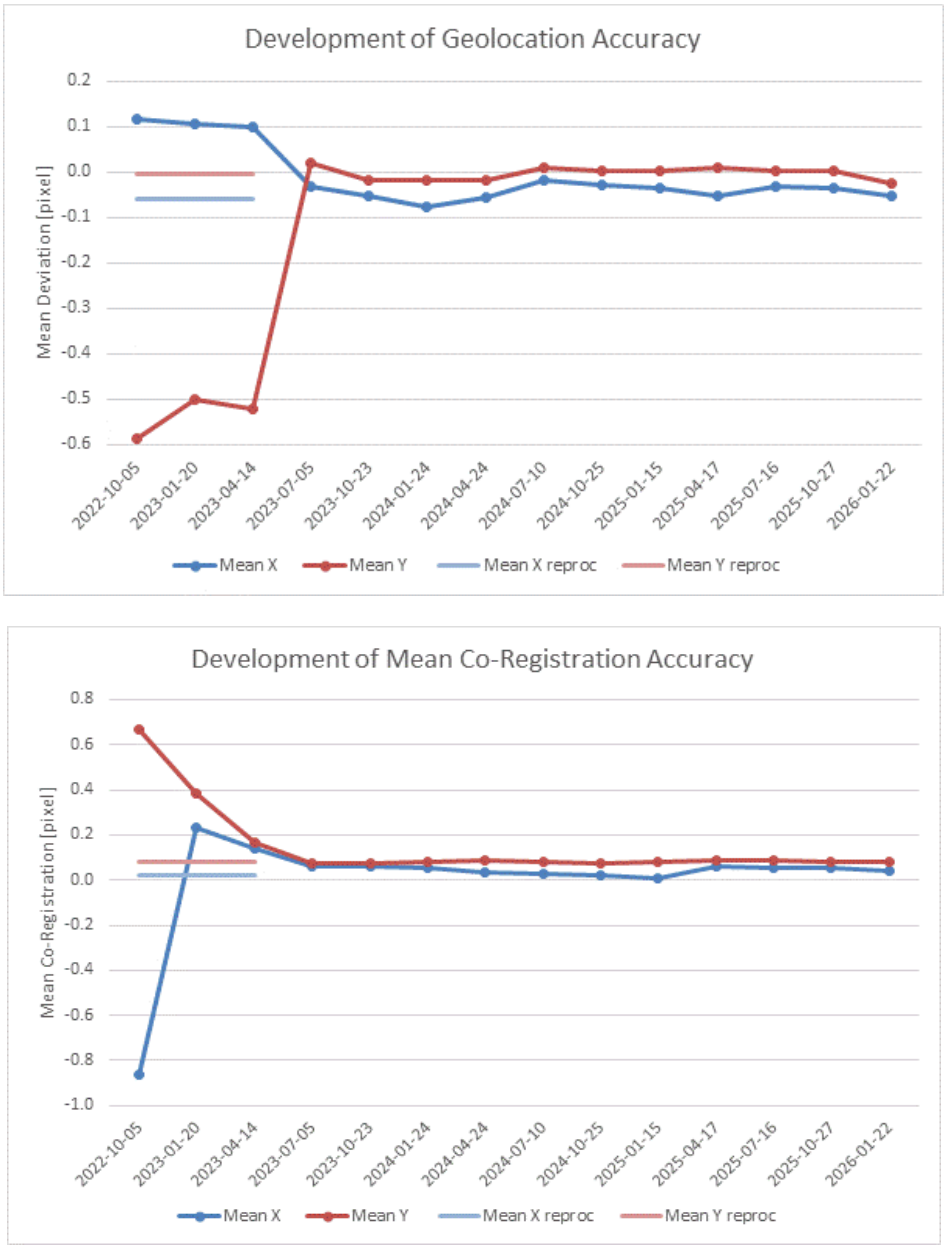

Figure 7-26 Development of co-registration accuracy based on the previous geometric QC reports. The values with re-processed L0 data and archived version ≥V01.03.00 are also shown

As most of the geometric processing – especially the matching against a reference image – is done on datatake level during L0 processing, the geometric accuracy and co-registration of data acquired earlier during the mission is not automatically improved when higher level products (L1B, L1C, L2A) are processed with the current processor version. However, after completing the L0 reprocessing of the whole archive, the geometric processing is executed with the latest processor version and geometric calibration table to make sure that the best geometric quality and co-registration is reached also for the reprocessed data. Today, the geometric performance of the products available in the Mission Archive with date earlier than 29.03.2023 is the same as for the products acquired after that date. Users can recognize reprocessed data by checking the metadata tag **archivedVersion**: if the version is 01.03.00 or higher, then the geometric performance should be as analyzed in this report, regardless of the acquisition date of the product.

7.6.4 Level 2A

7.6.4.1 **Validity of generated L2A "water" data**

7.6.4.1.1 Analyzed scenes

The following scenes were taken into consideration:

DataTake - ID	Tile - ID	Location	L2A Option	Cirrus / Haze Removal	Overall Quality
163513	31	2025-11-04	Water mode, water type "clear"	Cirrus	Nominal
169097	18	2025-12-17	Water mode, water type "clear"	Cirrus	Nominal
026843	10	2023-07-06	Water mode, water type "clear"	Cirrus	Nominal
170682	02	2025-12-25	Water mode, water type "clear"	Cirrus	Nominal
164236	05	2025-11-17	Water mode, water type "clear"	Cirrus	Nominal

Table 7-25 Datatake IDs of analyzed water products

The below listed parameters were checked for above mentioned scenes by EOMAP:

Parameter	Check
Masking (Land, Water, Clouds, etc.)	No issues found.
Adjacency correction	Updated*
Retrieval of atmospheric properties	Updated*
Cirrus – correction	No issues found.
Retrieval of water leaving reflectance	No issues found.
Quality Mask	Updated*

*Details to the updates are presented below.

7.6.4.1.2 Data Checks

For the checks described in the following, multiple scenes were used. The corresponding scene - IDs and locations can be found in Table 7-25.

- Masking

First, the geo mask is checked. The different parts of the scene shown masked (see Figure 7-27 and Figure 7-28) are classified as expected.

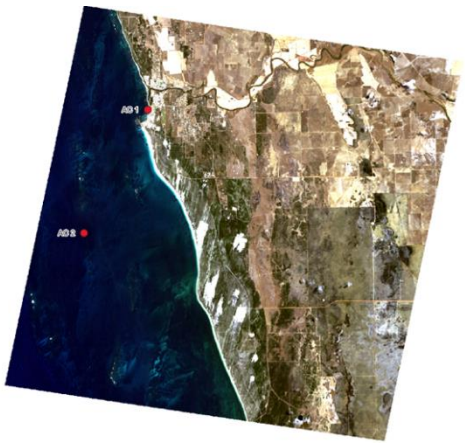

Figure 7-27 Scene-ID 169097; RGB-Quicklook with Bands 611.02nm – 550.69nm – 463.73nm

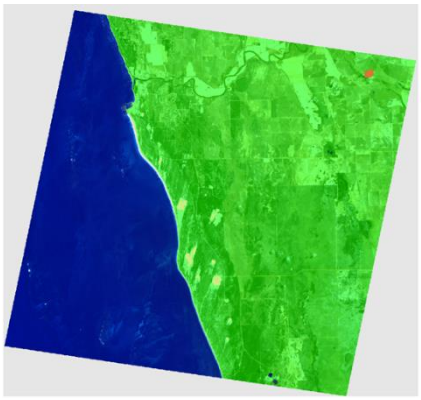

Figure 7-28 Scene-ID 169097; Geo Mask with Blue – Water, Green – Land, Orange – Clouds, Light-Grey – NA

- Cirrus and Adjacency Correction

Next, we check for the cirrus and adjacency correction using the two sites ‘AC1’ and ‘AC2’ shown in Figure 7-27.

The coordinates of the sample locations are as follows:

AC 1: LAT -29.26789005 | LON 114.92128392

AC 2: LAT -29.35498206 | LON 114.86761849

For sampling, we choose two locations, one located over shallow water, the other over deep water (see Figure 7-27 for the sample locations).

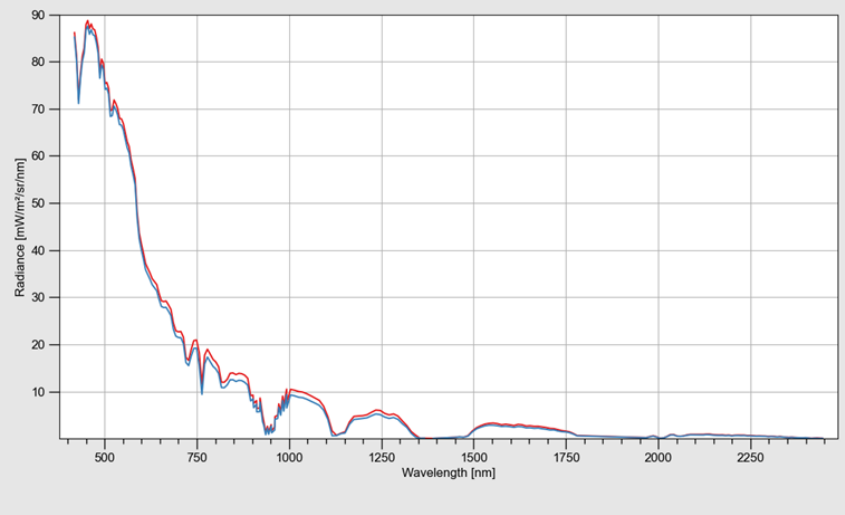

Figure 7-29 Scene-ID 169097; At-sensor-radiance sampled at location AC 1; red: measured, blue: adjacency corrected

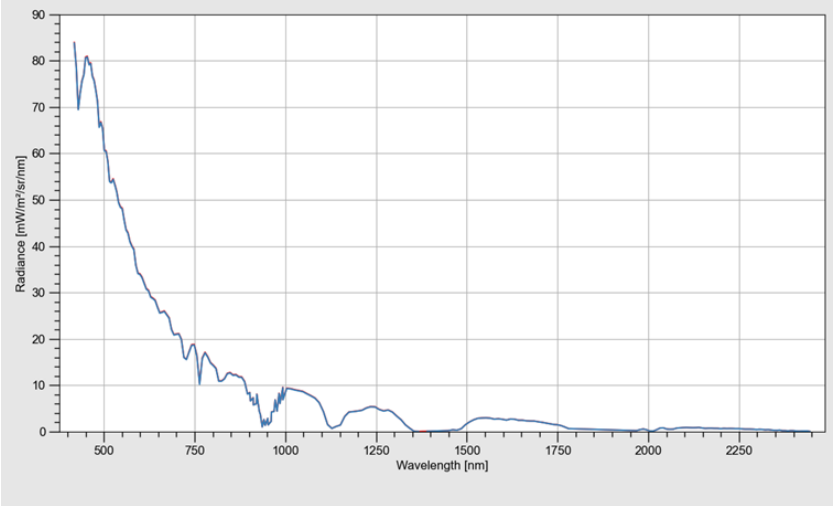

Figure 7-30 Scene-ID 169097; At-sensor-radiance sampled at location AC 2; red: measured, blue: adjacency corrected

Figure 7-29 and Figure 7-30 depict the sampled at-sensor-radiance - signal for location AC 1 AC 2, respectively. The effect of the applied correction is clearly visible in , due to the vicinity to bright land parts. In contrast, we cannot differentiate between the two curves plotted within . Here, the adjacency effect and thus the effect of the correction is supposed to be minimal, which is why the red curve is overlain by the blue one.

According to that, the adjacency correction works as intended.

- Reflectance Product

To get a better impression of the product normalized water leaving reflectance as the final one, shows the reflectance using the RGB channels 611.02nm, 550.69nm and 463.73nm.

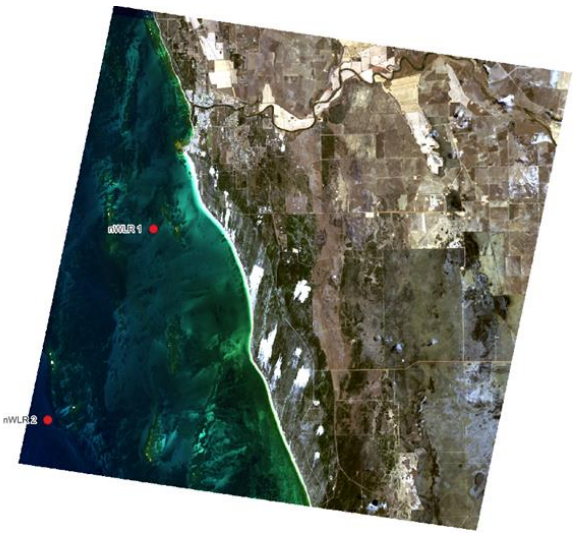

Figure 7-31 Normalized Water Leaving Reflectance of scene-ID 169097; wavelengths for RGB: 611.02nm – 550.69nm – 463.73nm

For the labeled locations in , the sampling coordinates are as follows:

nWLR 1: LAT -29.32534474 | LON 114.89489039

nWLR 2: LAT -29.43708774 | LON 114.82128007

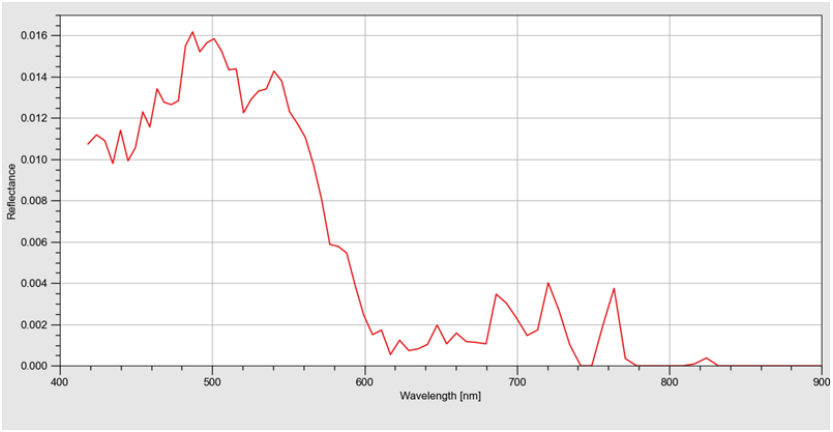

Figure 7-32 Scene-ID 169097; nWLR sampled at location nWLR 1

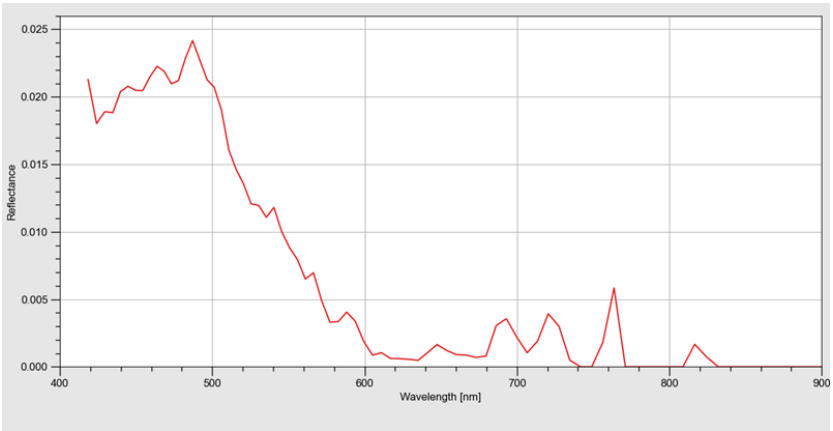

Figure 7-33 Scene-ID 169097; nWLR sampled at location nWLR 2

To evaluate the atmospheric correction, we sampled the normalized water leaving reflectance (nWLR) at the two locations ‘nWLR 1’ and ‘nWLR 2’ shown in Figure 7-32. We decided to locate nWLR 1 near the shore over optically shallow water. nWLR 2 was placed offshore over optically deep water. The spectrum plotted in Figure 7-32, as well as the one in Figure 7-33 show noisy characteristics over the full spectral range.

The reason for that is the presence of waves over the whole water body, as is depicted in Figure 7-33 below.

The sun glitter, caused by those waves, does affect the measured signal over the full spectral range. Especially its effect on the infrared region degrades the quality of the applied atmospheric correction, potentially leading to noisy spectra like shown above. An analysis of such datasets should be carried out very carefully, if at all.

Since the sun-glitter effect is not corrected, the atmospheric correction works as we expect it.

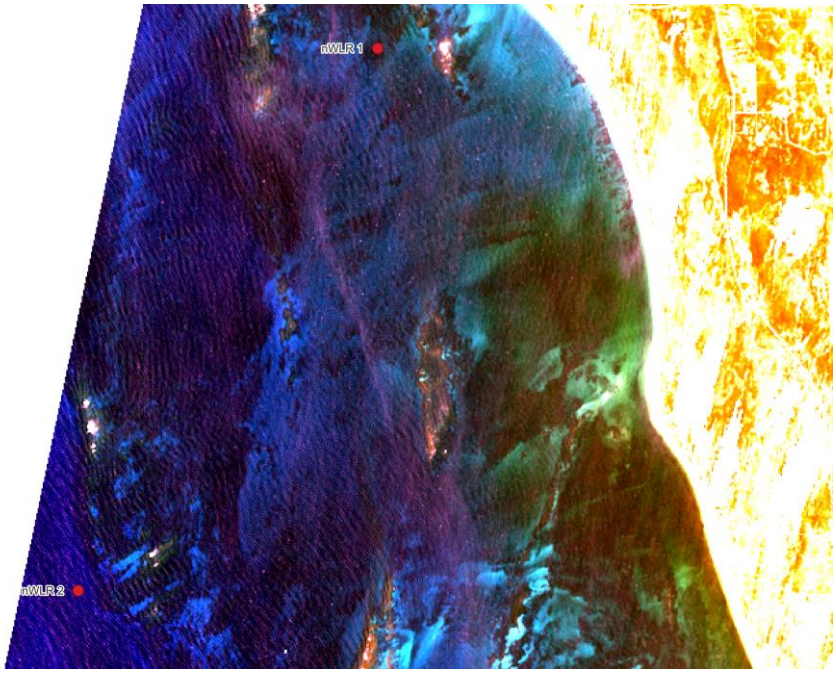

Figure 7-34 At-sensor radiance of scene-ID 169097 with adjusted histogram to depict present waves; wavelengths for RGB: 611.02nm – 550.69nm – 463.73nm

- Update for the generation of the quality mask

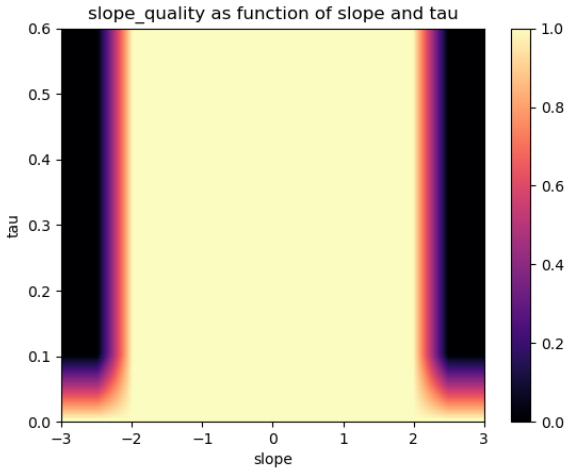

Figure 7-35 New quality range for slope

It was observed in relatively dark scenes, where the AOT was estimated to be close to or exactly zero, that the AOT slope quality could be zero even though it has little or no effect when AOT is close to zero. To circumvent this, the calculation of the aerosol slope quality was changed to depend on both AOT and aerosol slope (see Figure 7-35) as follows: If AOT > 0.1, the quality depends on the AOT slope only and linearly decreases from one (good quality) to zero (bad quality) for very large values (AOT slope larger than 2) and very negative values (AOT slope smaller than -2). Only in the case where AOT < 0.1 the quality depends on both AOT and AOT slope, preventing low quality values as AOT decreases.

Figure 7-36 RGB-Quicklook of scene-ID 164236; wavelengths for RGB: 611.02nm – 550.69nm – 463.73nm

The effect of the updated slope quality can be observed in a scene from Turkey, see Figure 7-36. The slope quality for pre-update and post-update are shown in Figure 7-37 and Figure 7-38, respectively. The AOT value for this clear scene is close to zero, but the slope quality in the pre-update version shows a pattern with many pixels with zero quality due to large absolute values of the AOT slope. In the post-update version, this effect is strongly reduced, and the AOT slope quality is predominantly larger than 0.8, which does not indicate a quality issue due to AOT or AOT slope.

Figure 7-37 pre-update: slope quality of scene-ID 164236; grayscale between 0 (bad quality, black) and 1 (good quality, white)

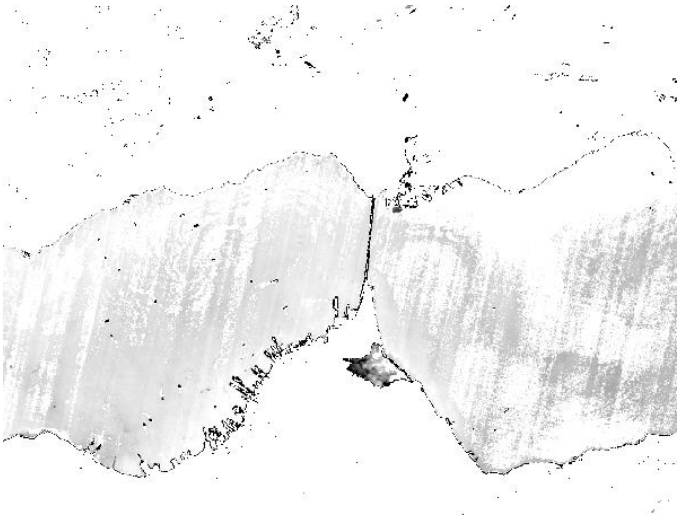

Figure 7-38 post-update: slope quality of scene-ID 164236; grayscale between 0 (bad quality, black) and 1 (good quality, white)

- Update height-handling within atmospheric correction over water

Up to now, a fixed value was used for the surface altitude within the correction workflow. Recently we found, that using such fixed value does lead to the presence of dark pixels in the final reflectance product, especially in case of lakes located in high altitudes. To overcome this, the recent update implements the usage of the actual height of the respective water body as described below.

The adjacency correction uses an effective surface altitude which is obtained by averaging over all pixels in the scene.

The atmospheric correction uses a per-pixel value of the surface altitude which is stored in a DEM.

Figure 7-39 RGB-Quicklook of scene-ID 148819; wavelengths for RGB: 611.02nm – 550.69nm – 463.73nm

Figure 7-39 shows the RGB – Quicklook of the scene we used to test the mentioned update. The lake in focus is the Plansee in Austria, located at a mean height of about 1400m.

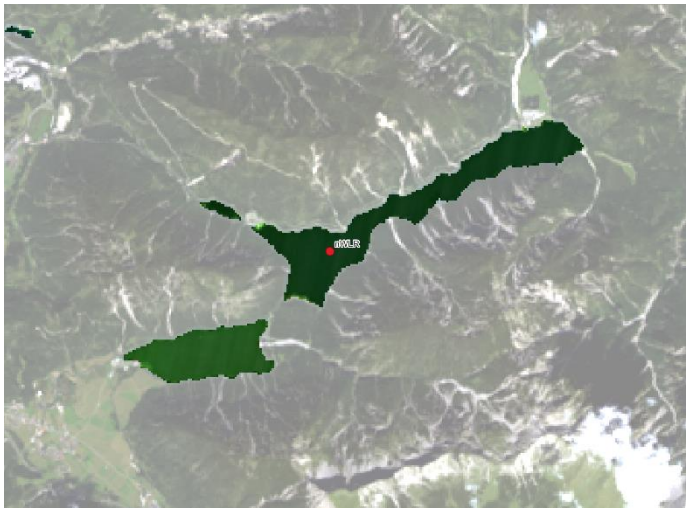

Figure 7-40 Pre-Update: nWLR of scene-ID 148819; wavelengths for RGB: 611.02nm – 550.69nm – 463.73nm

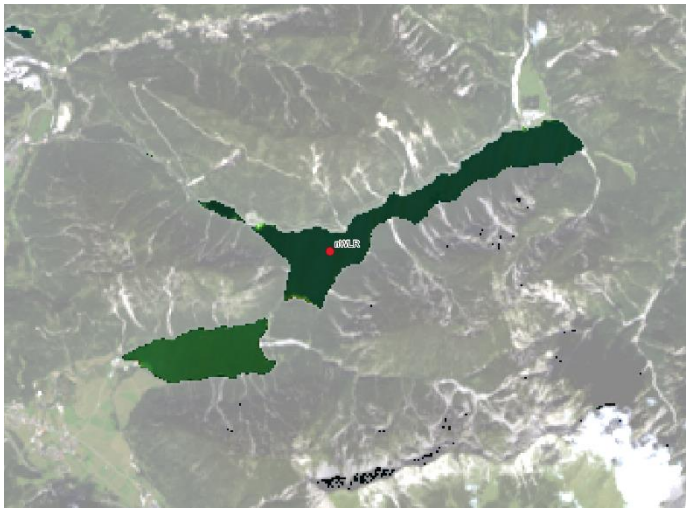

Figure 7-41 Post-Update: nWLR of scene-ID 148819; wavelengths for RGB: 611.02nm – 550.69nm – 463.73nm

Figure 7-40 and Figure 7-41 show the nWLR based on the pre-update processor version and the post-update version, respectively. Obviously, the effect of the update is barely visible using the shown RGB images. Thus, we sampled the signal at the location 'WLR', placed at the following coordinates:

nWLR: LAT 47.46977409 | LON 10.80091398

The resulting spectra are plotted in Figure 7-42. The plot does clearly show that using the actual height increases the resulting reflectance, especially in the blue and green region, in order to avoid dark pixels.

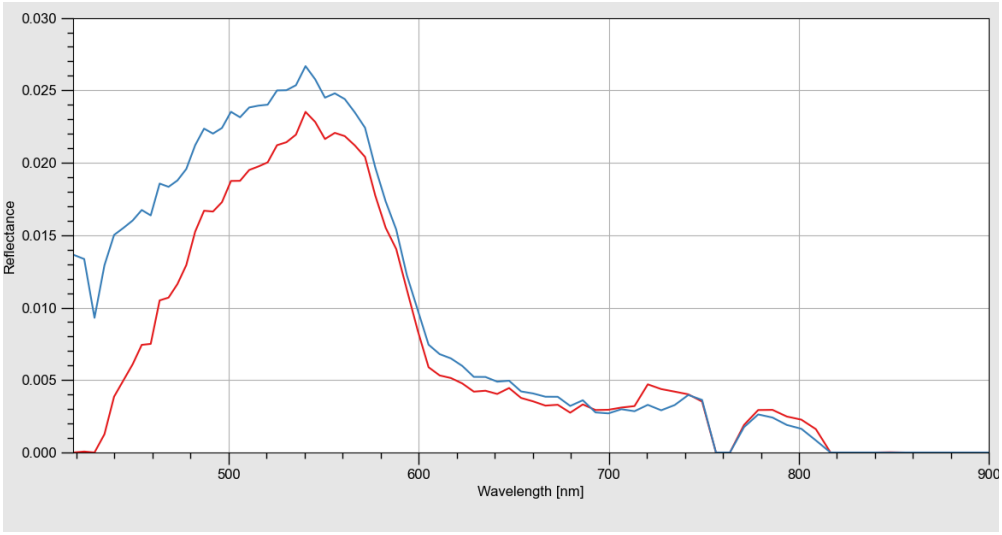

Figure 7-42 Scene-ID 148819; nWLR sampled at location nWLR; red: Pre-Update, blue: Post-Update

Figure 7-43 RGB-Quicklook of scene-ID 026843; wavelengths for RGB: 611.02nm – 550.69nm – 463.73nm

Figure 7-43 shows the RGB – Quicklook of another scene at an even more elevated water body, namely the Reserva National de Junin close to Lima in Peru located at a height of about 4100m.

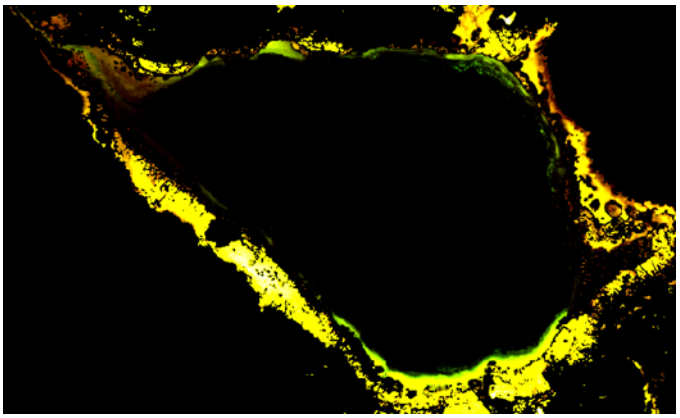

Figure 7-44 Pre-Update: nWLR of scene-ID 026843; wavelengths for RGB: 611.02nm – 550.69nm – 463.73nm

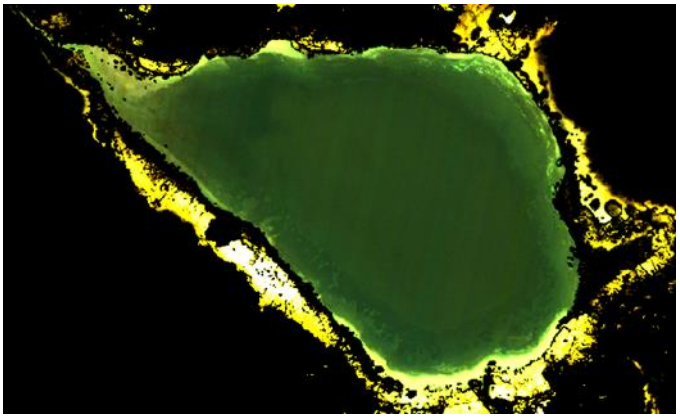

Figure 7-45 Post-Update: nWLR of scene-ID 026843; wavelengths for RGB: 611.02nm – 550.69nm – 463.73nm

Figure 7-44 and Figure 7-45 show the nWLR based on the pre-update processor version and the post-update version, respectively. In the pre-update version, almost all pixels of the water body are completely

dark, in contrast to the post-update version. Figure 7-46 shows the spectra located at the sampling position. The post-update version yields a reasonable water spectrum.

nWLR: LAT -11.003097 | LON -76.140278

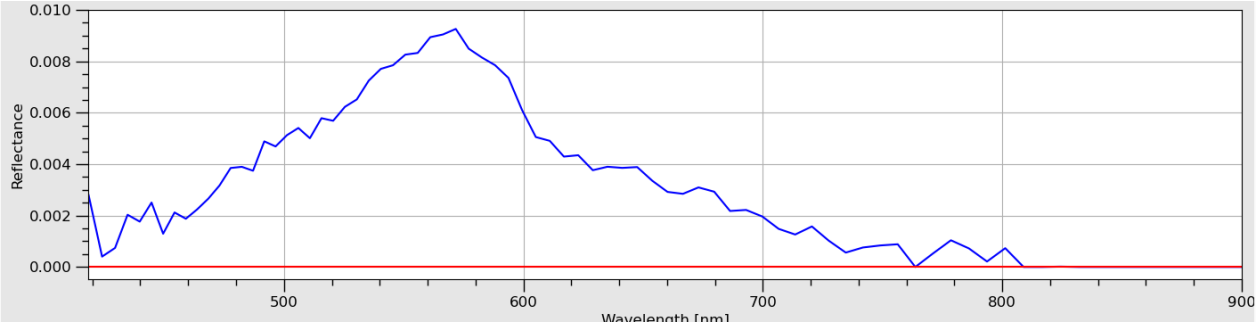

Figure 7-46 Scene-ID 026843; nWLR sampled at location nWLR; red: Pre-Update, blue: Post-Update

7.6.4.2 **Validity of generated L2A "land" data**

7.6.4.2.1 Analyzed scenes

Within the time interval between 01.10.2025 to 31.12.2025, an interactive in-depth analysis has been conducted for the following scenes:

Datatake -ID	Tile -ID	date	location	L2A option	cirrus and haze removal	Archived Version	processor version	Overall Quality	Quality Atm
167963	002	2025-12-18	Pinnacles, Australia	land	no	01.05.05	V010505	Nominal	Reduced
170303	005	2025-12-24	Near Groenfontein nature reserve, South Africa	land	no	01.05.05	V010505	Nominal	Nominal
164124	013	2025-11-11	Near Kassala, Eritrea.	land	no	01.05.05	V010505	Nominal	Nominal
168082	004	2025-12-13	Near La Ronge, Saskatchewan Canada	land	no	01.05.05	V010505	Reduced	Reduced (*) (SZA = 79°)
170541	003	2025-12-13	Near Chabarowsk Russian-China border region	land	no	01.05.05	V010505	Low	Low (SZA = 71°)

Table 7-26 Datatake IDs of analyzed land products

(*): note: quality atm. rating for L0 is "low"; reasons for this discrepancy are currently investigated.

For the selection of L2A data, several data takes acquired within the reporting period and covering different landscapes at different conditions were analyzed.

7.6.4.2.2 Data Checks

In the following, the different tiles were checked for the shape and magnitude of the BOA_ref spectra, and also the quality of the generated masks is evaluated when meaningful.

For all tiles the visual image impression is fine. For the masking, there are known issues of mis-classifications which are currently being investigated. The BOA_ref spectra all show the typical shape and magnitude, indicating the correct L2A correction.

- **Pinnacles, Australia (DT167963, 2025-12-18)**

The area over the Pinnacles test site depicted in Figure 7-47 and Figure 7-48 has been successfully observed in many EnMAP datatakes since the commissioning phase. For the masking (see Figure 7-49), as before, an incorrect flagging of parts of the bright beach sands at the coast with snow occurs, but inland bright sands are correctly excluded from the snow mask. This is likely caused by the high spectral similarity of slightly wet beach sands and snow/ice spectra, and can be tolerated. The flagging of haze-affected areas (Figure 7-49) over areas close to the sea seems plausible, while the flagging of a single cloud over bright inland sands is likely incorrect. Overall, the generated masks are as expected widely correct, showing only minor shortcomings.

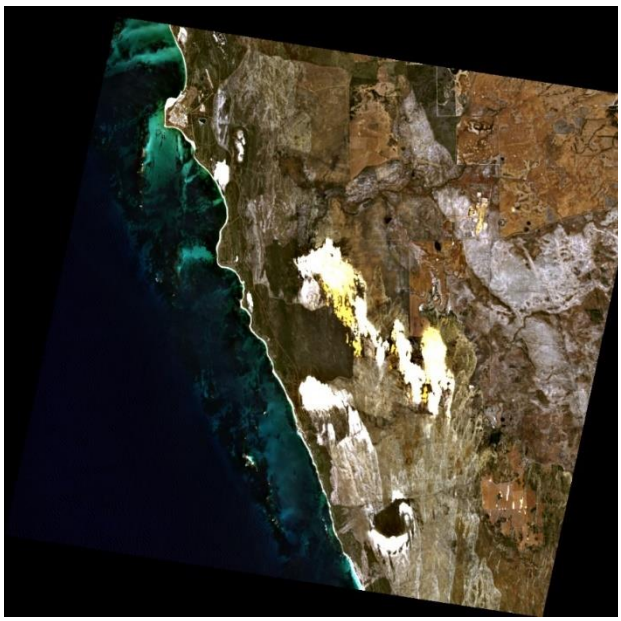

Figure 7-47 DT167963, true color composite

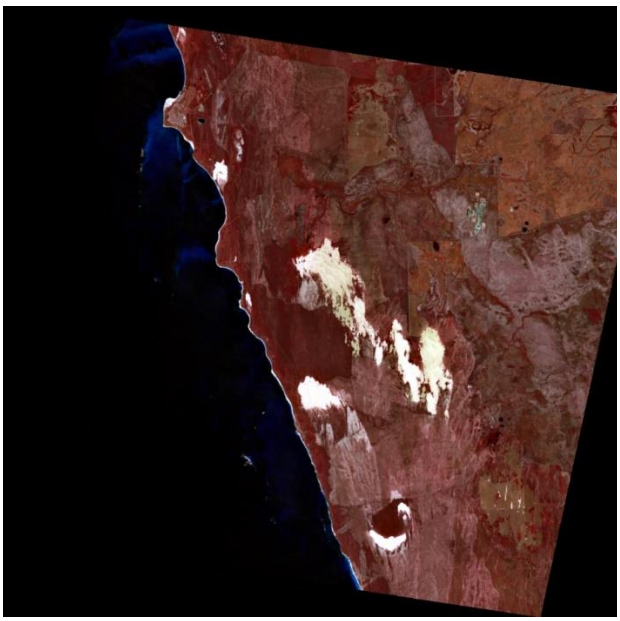

Figure 7-48 DT167963, CIR composite

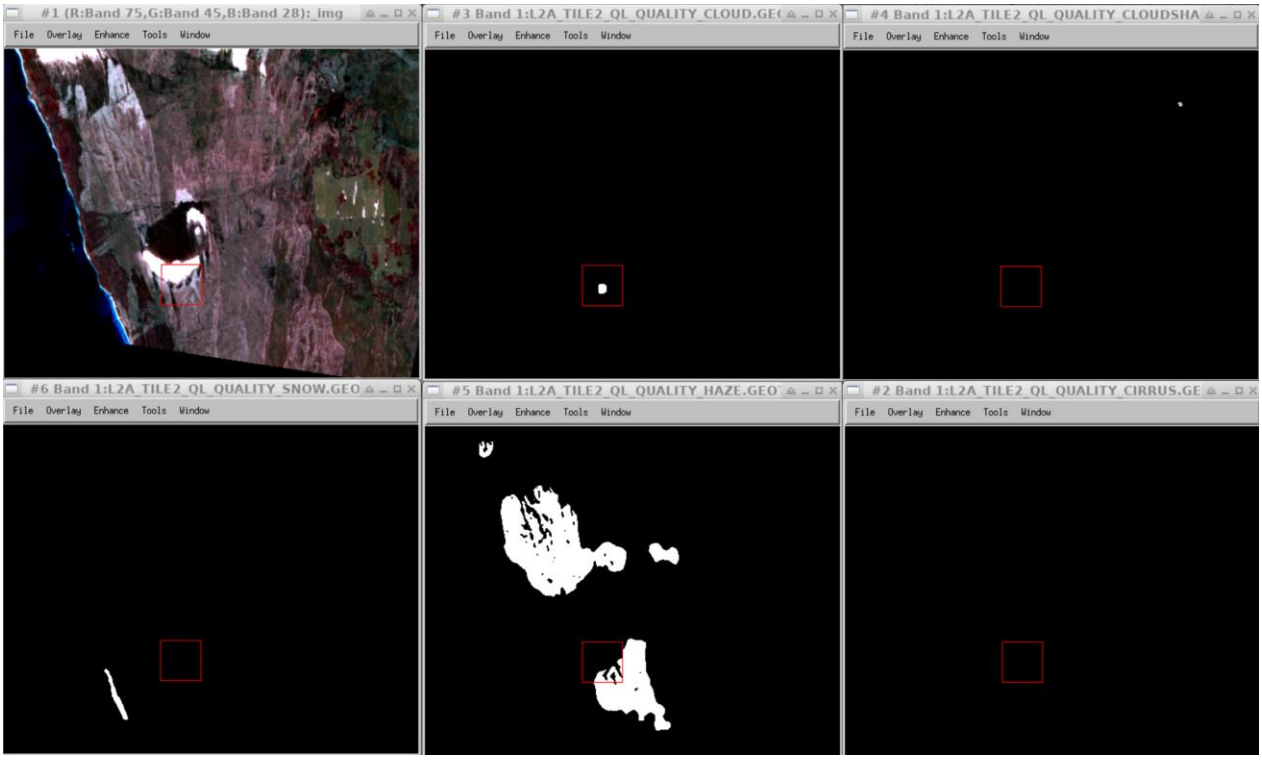

Figure 7-49 DT167963, from top left to top right: CIR image, cloud mask, cloud shadow mask; bottom left to bottom right: snow mask, haze mask, cirrus mask. Note that all other masks correctly empty and thus not depicted.

When having a look at the BOA reflectance spectra (Figure 7-50), the spectra of green and dry vegetation, as well as soil are as expected regarding shape and overall reflectance. Also, the water spectra (Figure 7-51) resulting from the “land” L2A processing are as expected, showing the correct processing.

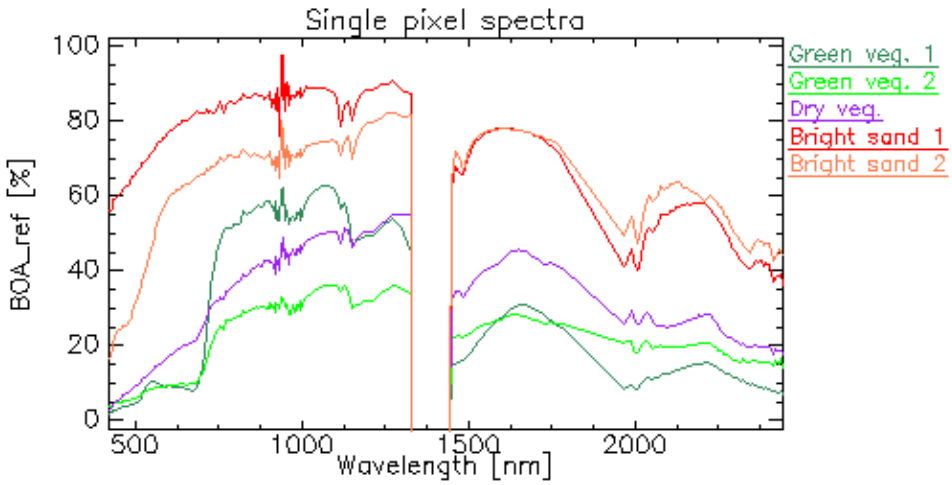

Figure 7-50 DT167963, single pixel spectra over land

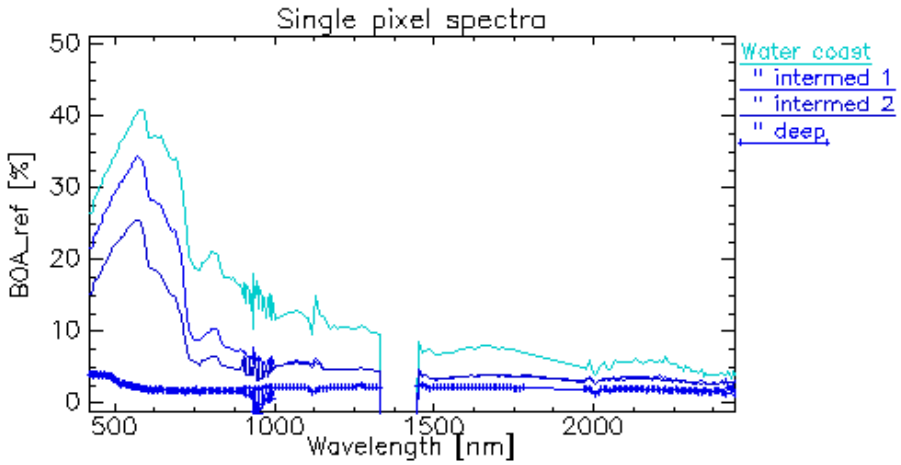

Figure 7-51 DT167963, single pixel spectra over water

- **Near Groenfontein nature reserve, South Africa (DT170303, 2025-12-24)**

The Groenfontein scene is located in a mountainous region (~14000 – 2000m a.s.l.). The L2A image impression of this scene (Figure 7-52) is clear, and the effects from terrain are well corrected with no major artefacts showing up.

The resulting BOA spectra show all typical features (Figure 7-53), with a slight overcorrection of the very dark irrigation ponds in the NIR region, resulting in a slightly negative reflectance.

Regarding the masking (Figure 7-54), the masks for snow, cloud, cirrus all correctly empty, and the haze mask is plausible. Only some water ponds are incorrectly flagged as cloud shadows due to the low overall reflectance (see Figure 7-53).

Overall, the L2A processing of this scene is valid and as expected.

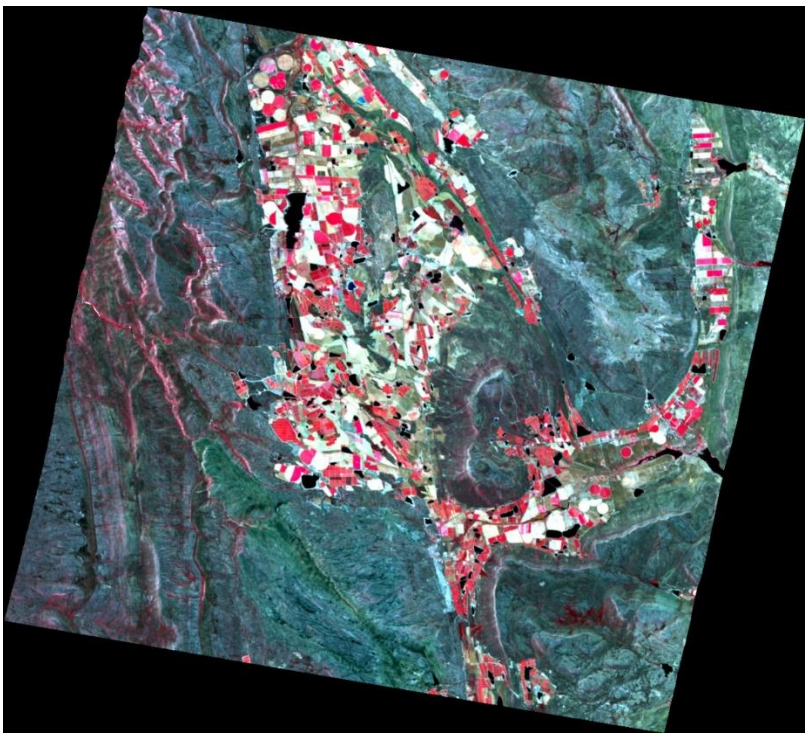

Figure 7-52 DT170303, CIR image

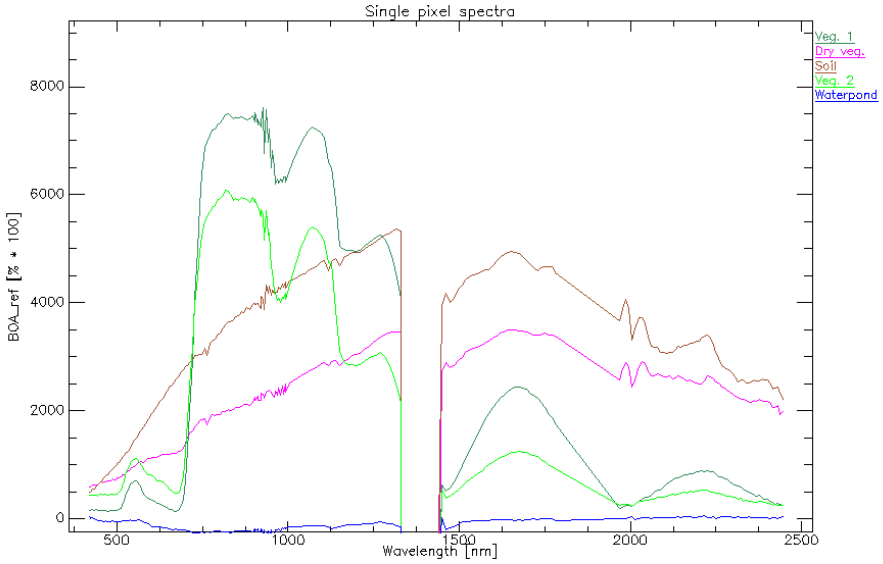

Figure 7-53 DT170303, single pixel spectra

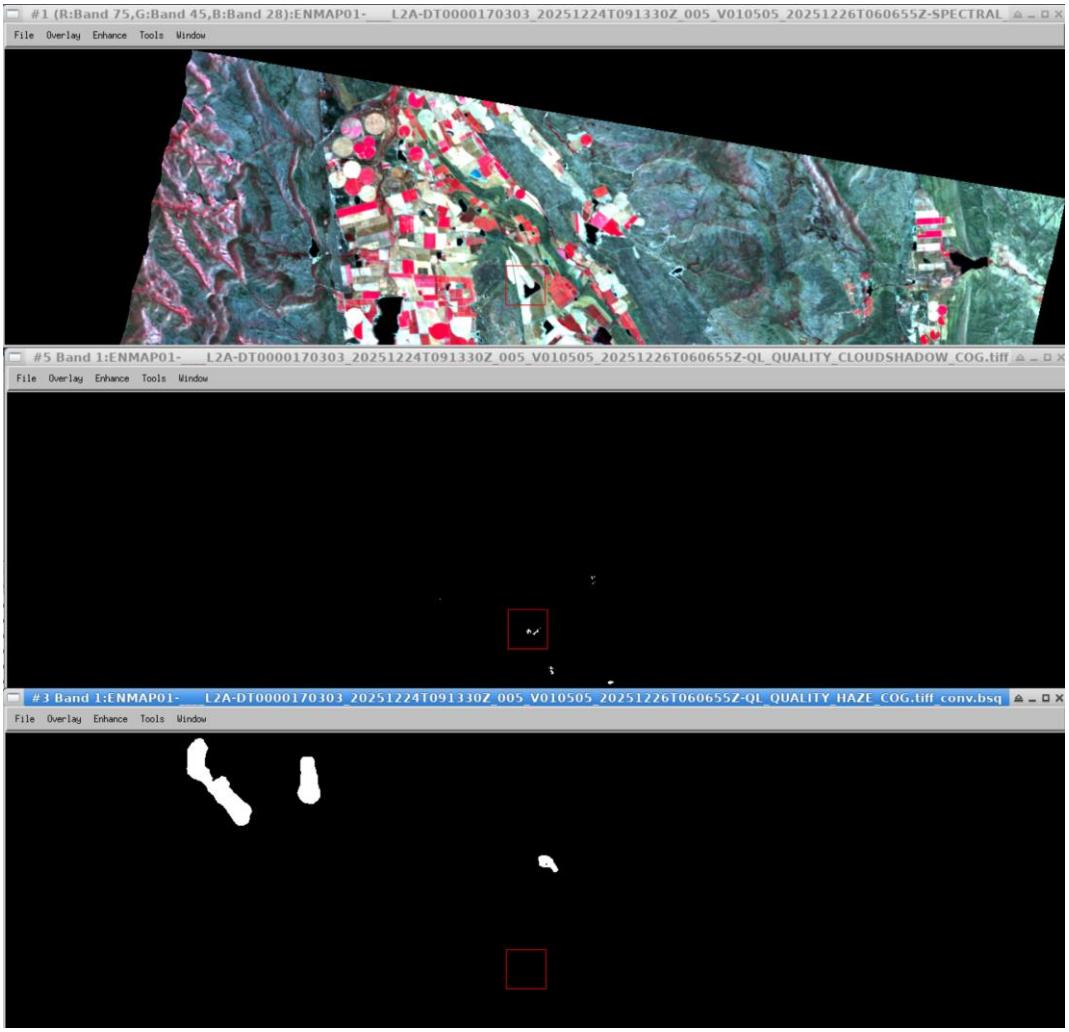

Figure 7-54 DT170303, from top to bottom: CIR composite (subset), cloud shadow mask, haze mask (all other masks correctly empty)

- **Near Kassala, Eritrea (DT164124, 2025-11-11)**

The EnMAP datatake acquired over Eritrea (Figure 7-55) shows the typical properties of a dryland scene, with the expected spectra of green and dry vegetation, bare soil and some dark (likely burnt) vegetation-free patches, which are shown in Figure 7-56. These spectra show the typical shape, spectral features and overall intensities, as well as the known shortcomings of EnMAP in the VNIR-SWIR detector overlay region. For the generated masks (Figure 7-57), the haze mask is generally plausible, as flags occur in areas of irrigated agriculture. But as haze is also flagged over build-up areas, this might be an incorrect confusion between classes. All other masks are correctly empty, indicating that dark (burnt) areas are not confused as cloud shadows.

Also for this scene, the L2A processing results in a dataset having the typical high EnMAP quality.

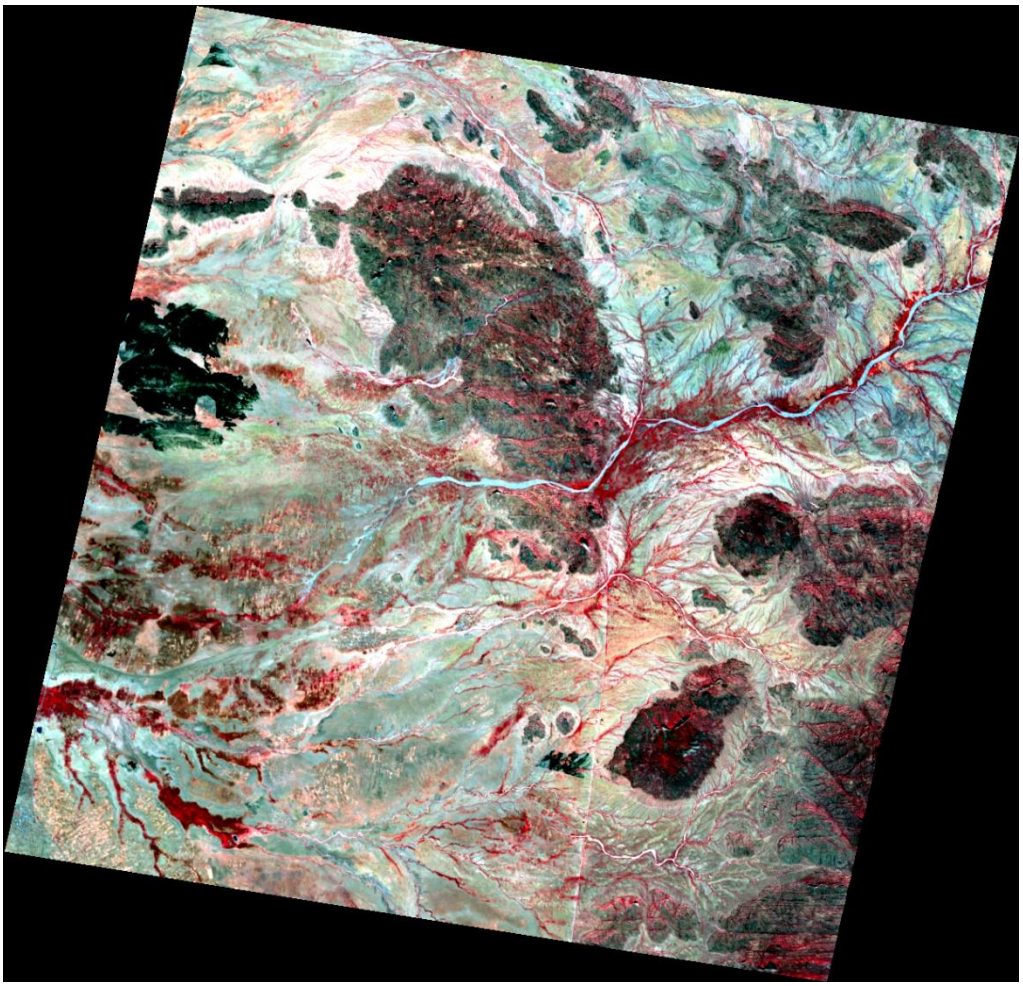

Figure 7-55 DT164124, CIR composite

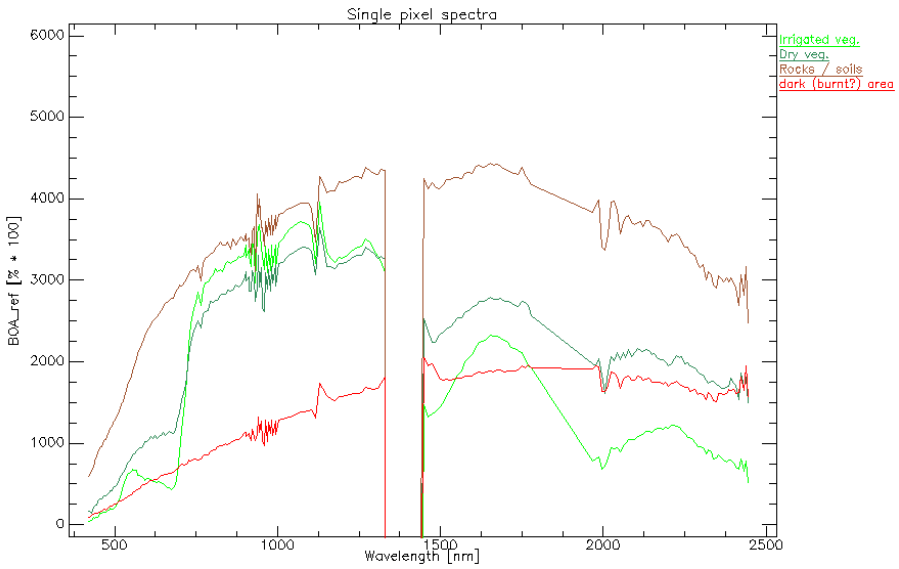

Figure 7-56 DT164124, single pixel spectra

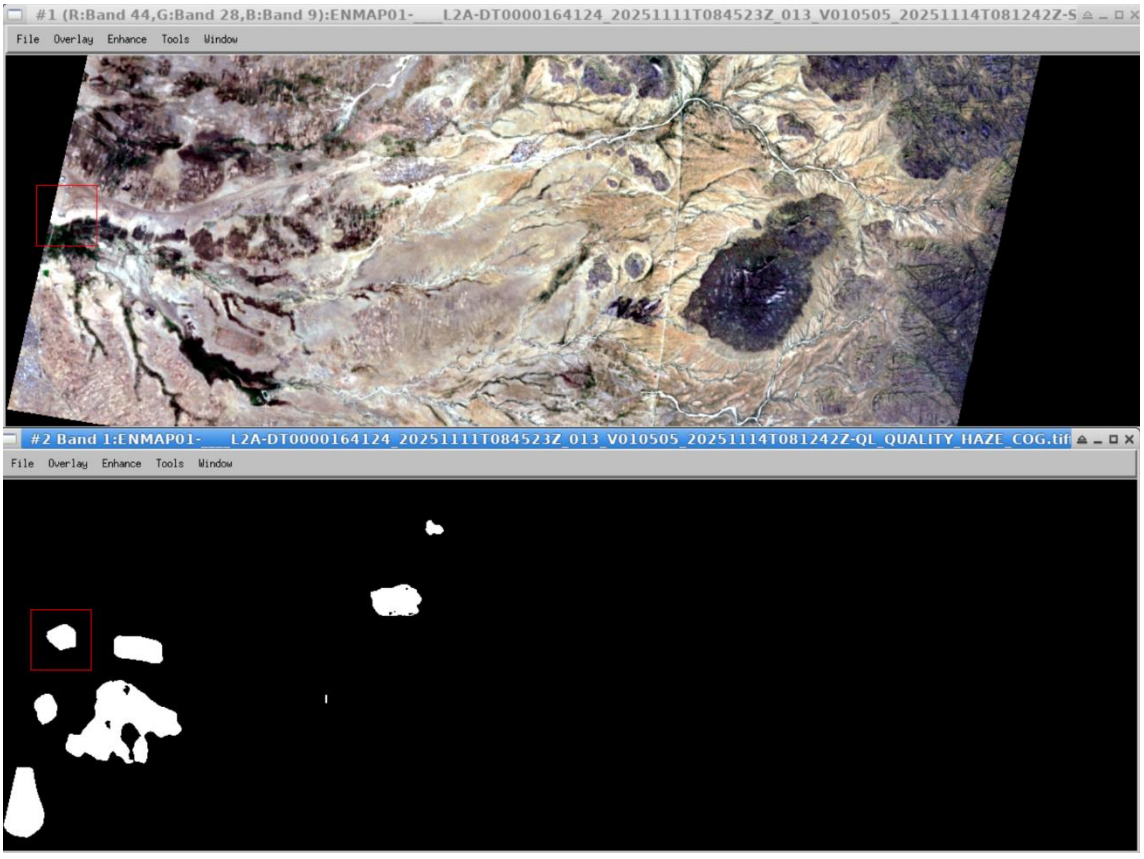

Figure 7-57 DT164124, top: true color composite (subset); bottom: haze mask; all other masks are correctly empty.

- **Near La Ronge, Saskatchewan Canada (DT168082, 2025-12-13)**

As a known shortcoming of the L2A processor for some snow & ice scenes was fixed in processor version 01.05.05, two such scenes processed with the improved processor were included in the QC checks.

It must be pointed out that these scenes were acquired having low light conditions (SZA of the La Ronge scene of 79°, and 71° for the Chabarowsk scene), thus having “reduced” or “low” overall quality ratings.

The scene acquired near La Ronge, Canada (Figure 7-58) shows a mixture of snow-covered rocks, snow and ice-covered inland lakes, and vegetation (shrubs and forests). For the generated masks (Figure 7-59), the snow mask is accurate, including all areas covered by snow & ice. Next, only one area of haze is detected over a dark rocky area, which is only a minor problem. More severe is the extent of the masked clouds, which incorrectly includes many snow- / ice-covered areas, many of which are already included in the snow mask. But as stated before, the overall quality of this scene is reduced due to the low-light conditions originating from the high Solar zenith angle of 79°.

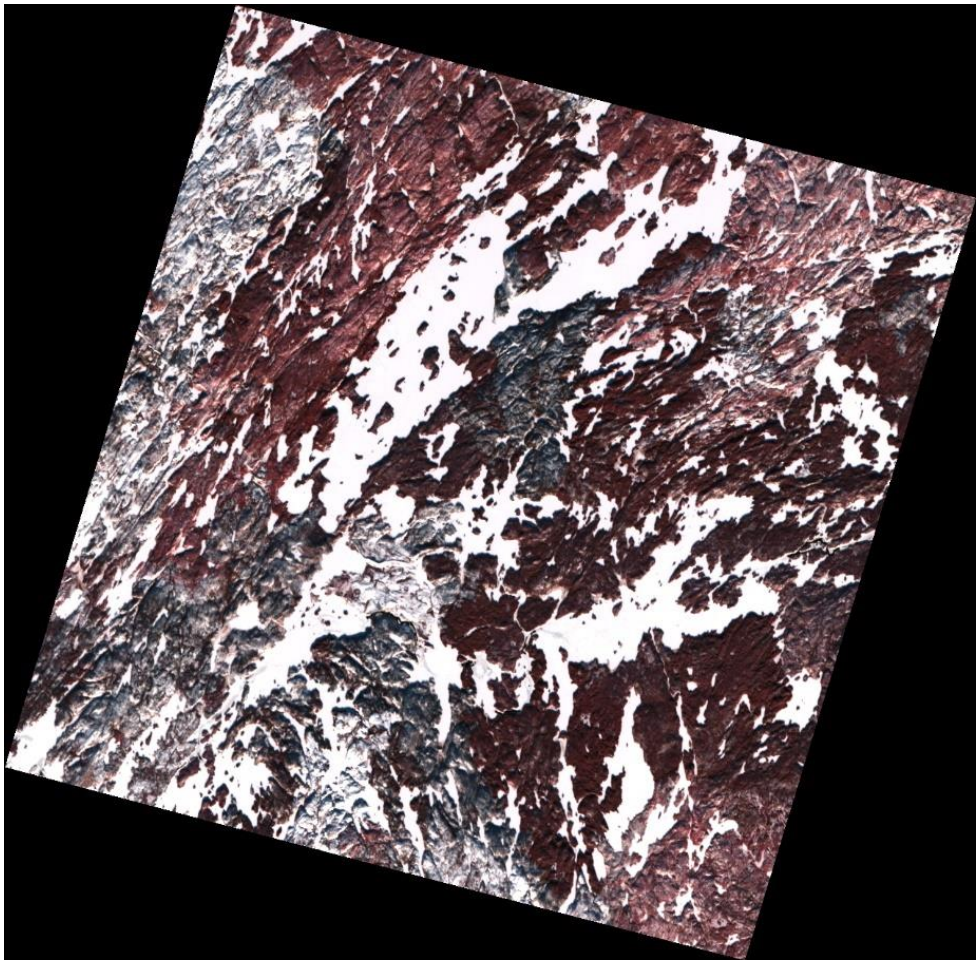

Figure 7-58 DT168082, CIR composite

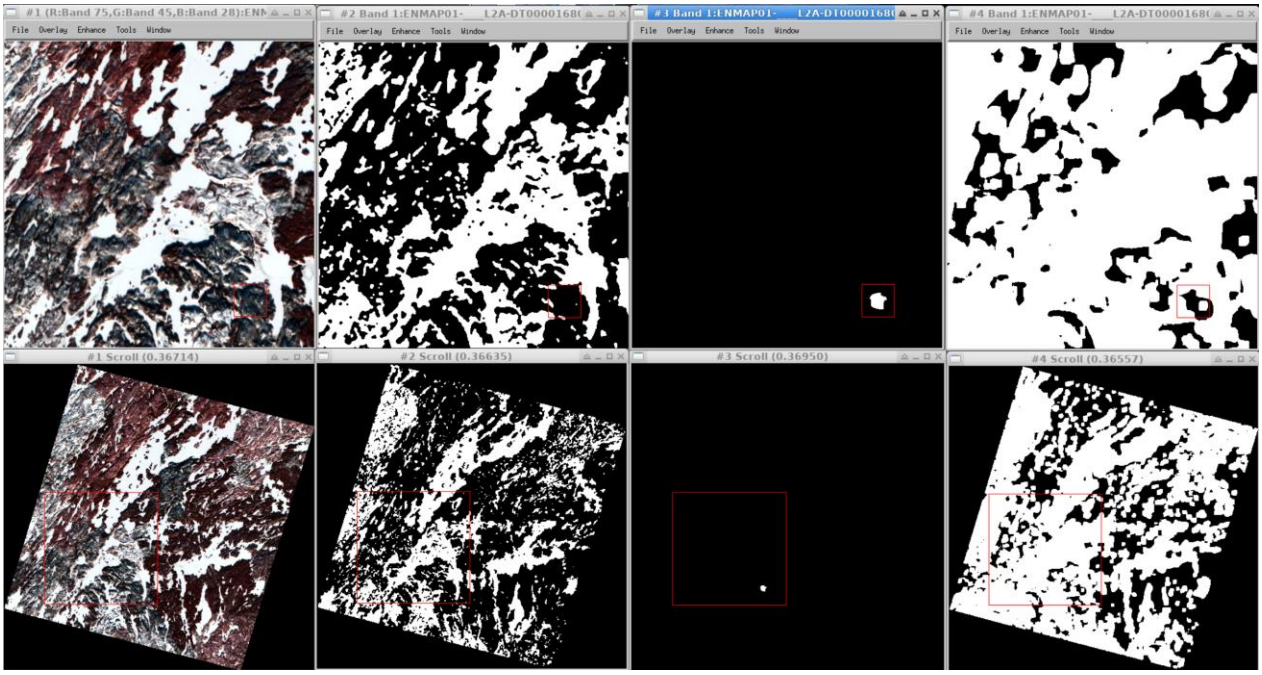

Figure 7-59 DT168082, from left to right: CIR composite (subset), snow mask, haze mask, cloud mask; all other masks are correctly empty.

Regarding the retrieved spectra (Figure 7-60), the shape and intensity look plausible. Given that there is likely a snow layer underneath the vegetation (shrub / small trees) causing a mixed signal in some cases, the sometimes higher signal in the VIS range can be explained.

When checking spectra of pure snow and ice pixels (Figure 7-61), these spectra are as expected, and no longer showing the incorrect “spikes” in the VIS (compare Figure 7-62 showing an extreme example from an older processor version and another scene).

To conclude, with the new processor version, the snow and ice spectra were improved for this scene, and the snow mask is accurate, while shortcomings in the cloud mask exist.

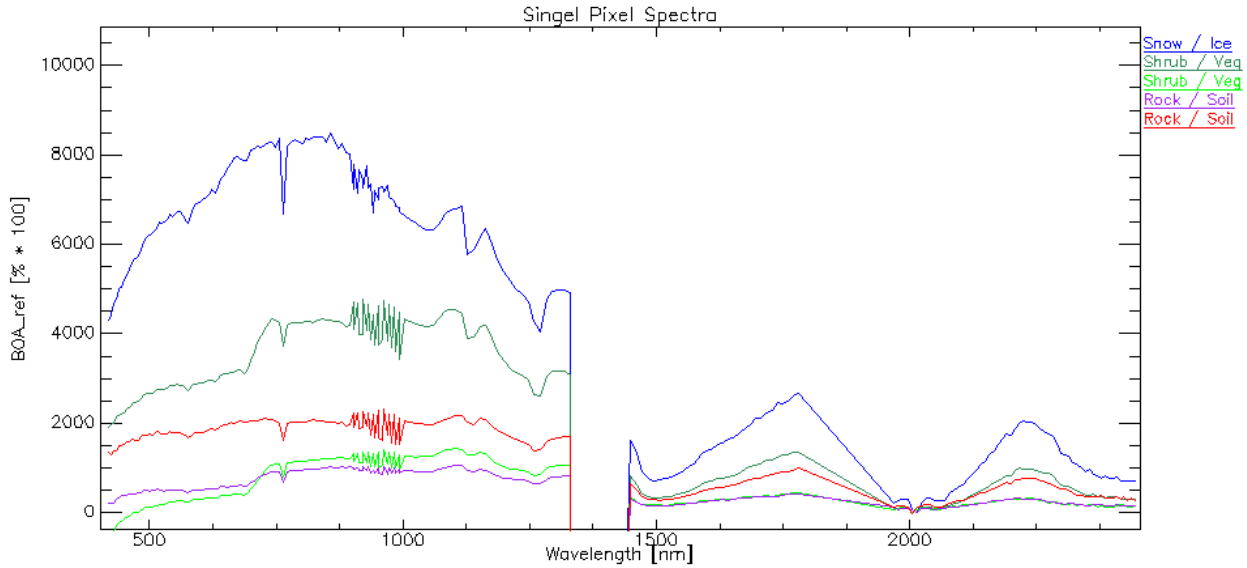

Figure 7-60 DT168082, single pixel spectra of different materials; note that there's likely a snow coverage beneath the vegetated areas causing a mixed signal.

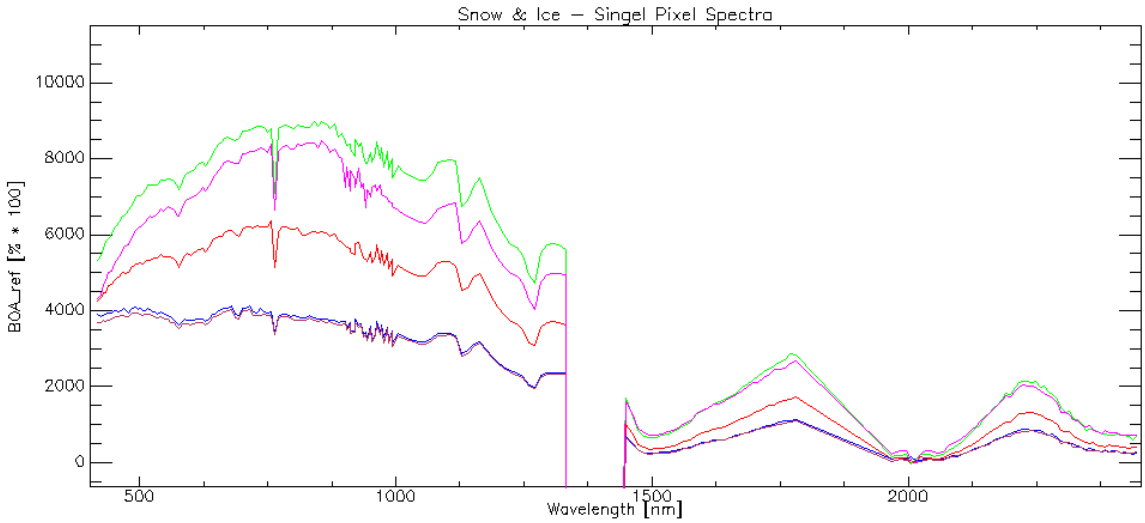

Figure 7-61 DT168082, single pixel spectra of various snow and ice surfaces

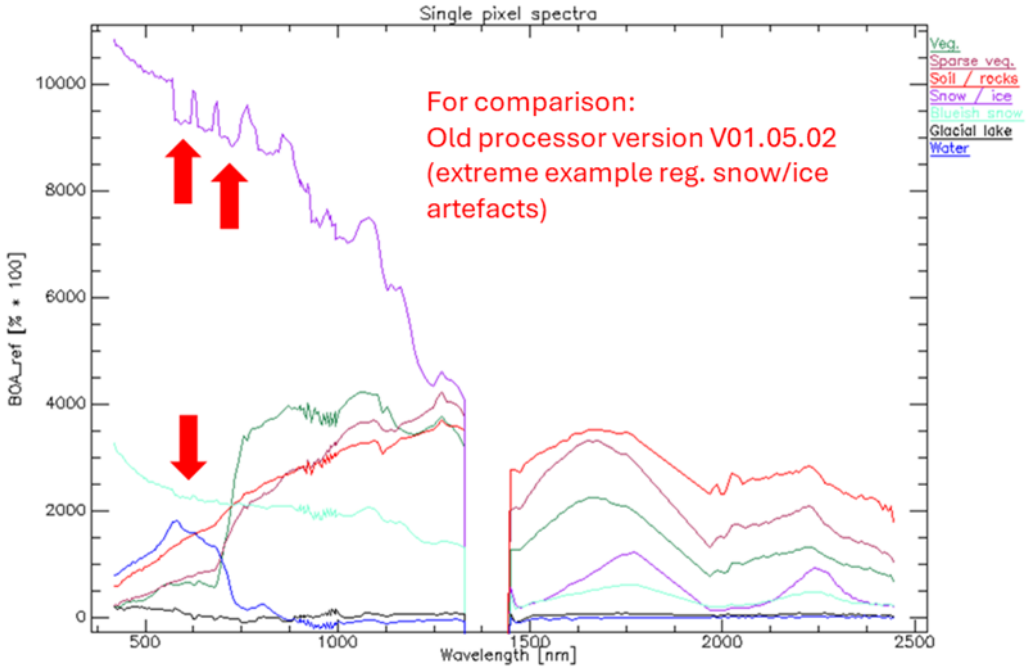

Figure 7-62 For comparison – extreme examples of previous processor shortcomings reg. ice and snow (different scene from 2025)

- **Near Chabarowsk, Russian-China border region (DT170541, 2025-12-13)**

As with the scene from Saskatchewan described before, also for this scene over Chabarowk the quality rating is “low” due to low-light conditions (SZA of 71°). This scene (Figure 7-63) also contains snowy regions, vegetation (likely with snow underneath), and also mountainous terrain in the northern part with some areas tilted towards the sensor thus having at some locations a more favorable sun illumination angle.

Most important, when checking the spectra of snow and ice (Figure 7-64), also for this scene the spectra look as expected, no longer showing the artefacts of the previous processor version. And also spectra of other materials show the typical shape and overall intensities (see Figure 7-65).

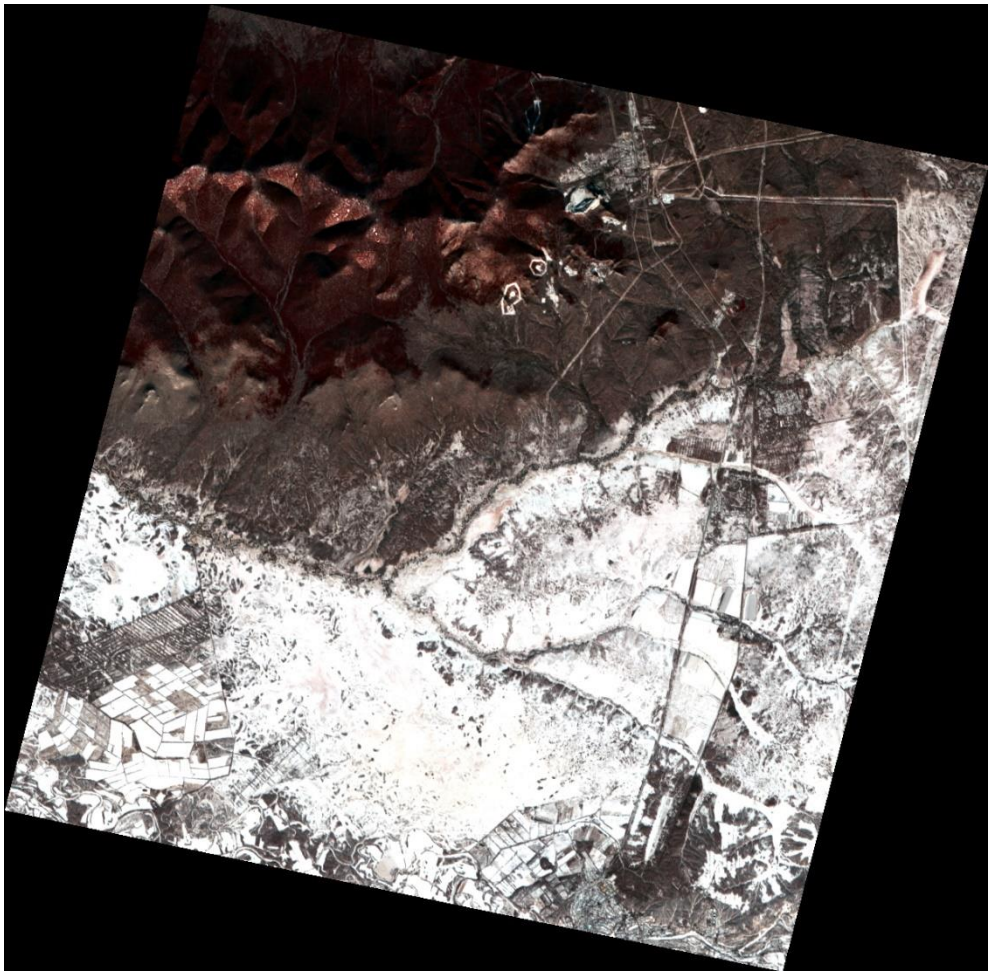

Figure 7-63 DT170541, CIR composite

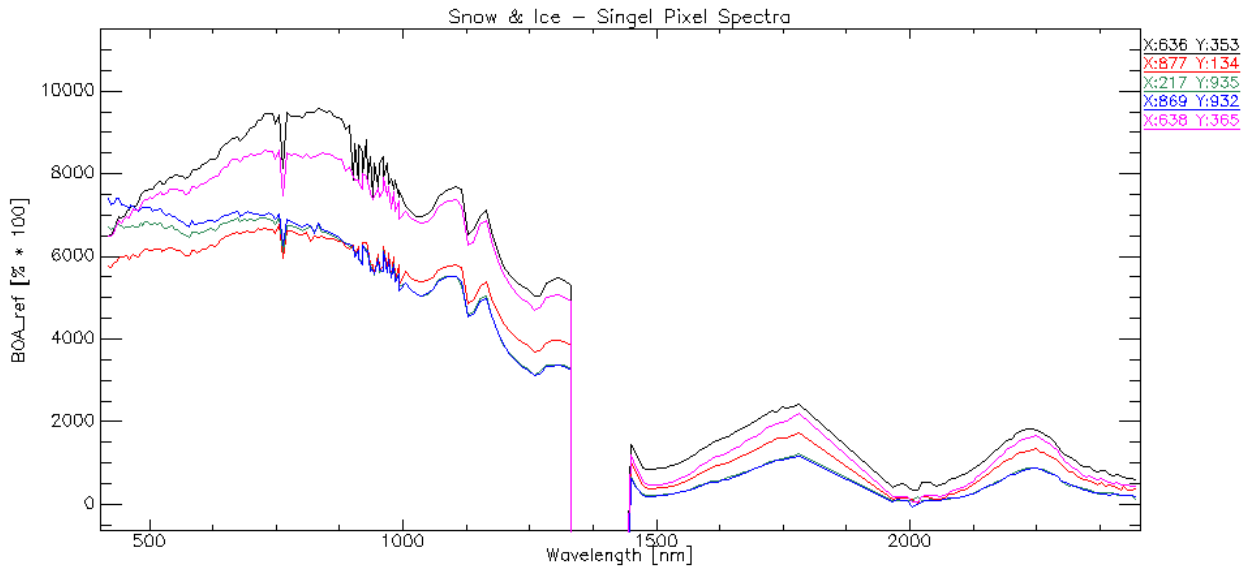

Figure 7-64 DT170541, single pixel spectra of snow and ice surfaces

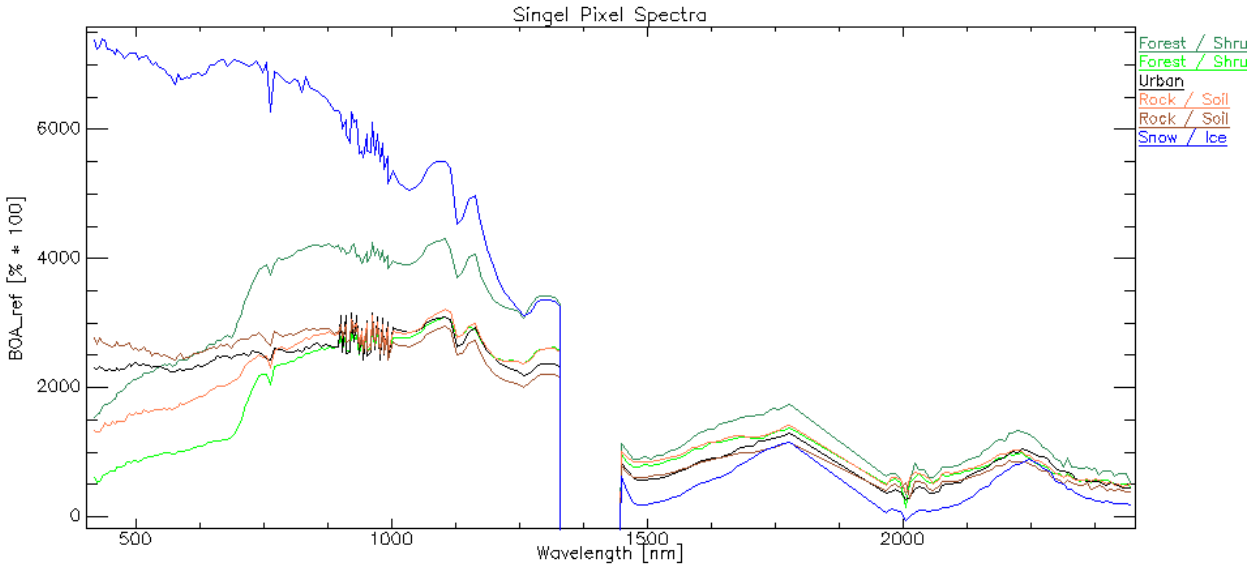

Figure 7-65 DT170541, single pixel spectra of various materials

For the generated masks (Figure 7-66), the snow mask is correctly flagging also smaller snow-covered areas like clearcuts of along roads. The haze mask is also mostly plausible, with some areas in deeper terrain shade also flagged (likely incorrect). But as with the scene before, the cloud mask also includes many -but not all- of the snow / ice areas, indicating problems for the separation of these classes in low-light conditions.

Thus, also for this scene the processing is valid, with the previous artefacts in snow & ice spectra corrected. As before, the snow mask is accurate, while the cloud mask incorrectly includes also snow pixels, at least for this low-light scene.

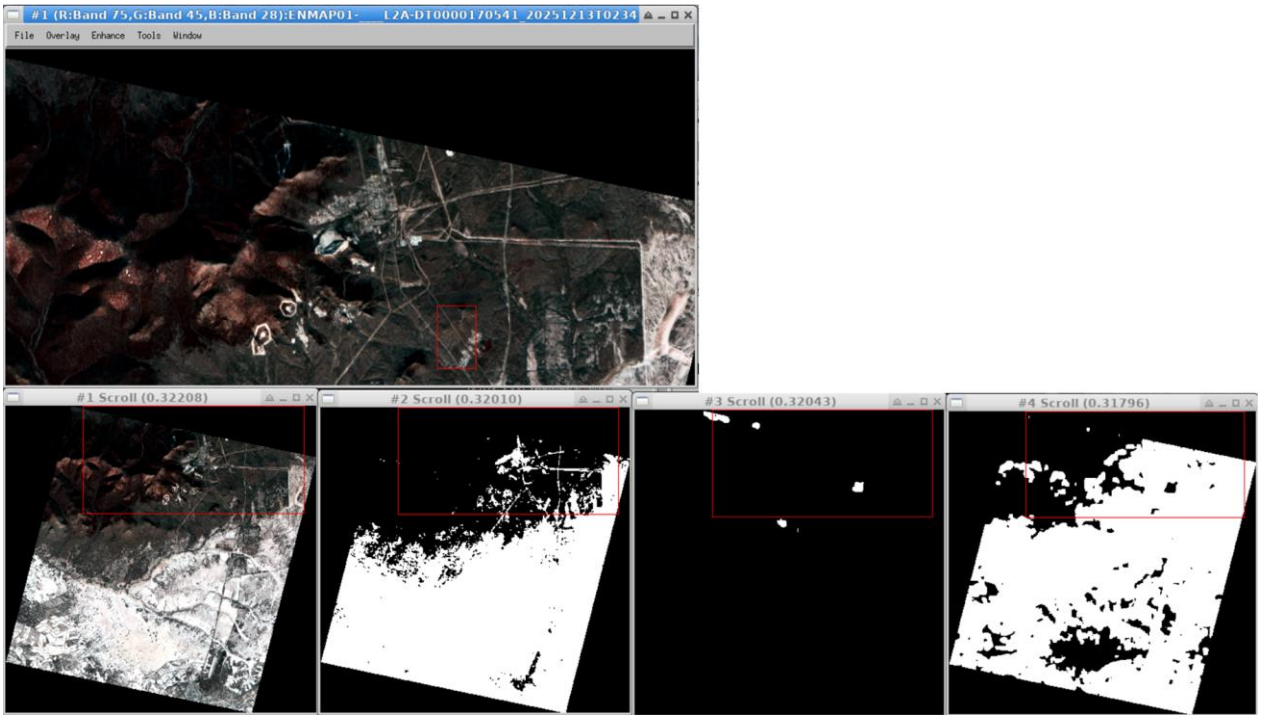

Figure 7-66 DT170541, top: CIR composite (subset); bottom row from left to right: CIR composite, snow mask, haze mask, cloud mask (all other masks are correctly empty).

8 External Product Validation

The standard quality parameters were validated in the external product validation process for the reporting period. The validation included 105 Level 1B, 182 Level 1C and 147 Level 2A products.

8.1 Level 1B

The following validation scenarios were performed to validate Level 1B products:

- TOA Radiance
- Signal-to-Noise Ratio (SNR)

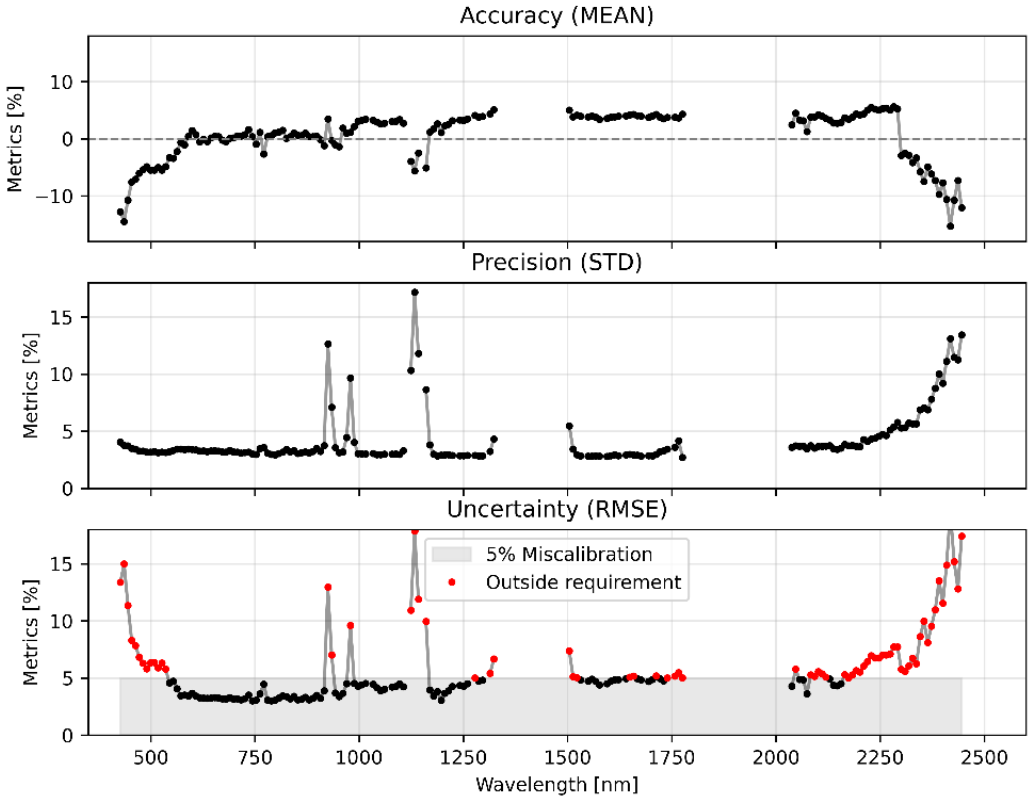

Figure 8-1 Errors between EnMAP TOA radiance and propagated TOA radiance from in situ measurements against wavelength for all arid validation sites based on 42 matchups.

New in situ data for the HYPERNETS station Gobabeb (GHNA) were recently published on the LAND HYPERNETS portal, downloaded, and successfully integrated into the TOA radiance and BOA reflectance validation. This increased the number of available matchups for the TOA radiance validation from 33 to 42. Also with the higher sample size, the results remain consistent with the previous report (MQR13): in the wavelength interval 550–1300 nm, the relative RMSE is within 3–4%, well below the mission requirement of 5%. In the 1500–1750 nm range, RMSE values of around 5% are observed and thus at the requirement threshold. Slight exceedances (<7%) occur in the 2000–2300 nm region, while larger deviations are visible at the detector edges (<600 nm and >2300 nm) (Figure 8-1).

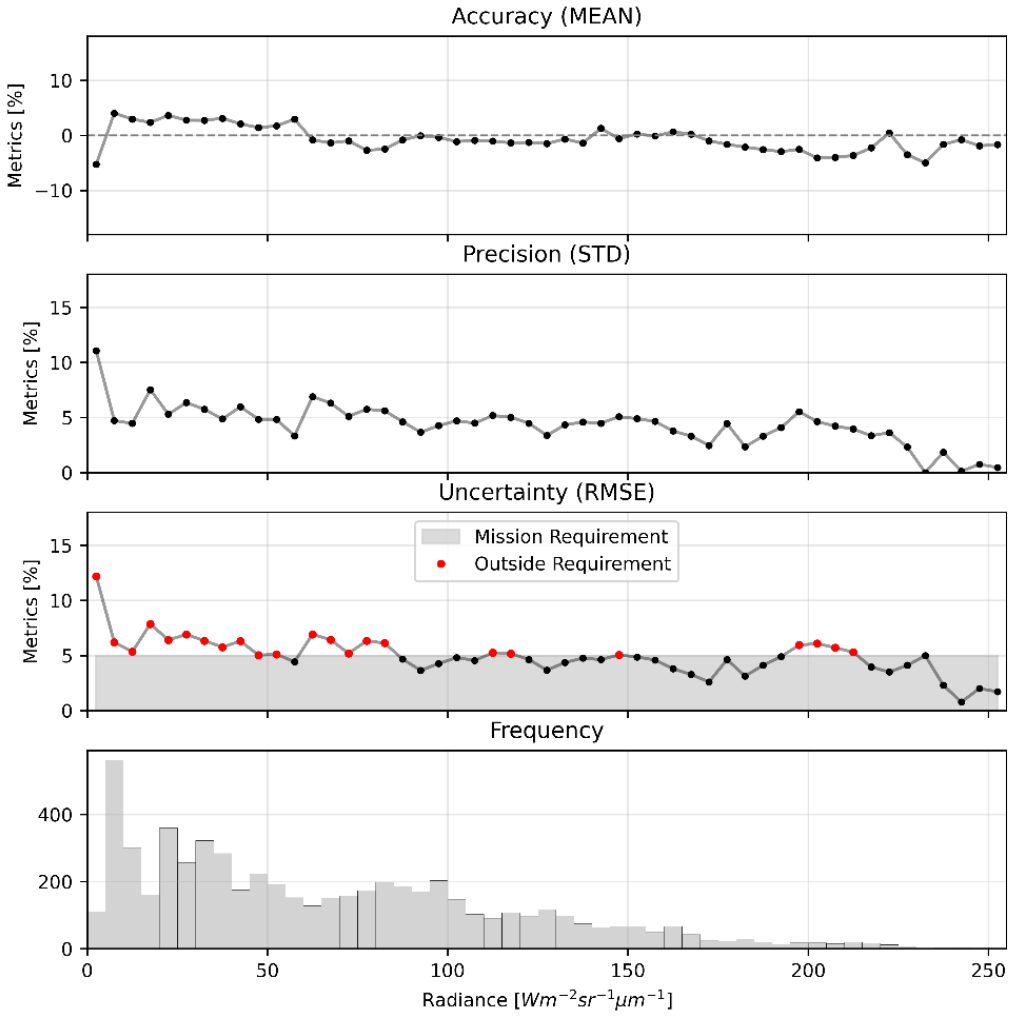

Figure 8-2 Errors between EnMAP TOA radiance and propagated TOA radiance from in situ measurements against radiance level for all arid validation sites based on 42 matchups.

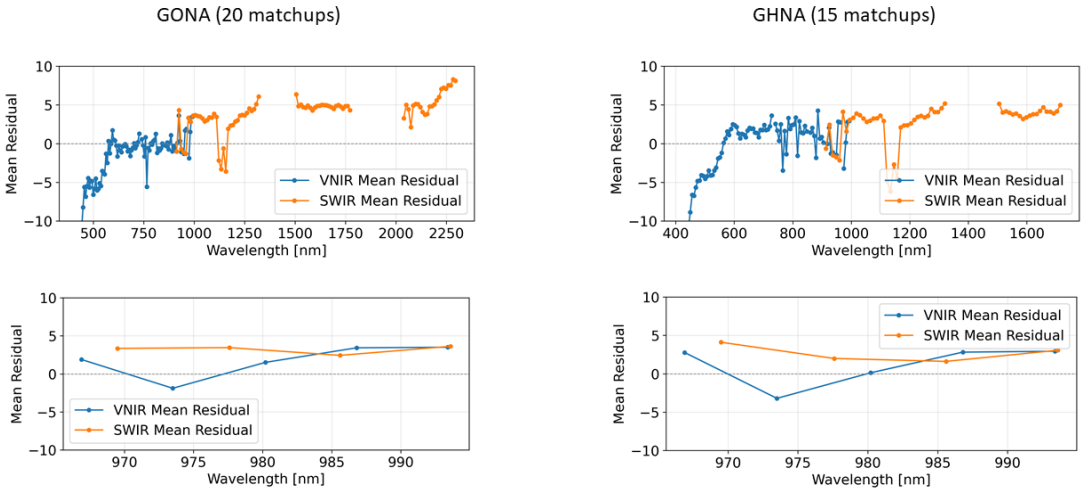

Figure 8-3 Mean difference between EnMAP TOA radiance and propagated TOA radiance from in situ measurements against wavelength at GONA (left) based on 20 matchups and GHNA (right) based on 15 matchups. The upper row shows the whole wavelength spectrum, the lower row shows a zoom to 960 to 1000 nm.

Furthermore, the additional GHNA matchups enabled a direct comparison between the Gobabeb RadCalNet station (GONA) and GHNA (Figure 8-3). Consistent with the behaviour reported for GONA in MQR12, the SWIR detector shows a clear positive bias of approximately 4–6 W m^{-2} sr^{-1} μm^{-1} relative to the in-situ radiance. The VNIR detector exhibits a negative bias up to ~550 nm at both sites. At longer wavelengths, the VNIR shows no bias at GONA, whereas GHNA shows a bias of approximately 2 W m^{-2} sr^{-1} μm^{-1}. Overall, the difference between EnMAP and in situ TOA radiance shows consistent behaviour for both stations. In the overlap region (985–1000 nm), VNIR and SWIR exhibit a comparable positive bias for both stations, which contrasts with the BOA reflectance validation and was already noted in MQR12.

The SNR assessment was updated based on 202 tiles with the product version 01.05.02 (VNIR 105 and SWIR 97) and was found to be very stable (VNIR: 401:1; SWIR: 260:1) compared to the previous evaluations and inside the mission requirements (VNIR > 343:1 @495 nm SSD 4.7 nm; SWIR > 137:1 @2200 nm & SSD 8.4 nm).

8.2 Level 1C

The following Level 1C validation scenarios have been performed:

- VNIR-to-SWIR spatial co-registration
- Absolute spatial accuracy

The spatial co-registration between VNIR and SWIR has been analyzed for 105 products with the product version 01.05.02. Compared to the previous report, the RMSEs in X and Y direction remain stable (6.0 and 6.4 m). Overall, the spatial co-registration performance is stable and well within the mission requirement of less than 30% of a pixel.

The quality of the absolute spatial accuracy is also stable. An RMSE of 10.3 m in X and 12.9 m in Y direction derived from 182 tiles with the product version 01.05.02 was achieved which is well inside the mission requirements (<30 m with GCPs in the image, <100 m without GCPs).

8.3 Level 2A

Land

Following the integration of the additional GHNA matchups, the total number of matchups increased from 50 to 59. Analogous to the TOA radiance results, the SWIR detector exhibits a positive bias of approximately 1.5–2% reflectance, whereas the VNIR shows a negative bias of about 2% at the lower end of the spectrum for both stations (Figure 8-7). For the VNIR at higher wavelengths (550–900 nm), no bias is observed at GONA, while GHNA exhibits a small positive bias of approximately 0.75%. In the overlapping spectral region (960–1000 nm), the SWIR displays higher reflectance values by approximately 1.5–2% for both stations.

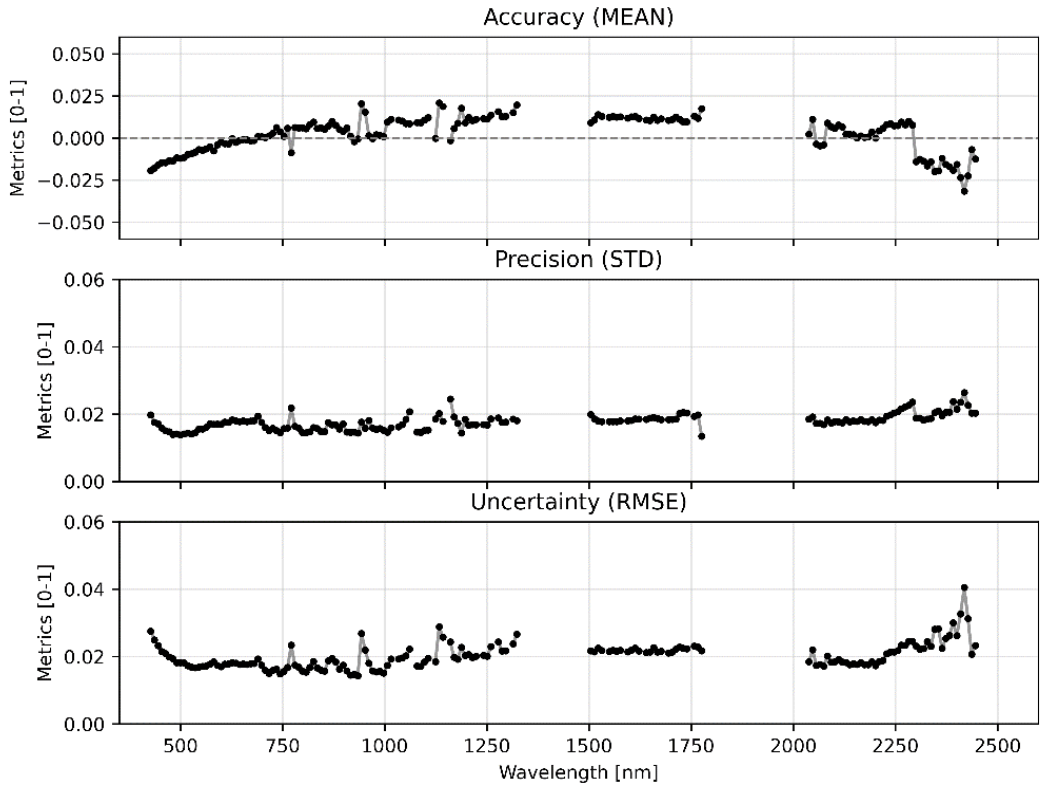

Figure 8-4 Errors between EnMAP and in situ BOA reflectance against wavelength for all validation sites based on 59 matchups.

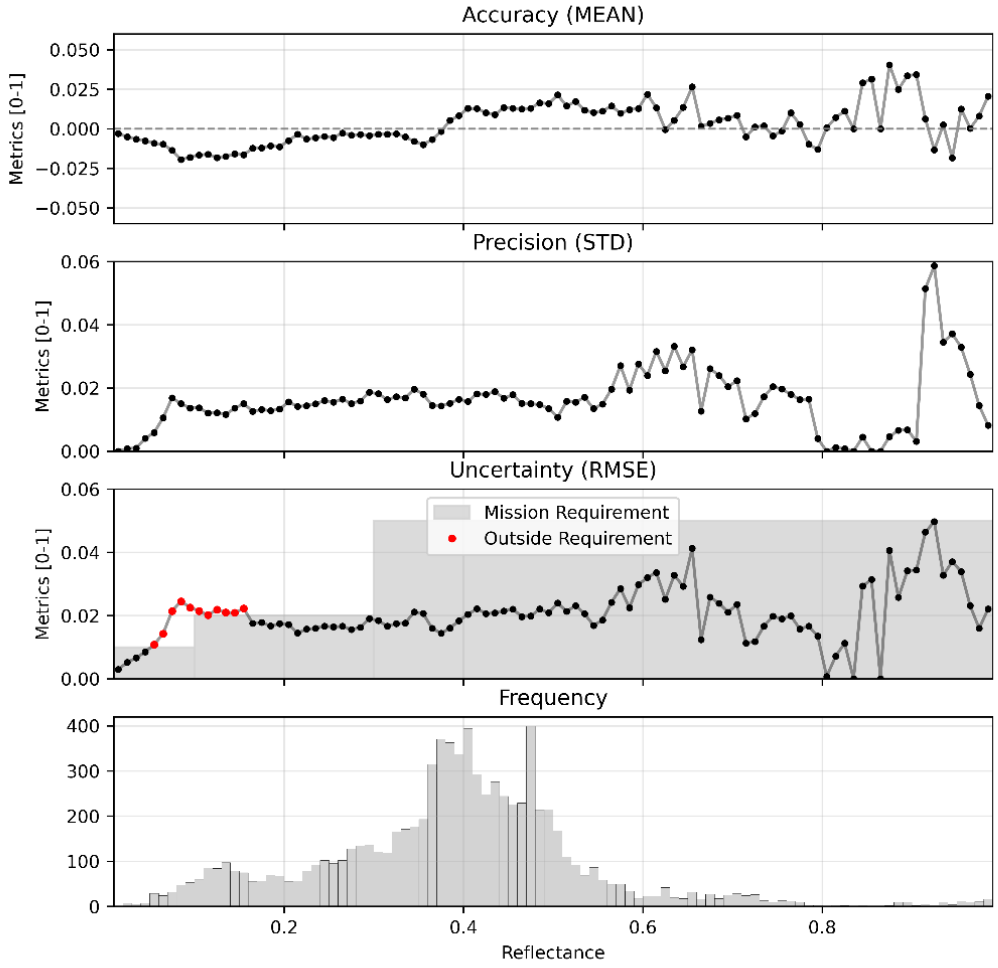

Figure 8-5 Errors between EnMAP and in situ BOA reflectance against reflectance level for all validation sites based on 59 matchups.

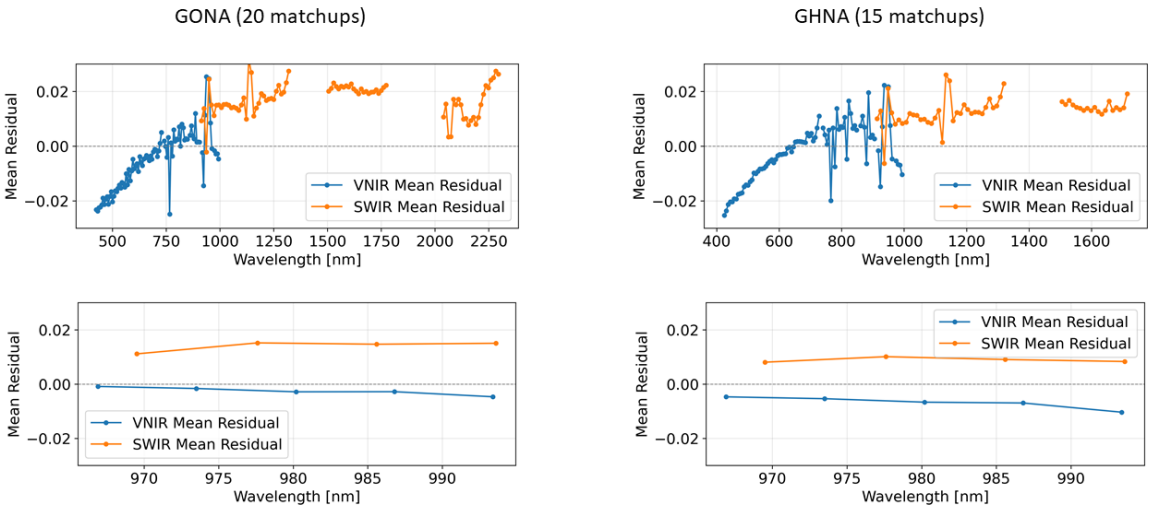

Figure 8-6 Mean difference between EnMAP BOA reflectence and BOA reflectance from in situ measurements against wavelength at GONA (left) and GHNA (right). The upper row shows the whole wavelength spectrum, the lower row shows a zoom to 960 to 1000 nm.

Water

A total of 24 additional matchups have been incorporated into the water validation since the previous report. These include 5 matchups for the Acqua Alta Oceanographic Tower (AAOT), 4 for Lucinda Jetty, 2 for Magest, and 2 for Lake Garda. In addition, 8 matchups from the Mackenzie campaign were added, along with two matchups for the newly established site Alkor and one for the newly established site Wraysbury. This increases the total number of available matchups to 88. Based on the 88 matchups, the uncertainty remains well within the mission requirements for wavelengths below 650 nm. For wavelengths above 650 nm, the uncertainty partly exceeds the mission requirements (Figure 8-7). As illustrated in Figure 8-8, the uncertainty increases with increasing reflectance level, which is attributable to a growing negative bias at higher reflectance values.

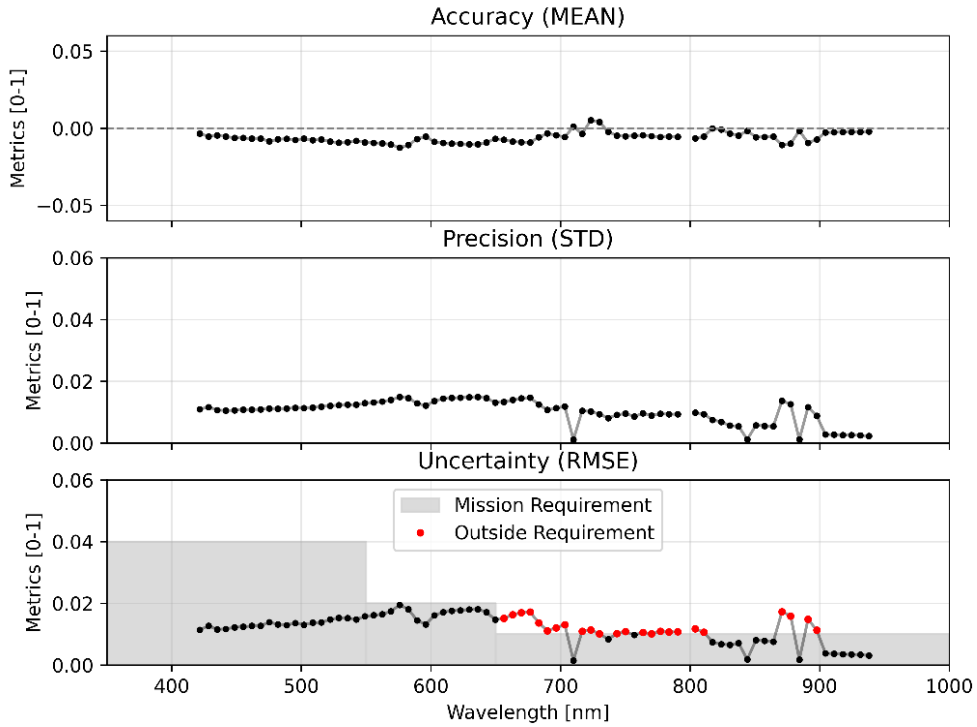

Figure 8-7 Errors between EnMAP and in situ BOA Normalized Water-Leaving Reflectance against wavelength based on 88 matchups.

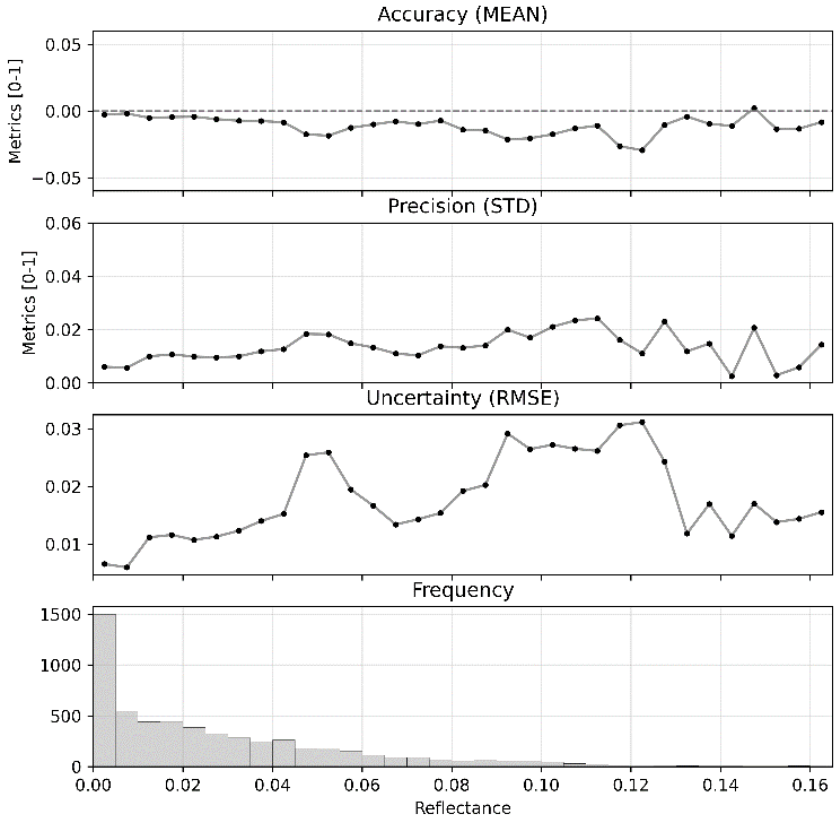

Figure 8-8 Errors between EnMAP and in situ BOA Normalized Water-Leaving Reflectance against reflectance level based on 88 matchups.

8.4 Summary of External Product Monitoring

Overall, the validation and quality monitoring activities carried out during the reporting period indicate that the EnMAP product quality is stable and compliant with the mission requirements. The observed differences between the VNIR and SWIR detectors in the overlapping spectral region are consistent for both the RadCalNet station (GONA) and the HYPERNETS station (GHNA) at Gobabeb. This consistency suggests that the detected differences are unlikely to originate from the in situ instruments.

9 Others

EnMAP Mission Operations and Status Publications:

- Giardino, C., Pellegrino, A., FABBRETTO, A., & Panizza, L. (2025), ACIX-III AQUA: Evaluation of atmospheric correc-tion processors for hyperspectral satellite over inland and coastal waters. Zenodo. doi: 10.5281/zenodo.17660438

- Kokhanovsky, A., Chevrollier, L.A., Wehrle, A., Segl, K., Chabrillat, S. (2025). A simple analytical model for the reflection function of flat glacier ice surfaces and its application for optical remote sensing of glaciers, Journal of Quantitative Spectroscopy & Radiative Transfer. https://doi.org/10.1016/j.jqsrt.2025.109717.
- Asadzadeh, S. and Chabrillat, S. (2025). Leveraging EnMAP hyperspectral data for mineral exploration: examples from different deposit types, Ore Geology Reviews 186, 106912. https://doi.org/10.1016/j.oregeorev.2025.106912

EnMAP Mission Operations and Status Presentations:

- VH-RODA: „Long-term Inflight Spectral and Radiometric Calibration of EnMAP” by D. Marshall. 17-21 November 2025. ESA – ESRIN (Frascati, Italy)

- GSICS Lunar Calibration Subgroup: “EnMAP Moon observations” by M. Pato. 13. November 2025 (online meeting).